Strain and Structure of a Temperate, Maritime Glacier: *Te Moeka o Tuawe* / Fox Glacier, South Westland, New Zealand

John Richard Appleby

Thesis submitted in fulfilment of the degree of Master of Science in Physical Geography, at Massey University, Palmerston North, New Zealand.

November 2007

"Raki, the Sky Father, wedded Papa-tui-nuku, the Earth Mother. After the marriage, the four sons of Raki who were named Ao-raki, Raki-ora, Raki-rua, and Raraki-roa came down to greet their father's new wife in the canoe of the eldest brother Ao-raki, known as Te Waka o Aoraki. They cruised around Papa-tui-nuku, then, keen to explore, the voyagers set out to sea, but no matter how far they travelled, they could not find land. They decided to return to their celestial home, but the karakia which should have lifted the waka back to the heavens failed and the canoe fell back into the sea and turned over onto its side, and settled with the west side much higher out of the water than the east, thus the whole waka formed Te Waka o Aoraki, the South Island. Ao-raki and his brothers clambered on to the high side and were turned to stone, where they remain today, Aoraki being the highest peak, surrounded by his younger brothers. The permanent snows of these peaks were known as whenuahuka and the great snow fields hukapapa. The glaciers that flowed out of them were called huhapo. Nearby in the darkened valleys was kopakanui or ice and in places cut off from the sun was thick ice of waiuka meaning solid water"

-Maori Mythology

Abstract

The study of glaciers has an immense significance for understanding and predicting global environmental change. The Earth is a dynamic system, consisting of individual units such as the cryosphere, an understanding of which may provide the basis for predicting future environmental change on a global scale. The dynamics of a glacier, a major indicator of the climatic and environmental situation is often presented as supraglacial structures, which reflect glacier formation, deformation and flow. Although structural attributes such as folds, faults, crevasse traces and foliation are commonly described in glaciers, the origin and significance of many of these structures remains unclear.

This research project mapped the surface structures of Fox Glacier, using remote sensing in the form of aerial photographs and field observations, to produce a structural glaciological interpretation of the glacier surface, structural field maps of individual structures, and a schematic structural evolution of Fox Glacier. In addition, cumulative strain, and strain rates were calculated for three different areas of the lower Fox Glacier. The relationship between the observed structures and the measured strain rates has also been considered.

Fox Glacier is located in the South Westland region of the South Island of New Zealand. From the Main Divide of the Southern Alps up to 3000m altitude, Fox Glacier flows for 13 km, terminating at an altitude of 270 metres in temperate rainforest, 17 km from the present coastline. The steep gradient allows for relatively rapid ice flow. Despite being a very dynamic glacier, very little research has been carried out on Fox Glacier in recent years with most research in the area being concentrated on its neighbour the Franz Josef, and even more so on the glaciers of the Eastern side of the Main Divide (e.g. the Tasman and Mueller glaciers).

There is a high level of spatial variability in structural types observed, and the cumulative strain and strain rates measured on the surface of the Fox Glacier, with the variations being linked to valley topography including long-profile gradient and valley width. Strain rates of

208.78 y^{-1} and -162.06 y^{-1} were recorded on Fox Glacier. A relationship can be determined between observed glaciological structural features and measured strain rates, suggesting strain rate has an influence on the type, magnitude, location and frequency of these features, however, the study is only a 'snap-shot' of the strain conditions experienced in the most dynamically active time, during the summer ablation season.

Developing predictive models of the structural evolution of glaciers may help further understanding of how glaciers respond to a change in climatic input, especially climatic warming. This is particularly important for larger ice sheet outlet glaciers whose structure and flow appear to reflect and control dynamics of the ice sheet behind

Acknowledgements

The completion of this MSc thesis would not have been possible without the help, advice and encouragement from a number of people whom I wish to thank and acknowledge:

- Dr Martin Brook, whose knowledge of, and enthusiasm for glaciers and glacial processes has been a catalyst for my own enjoyment and involvement in glacial research.
- Dr Ian Fuller and Mr David Feek of the Geography Programme at Massey University, for technical and field assistance and advice. Also for the loan of the Trimble RTK GPS unit from the Geography Department.
- Associate Professor Bruce Van Brunt of the Institute of Fundamental Sciences at Massey University for guidance and advice on all things mathematical, and also a great enthusiasm for the mountains of New Zealand's Southern Alps.
- Marius and all of the guides and staff of Alpine Guides Westland, for advice, assistance and entertainment whilst undertaking the seven weeks of fieldwork at Fox Glacier.
- Lee and all of the pilots and staff of Glacier helicopters, Fox Glacier for invaluable help with logistics and transport.
- Department of Conservation / *Te Papa Atawhai* for allowing research in the Westland *Tai Poutini* National Park.
- Funding from the Massey University Geography Programme Graduate Research Fund (GRF).
- All of the staff and postgraduate students of the Massey University Geography Programme, for providing a supportive, professional and fun working environment.
- My Parents, for having to keep topping up my bank account!

Table of Contents

Chapter 3: Methodology of Research

Chapter 4: Results

Chapter 5: Discussion

Chapter 6: Conclusions

Appendices

References

List of Figures

List of Tables

Chapter 1: Introduction

1.1 Introduction

The Earth is a dynamic system in which the atmosphere, geosphere, hydrosphere, biosphere, and cryosphere interact with one and other. Understanding how each of these spheres act in unison, may ultimately provide the basis for predicting future environmental change on a global scale. Firstly, however, we must understand how they act in isolation. The interrelations between the cryosphere (namely the Earth's glaciers) and global change (primarily climate change) are largely due to changes in the size and shape of the glaciers (Knight, 2006).

The shape of a glacier is often presented as supraglacial structures, which reflect glacier formation, deformation and flow. Although structural attributes such as folds, faults, crevasse traces and foliation are commonly described in glaciers, the origin and significance of many of these structures remains unclear (Glasser *et al*., 2000). The types, frequency and formation of these features can be dictated by the climatic situation locally and the environmental situation globally (Gardner and Sharp, 2007).

Because of their small extent, and often high precipitation, mountain glaciers are rather sensitive to climate variations and changes in the environment (Kaser, 2006; Bugmann *et al*., 2007). The elevation (c. 3000m) of the Main Divide of the Southern Alps in New Zealand's South Westland provides a gathering ground for névé fields, which nourish a number of valley glaciers. The largest glaciers flow east and south to the Tasman valley, but on the western side of the divide the Franz Josef and Fox Glaciers have long been noted for their spectacular appearance and the low altitude (200m) of their termini (Soons, 1992). This large gathering ground coupled with relatively narrow valleys (<1km) mean small changes in the climatic situation, create magnified changes in the flow patterns and structure of the west coast glaciers

1.2 Description of Study Area

Fox Glacier is located in the South Westland region of the South Island of New Zealand (Figure 1.1). South Westland is a narrow strip of land bordered by the Tasman Sea in the west and the Southern Alps in the east. The Main Divide of the Southern Alps (Figure 1.2), in excess of 3000 metres altitude, provides a barrier to the westerly air flow known as the 'roaring forties', producing up to 15 metres of precipitation each year (Coates and Chinn, 1992). Some of this precipitation is collected in the névé of the Fox Glacier, one of the largest in New Zealand, having a collection area of approximately 25 km^2 (Sara, 1974). From approximately 2700 metres above sea level (a.s.l), ice flows from the névé and down the Fox valley, forming a glacier that extends approximately 13 km to its snout (Figure 1.2), terminating at an altitude of 270 metres, around 17 km from the present coastline (Purdie, 2005).

From the névé the glacier flows in a north-westerly direction down the upper icefall into a valley confined by Chancellor Dome, and Paschendale Ridge. Below this upper icefall the gradient lessens, as the ice moves along Victoria Flat, an area that has, in the past, marked the confluence of the Fox and Victoria Glaciers. The ice then flows down another steep icefall (the lower icefall), and follows the constraining valley, giving the lower part of the glacier a westerly aspect.

It is thought that Fox Glacier is exceptionally sensitive to variations in precipitation due to the relatively large size of its névé in comparison to the main valley; meaning small changes in accumulation can produce dramatic changes in the position of the snout (Coates & Chinn, 1992). This combined with the steep gradient and rapid ice flow, means that Fox Glacier is highly dynamic. However, very little research has been carried out on the Fox Glacier in recent years (e.g. Gunn, 1964; Sara, 1974; Purdie, 2005; Purdie *et al*., 2007, Purdie *et al*., 2008) with most research in the area being concentrated on the neighbouring Franz Josef Glacier (e.g. Hooker and Fitzharris, 1999; Davies *et al*., 2003; Goodsell *et al*., 2003; McKinzey *et al*., 2004; Goodsell *et al*., 2005), and on the debris covered glaciers to the east of the Main Divide (e.g. Hochstein *et al*., 1998; Kirkbride and Warren, 1999; Warren and Kirkbride, 2003; Rohl and Roehl, 2006; Mager and Fiztsimons, 2007).

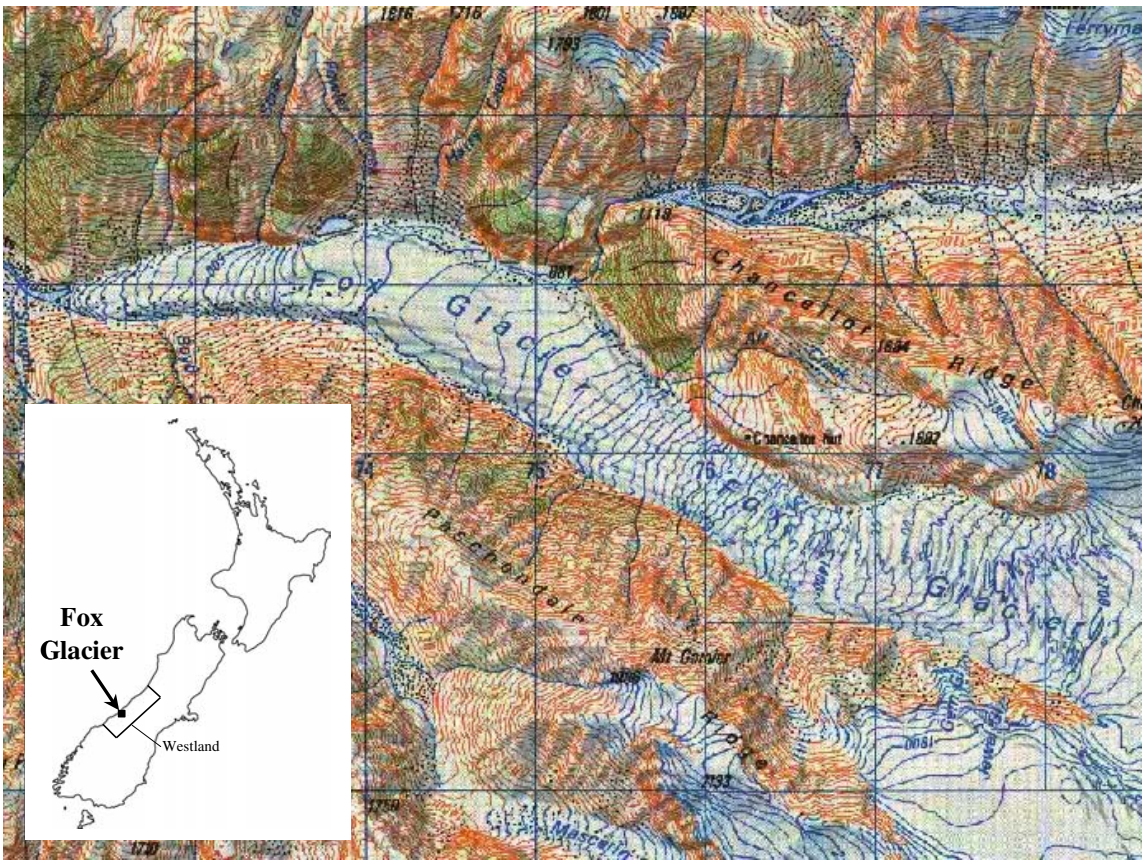

Figure 1.1: Location and topographical map NZMS 260 H35/H36 of Fox Glacier / *Te Moeka o Tuawe* at a scale of 1:50 000 (Land Information New Zealand, 2003).

1.3 Importance of Glacial Research

Past and modern glacial environments provide an important key to our knowledge of past, present and future global environments and climates. The effect of modern glaciers on a global scale can be looked upon at two levels. Firstly, they impact upon humans and habitats in their nearby surroundings, through meltwater outbursts and rapid advances, and secondly at a larger scale impact on global sea-level (Nesje and Dahl, 2000). Glaciers and ice sheets both affect and are affected by changes in Earth's climate. They can be seen as frozen fresh-water reservoirs, covering approximately 10% of the Earth's surface, containing in excess of 80% of the World's fresh water (Benn and Evans, 1998). Mountain glaciers experience a constant natural fluctuation in volume and length driven by precipitation and temperature (Anderson and Mackintosh, 2006), however, the current

retreat of glaciers, and the break-up of ice sheets, may be of a greater magnitude and speed than those previously seen during natural fluctuations (Bamber *et al*., 2007). It should be remembered that the hypsometry of individual glaciers and ice caps plays an important role in their response, thus making it difficult to generalize results (Oerlemans *et al*. 1998).

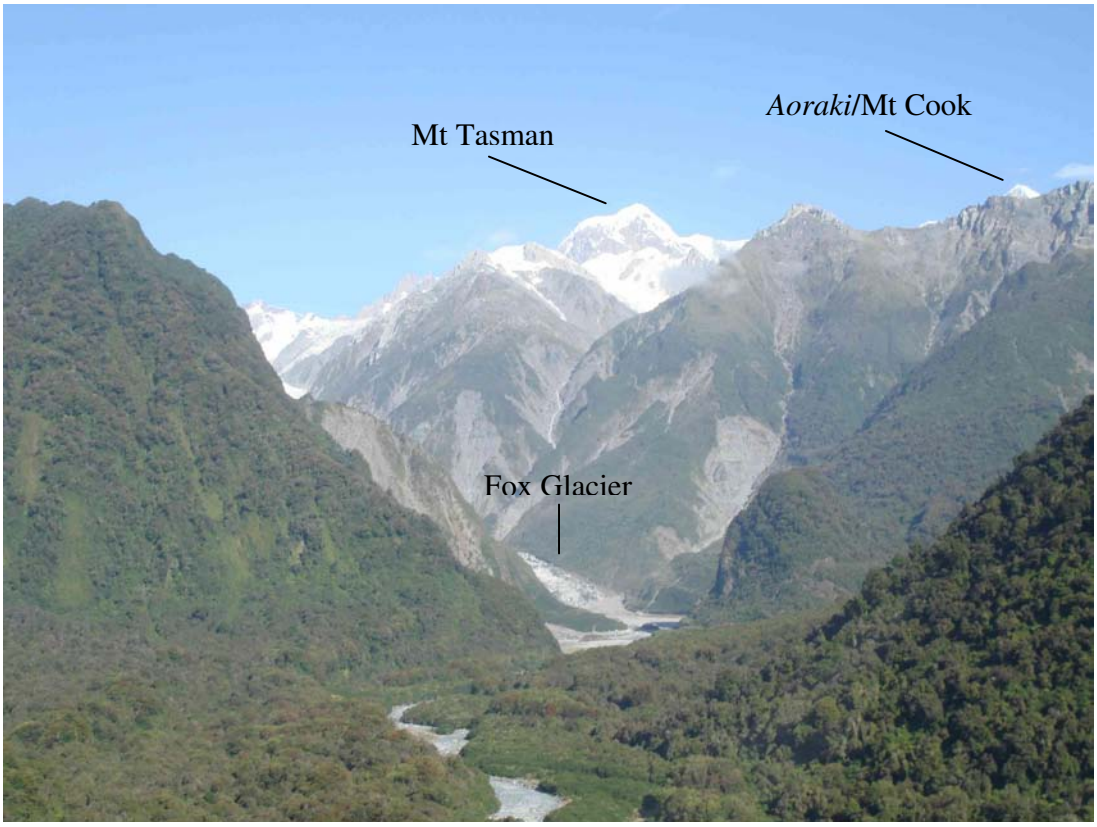

Figure 1.2: Fox Glacier flowing from the Main Divide of the Southern Alps into temperate rainforest, with New Zealand's two highest mountains *Aoraki*/Mount Cook (3754m) and Mount Tasman (3497m), towering above. (Photo: J. Appleby)

Understanding the link between structure and strain allows a glaciers flow regime and behaviour to be understood from such sources as aerial photographs or satellite imagery (Goodsell *et al*, 2005[a]). Glacier-based tourism is of great importance in New Zealand's Southern Alps, particularly on the west coast. Hence, understanding the movement, structure and response to climate is therefore not only of significance in predicting the future response of glaciers to climate, but also in managing the safety and economic future of the people and communities that live and work in such dynamic glacial landscapes.

1.4 Thesis Structure

This thesis is divided into six chapters. Chapter Two is a review of previous literature and research related to Fox Glacier, structural glaciology, and the study of strain and stress measurements. Chapter Three outlines the methods used in this study to measure strain, and to map structures on the glaciers surface. Chapter Four presents the results obtained from this study using methods discussed in Chapter Three, and presents data including maps produced from aerial photographs and field observations, and calculations of strain experienced on the surface of the ice. Chapter Five provides a discussion of these results and explores the potential for future research. Following this, Chapter Six provides conclusions and a summary of the key findings of the research. Appendices and a reference section follow Chapter Six.

Chapter 2: Literature Review

2.1 Historical Background

Early observations of New Zealand's glaciers date from the mid 1800s, with the earliest recorded glacial maps being of the termini of the Tasman, Godley and Classen Glaciers, produced in 1862 by government surveyor and geologist, Julius von Haast (Gellatly, 1985). Fox Glacier (Figure 2.1) was first surveyed by Douglas and Wilson in 1894 and 1895, with the next detailed maps being produced by Greville and Bell in 1910 (Bell, 1910). Following these early observations, glacier research for the first half of the last century was dominated by observations of glacier termini changes. Many of these surveys were published in early volumes of the *Journal of Glaciology*, giving New Zealand's glaciers a level of international scientific exposure that has not been repeated since (Fitzharris *et al*., 1999).

Despite the early voyages along the west coast by Abel Tasman in 1642, the earliest European record of Fox Glacier comes from explorers Frances and Young in the logbook of their ship *Mary Louisa* as it sailed along the west coast of the South Island:

> *"At noon, abreast of Mount Cook, close in shore, we could see distinctly that it was an immense field of ice, entirely filling up the valley formed by the spurs of the twin peaks, running far down into the lowland. It was a pale green colour, and appeared to be quite a mile in width towards the lower end of the valley…"*
>
> -Extract from the log book of the Mary Louisa recorded on 14th June 1859 (after Sara, 1974).

Originally named the Albert Glacier by Haast to complement the smaller, Victoria Glacier (a tributary of Fox Glacier) lying parallel and to the north, its name was changed to Fox Glacier in 1879 after the visit of the then Prime Minister of the Colony, Sir William Fox (Sara, 1974). The name Albert Glacier is still retained in the upper part of the névé.

Figure 2.1: Fox Glacier/*Te Moeka o Tuawe* which flows 13km from below Douglas Peak (3077m) on the Main Divide of the Southern Alps to the Fox River at approximately 200m above sea level. (Photo: J. Appleby)

Interest in glacial structure dates back to the first days of glaciology, when early researchers such as Forbes (1845) and Tyndall (1859) compared foliation in ice with geological structures, and suggested mechanisms for ice flow and deformation. The nineteenth century was a time when the fundamental physical principles of glacier flow and mechanics were being examined, and a number of authors used ice structures to support their ideas about ice deformation (Hambrey and Lawson, 2000). The first mention of any structure present on Fox Glacier was inferred, indirectly, by Douglas (1896), who wrote:

"As a mere mass of ice in the valley, the Fox Glacier cannot compare for a moment with the Franz Josef, its icefall is inferior, and the surface of the glacier not so broken up into picturesque pinnacles….."

As with all landform features in New Zealand, Fox Glacier has both cultural and spiritual significance to local Maori. The Maori name for the Fox Glacier, *Te Moeka o Tuawe*, is derived from *Tu Awe*, an ancestor of *Ngāi Tahu*, the local tribe, who fell to his death whilst exploring in the area. The bed of the glacier became his final resting place (*moeka*), with the valley being filled with ice through the tears of his lover *Hine Hukatere*, from which the name of the Franz Josef Glacier, *Kã Roimata o Hine Hukatere*, meaning '*the tears of the avalanche girl'*, is also derived (Alpine Guides Westland, 2007).

2.2 Stress, Strain and Structure of Glaciers

The concepts of stress and strain are fundamental to a clear understanding of why and how glaciers flow, and of many aspects of their interaction with the landscape such as response to climate change (Benn and Evans, 1998). The way in which a glacier flows is fundamental in understanding glacial processes such as erosion and deposition and how mass and energy is processed through the glacial system.

Understanding the processes involved in how a glacier behaves, flows, and changes, may allow us to predict and therefore manage potential hazards such as glacial lake outburst floods or glacial surges; it can also assist us in understanding how different glaciers respond variably to climate change. Along with using research to predict the future, we can also use it to reconstruct the past. If a uniformitarianistic approach is taken, the present can be seen as the key to the past. The processes we see occurring in today's glacial landscapes are a good proxy of processes that occurred in the past, and so if we can assign landform products to specific glacial behaviour, we can deduce what glacial processes have occurred in the past by studying landforms from previous glacial activity.

Little work has been done on relating stress and strain to the structure of temperate maritime glaciers. This is especially true of the glaciers of New Zealand, which are only now beginning to be studied and understood. Structural glaciology is more commonly studied in the European Alps on glaciers such as Bas Glacier D'Arolla in Switzerland (e.g. Goodsell *et al.*, 2002; Mair *et al.*, 2002; Goodsell *et al.*, 2005; Swift *et al.*, 2005), Antarctica (e.g. Scofield et al., 1988; Läufer and Phillips, 2005; Samyn *et al.*, 2005), Scandinavia (e.g. Fischer *et al.*, 2003), and the Arctic, especially Svalbard (e.g. Hambrey *et al.*, 1996; Woodward *et al.*, 2002; Farbrot *et al.*, 2005).

2.3 Stress, Strain and Deformation

In everyday use, stress and strain are used interchangeably, but they are actually quite different components of a force. Stress can be seen as a measure of the force acting on an object or material, whereas strain can be considered a measure of the amount of deformation that the material experiences. The two components are interlinked with stress being directly proportional to strain according to a relationship described as Hookes Law (Figure 2.2) (Cutnell and Johnson, 2004).

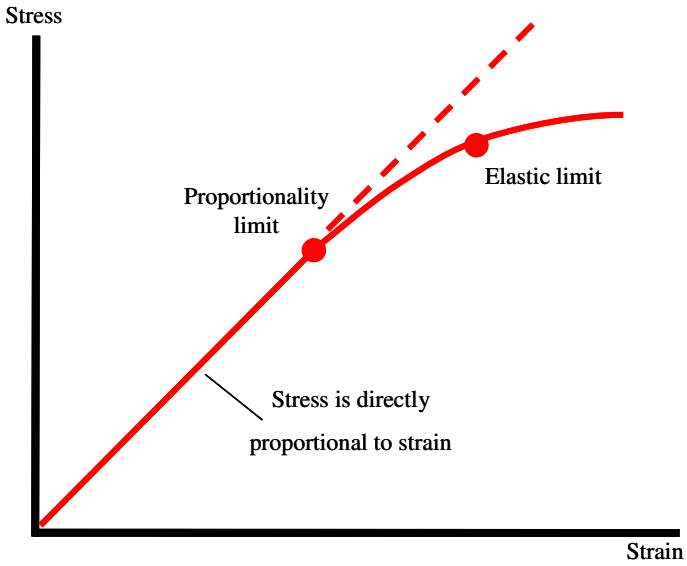

Figure 2.2: Proportionality of stress and strain according to Hooke's law. Up to the proportionality limit stress is directly proportional to strain. Beyond this point, ductile deformation of ice occurs up to the elastic limit, at which point ice cannot resist strain and experiences fracture (Cutnell and Johnson, 2004).

This law of proportionality occurs up to the proportionality limit, at which point they are unequal. Eventually a material will reach an elastic limit, at which point the material cannot return to its 'un-stressed' form and permanent deformation occurs (Paterson, 1994). When ice is deformed under increasing stress, it undergoes a transition from elastic to ductile behaviour, crossing the elastic limit threshold, when considered using Hookes Law. Natural ice masses experience moderate or low stresses for tens or hundreds of years and surface features such as crevassing are thought to be a product of these long stress histories (Vaughan, 1993), although much higher stresses acting over a shorter time would be expected in a glacier flowing as rapidly (approx. 0.9 m/day) as Fox Glacier (Purdie *et al*., 2007). At higher stresses, according to Jaeger and Cook (1979), ice becomes brittle and its ability to resist load decreases with increasing deformation. Fracture is a continuous process throughout the brittle regime until sudden failure occurs, producing, in conjunction with ablation, the often dramatic surface topography of valley glaciers.

Stress is measured in units of Newtons per square meter (Nm^{-2}), commonly termed Pascals (Pa). However, for the magnitudes of stress involved in glaciology, the bar is a more manageable unit, where 1 bar is 100 kPa or 10^5 Pa. Strain can be considered as a total or cumulative value describing the total strain experienced by a material due to the stress applied, but is more commonly expressed as a dimensionless ratio of the difference between initial length and final length, describing the rate at which the body of ice deforms in response to the applied stress (termed strain-rate) and is expressed in units of $time^{-1}$ (Hubbard and Glasser, 2005).

Stresses are vector quantities, meaning they have both magnitude and direction (Hooke, 2005). Stresses that are directed normal to the surface on which they are acting are called normal stresses; in this case, the mass of the ice causing a downward stress on the glacier bed. Those stresses acting parallel to the surface are shear stresses This is the force of the ice moving down-valley under the influence of its mass and gravity (Figure 2.3). The parallel shear stress acting on a body of ice is largely controlled by ice thickness and surface slope (Echelmeyer and Kamb, 1986), which in turn can be greatly influenced by the mass balance gradient of the glacier.

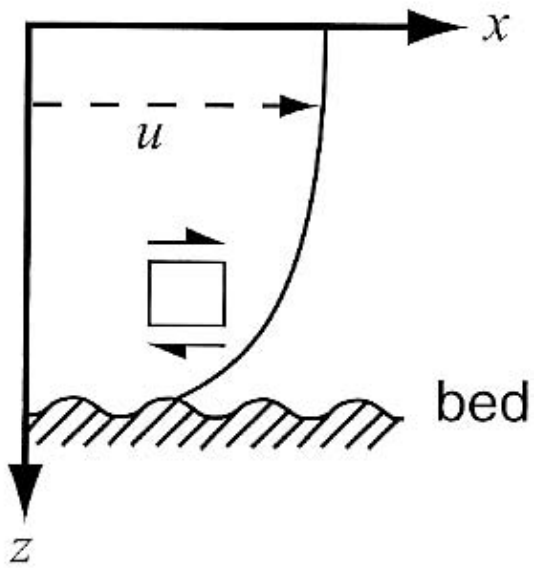

Figure 2.3: Normal force due to mass of ice *z*, and shear-stress force *x*, of a body of ice. Horizontal velocity is defined *u*, whilst perceived shear stress is demonstrated by the arrowed-box (Hooke, 2005).

2.3.1 Mass Balance, Stress and Strain

Mass balance can be seen as a driver of stress and strain in glacial ice due to the gradient created by ablation, accumulation and gravity (Figure 2.4). The rates at which annual ablation and accumulation change with altitude are termed the ablation gradient and accumulation gradient and together define the mass balance gradient (Benn and Evans, 1998). Steep mass balance gradients result from heavy precipitation in the névé and upper accumulation area and high ablation rates in the ablation area lower down the glacier, and correspond with high throughputs of ice (Kuhn, 1984). It would appear that Fox Glacier demonstrates these trends well, with a névé receiving approximately 11 to 15m of precipitation each year, whilst the glacier terminates at a very low altitude, with the snout experiencing average ablation rates of 129 mm d^{-1} during the summer ablation season (Purdie, 2005).

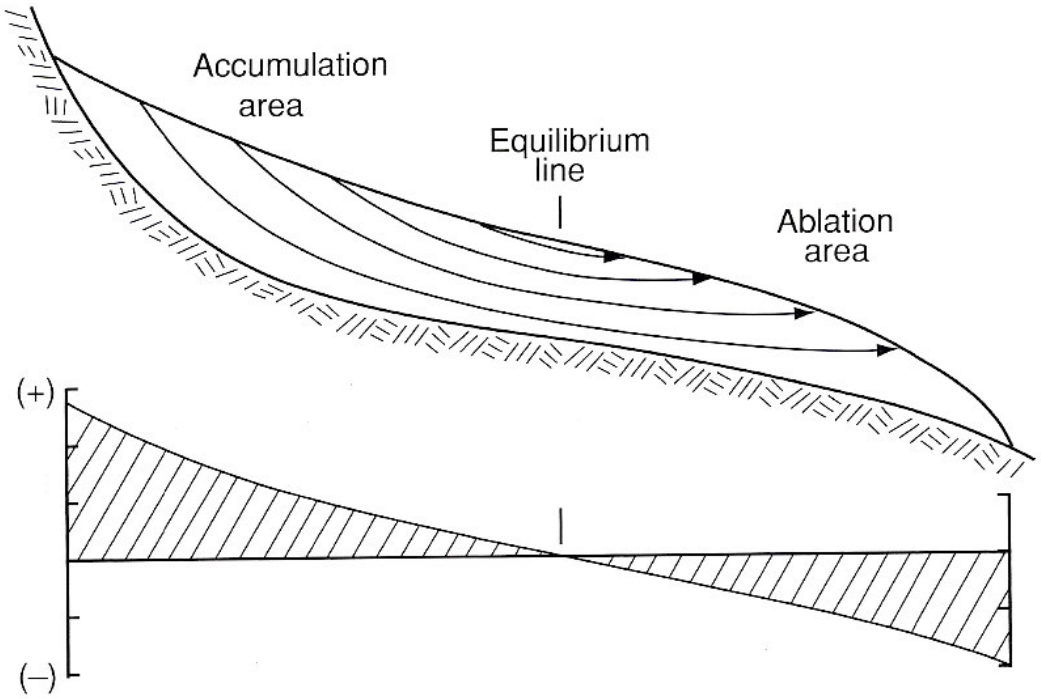

Figure 2.4: Longitudinal cross section of a valley glacier showing schematic representations of mass balance and gradient (Hooke, 2005).

This in-balance of mass in conjunction with the steep gradient of valley glaciers such as Fox Glacier creates substantial momentum and relatively rapid movement of ice. Movement can be considered one of the fundamental causes of stress, strain and deformation seen in valley glaciers, ice sheets, or ice caps.

2.3.2 Flow of Ice

Ice flow is one of the fundamental characteristics of glaciers and ice sheets, although until the mid-nineteenth century, the fact that glaciers moved at all was unknown to the scientific community (Hambrey and Alean, 2004). Many processes and properties of the surrounding environment influence glacier movement (Benn and Evans, 1998) including thermal regime, substrate composition, ice thickness and glacier hydrology.

Ice thickness influences glacier motion through an increased gravitational force on the ice mass, and an increase of pressure at the base (Benn and Evans, 1998). The more massive an

object at the top of a slope, in this case ice, the more potential energy it contains (Cutnell and Johnson, 2004), and so the greater kinetic energy will be available in the system as the ice moves down slope. The thickness of the ice also determines the pressure melting point (pmp) and therefore how much melt water is available at the sole of the glacier. Basal melt water has a lubricating effect on the glaciers sole and may allow movement via enhanced basal sliding. Basal sliding includes processes such as basal creep, regelation slip, and hydraulic jacking. Weertman (1964) suggested a water layer of only a few millimetres thickness might change the sliding velocity of ice appreciably. In a temperate glacier, such as Fox Glacier, basal sliding is considered as the main component of flow (Nienow *et al*., 2005), and may account for around 90% of overall movement (Hambrey and Alean, 2004).

In addition to basal sliding, glaciers move by internal deformation of the ice. Ice will respond to an applied shear stress by demonstrating strain in the form of deformation. This internal deformation of the ice occurs via either ductile deformation or brittle fracture. Ductile deformation or creep occurs as ice crystals move around each other, or change their individual shape to fit in with the surrounding crystals. Deformation such as this may occur in crystals by gliding along lines of weakness, known as cleavage plains, or along defects within the crystals themselves (Weertman 1983). Movement between crystals occurs by the change in size and/or shape of crystals at the grain boundary under a process known as recrystallization (Alley, 1992). Internal deformation may be strikingly obvious if it occurs in a body of ice constructed of layers, often exhibiting a highly folded stratigraphy when deformed by crystal movement or change in size or shape. In some situations, ice cannot creep and deform fast enough, and brittle fracture occurs when the ice passes a threshold of failure. As the ice fractures, large-scale faulting and folding may occur with features such as crevasses being the result (Harper *et al*., 1998; Harper *et al*., 2001).

It is not only ice that deforms to allow movement. Sediments beneath a glacier may undergo strain in response to stress imposed by the overlying ice (Larsen *et al*., 2007). Such subglacial deformation accounts for a substantial share of the forward motion of some glaciers (Boulton and Jones, 1979; Humphrey *et al*., 1993; Benn and Evans, 1998). Water causes an increase in volume of the subglacial material or till via a process called dilation.

As the material is now less compact, its shear strength and so resistance to applied forces is reduced. Grains of the material effectively climb over and around each other as the shear stress from the ice is transmitted to the till. This creates a lubricating layer at the ice-bed interface.

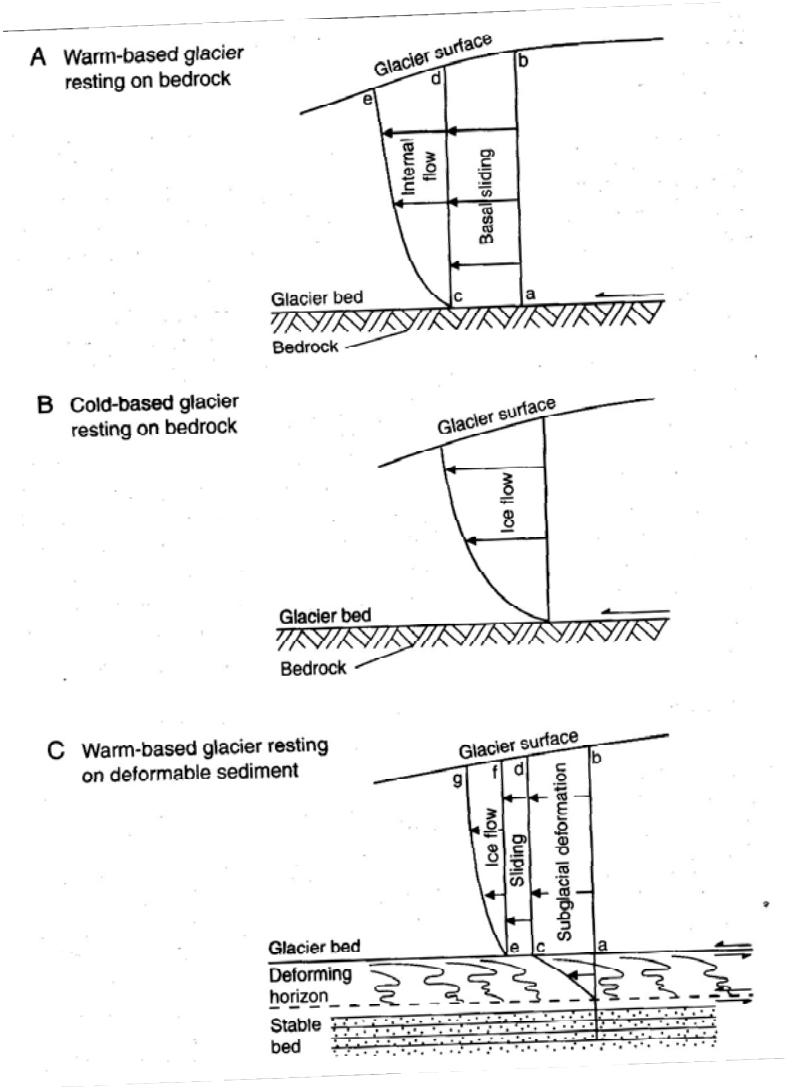

Figure 2.5: Horizontal velocity and flow profiles of glacial ice according to basal thermal regime and the presence or absence of a deformable bed (Boulton, 1996).

Boulton (1996) suggested theoretical velocity profiles for glaciers using the three main basal thermal regimes (Figure 2.5). Although simplistic and stylised, these profiles give a good indication of how a glacier is moving at a given temperature and ice-bed interface condition.

2.3.3 Flow Laws of Ice

A number of 'flow laws' have been established from laboratory-based experiments to describe the response of ice to applied stresses. The most widely used of these is Glen's flow law introduced by Glen (1955). This law was first adapted and used for glacial research by Nye (1957) and can be written as,

$$\dot{\varepsilon} = A t^n \qquad (2.1)$$

Where: $\dot{\varepsilon}$ = Strain rate (a^{-1})

t = Shear stress (kPa)

A = Constant related to ice hardness (viscosity) (s^{-1} $(kPa)^{-3}$)

n = Constant (approx. 3)

Glen's Flow Law describes many of the key features of glacier behaviour including:

- That the majority of deformation occurs near the base, where the stresses are highest;
- it explains how internal deformation occurs in glaciers where there is no basal sliding;
- it aids in explaining why strain in temperate glaciers is higher than in cold glaciers;
- it shows that the rate of deformation is intimately related to the shear stress in the form of a power law (Sugden and John, 1976).

However, Sugden and John (1976) point out that whilst Glen's Flow Law explains the role of shear stresses in glaciers, it does not take into account longitudinal strain variations, which may contribute to an increase in the strain rate, enhancing the deformability of the ice. Also, the flow law assumes ice crystals are aligned randomly, when in most cases they

tend to align themselves according to the direction of flow, increasing the plasticity of the ice (Ancey, 2007).

Although Glen's Flow Law has become fundamental to most studies of glacier motion, it is unrealistic to believe there is only one flow law applicable to ice deformation, because several processes are responsible for ice creep (Benn and Evans, 1998). The relative importance of the processes considered by Glen (1955) change spatially and temporally, thus necessitating the formulation of different laws depending on the dominant processes existing within the unit of ice being studied.

2.3.4 Field Measurement of Stress and Strain

According to Milnes and Hambrey (1976), the simplest method of estimating two-dimensional surface strains on glaciers is to use a velocity-contour and flow-line map, determined from the survey of stakes inserted into the ice surface. This method was first proposed by Nye (1959), and has become the norm for most research into stress, strain and deformation in ice bodies (e.g. Wu and Christensen, 1964; Meier *et al*., 1974; Hambrey and Müller, 1978; Vaughan, 1993; Goodsell *et al.*, 2005[a]).

The general method involves the drilling of stakes into polygon patterns, often diamonds or triangles, usually longitudinally down glacier or transversely across glacier. The relative location of each stake can then be repeatedly plotted using either a total station for optical surveys or, more commonly, differential global positioning systems (GPS). By measuring the change in length of the sides and diagonals of these patterns, it is possible to calculate with considerable accuracy all components of the rate of strain in the body of ice, after making use of various mathematical equations and models (Nye, 1959).

2.3.5 Mathematical Modelling

Often fieldwork is not practical due to constraints such as access, cost, or time and so researchers have tried to formulate mathematical models to predict the behaviour of glacier ice under certain conditions without the need for field investigations. Recent developments in glacier modelling have facilitated the prediction of stress and strain fields (Hubbard *et al.*,

1998) and the evolution of structures (Hubbard and Hubbard, 2000). Mathematical models allow for the creation of accurate predictions of deformation such as in Figure 2.6, for example. Field observations suggested that Hubbard and Hubbard's (2000) modelled data depicted the deformation and rotation of primary stratification and crevasse traces in the Haut Glacier D'Arolla, Switzerland, to a high degree of accuracy. However, due to their complexity, mathematical models can easily have flaws resulting in realistic but incorrect predictions (Hooke, 2005).

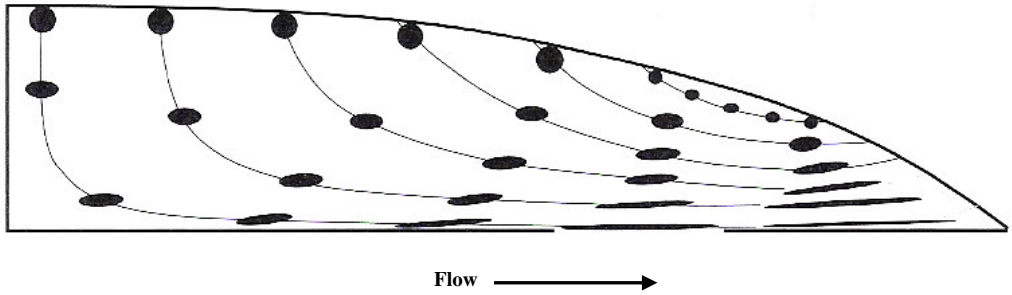

Figure 2.6: Schematic illustration of the deformation of a spherical object as it moves down glacier from the accumulation to ablation zone (Hooke, 2005).

It must be remembered also, that each glacier is unique in its behaviour, with a vast range of variables including topography, climate, aspect, and mass balance regime. Generalised models are useful for predictions or explanations of structural ice deformation but should be considered critically when extrapolated to other glaciers, upon which the data used to develop the model was not collected.

Beyond the scope of this research, stress, strain and deformation can also be modelled at the molecular level, taking into consideration crystal lattice structure, vibration and dislocation as discussed by workers such as Petrenko and Whitworth (1999), Thorsteinsson (2001), Hamelin *et al.* (2004), and Hooke (2005).

2.4 The Ice and Rock Deformation Analogy

A number of researchers (e.g. Hambrey and Lawson, 2000) have noted that the manner in which ice deforms in glaciers, producing a variety of ductile and brittle structures, resembles deformation in rock. However, Hambrey and Milnes (1977) noted that deformation in a typical alpine glacier takes place at a rate of six orders of magnitude faster than the deformation of sediments in Alpine orogenic belts.

Ice can be seen as a sedimentary rock in which new layers of sediment are added each year either through the accumulation of precipitation or the redistribution of snow from wind transport or avalanching. The accumulated snow then undergoes metamorphic change through the actions of pressure and temperature, before finally experiencing denudation by wind, water and fracture. In geological terms, according to Ragan (1969), flowing ice is an easily accessible, essentially monomineralic metamorphic rock (Herbst *et al.*, 2006) undergoing active deformation and recrystallization at high temperature.

For these reasons, the study of structural deformation in ice has been suggested as a quick and accurate measure of how rocks behave in similar conditions, allowing an understanding of geological processes over a period not normally associated with this field of study. Ice can be studied in a natural environment, with the results then being extrapolated to rock, and laboratory-based investigations in which the deformation processes can be replicated under controlled conditions are possible; something not possible with geological research (Karato *et al.*, 1998). Flowing ice is an attractive structural model having advantages of experimental models whilst avoiding the drawbacks (Ragan, 1969).

2.5 Glacial Structure

An important component of the study of a glacier's behaviour in conjunction with the measurements of the stress and strain rates it may be experiencing is the analysis of surface, or supraglacial, structure and the construction of a structural map. Supraglacial structures reflect glacier formation, deformation and flow. Glacier ice exhibits a wide variety of internal and superficial structures such as crevasses, icefalls, ogive banding, and layering (Nesje and Dahl, 2000).

There are two main categories of glacier structures as described by Hambrey (1994). The first of these is primary structure, involving deposition and accretion of material in the glacier and no deformation of the ice. These structures include regelation layering, lenses and bubbly ice deposits. Secondary structures occur through either plastic or brittle deformation of ice when internal creep of an ice mass causes stress to exceed the tensile strength of the ice, as discussed in 2.1.1. Characteristic glacier structures include crevasses, crevasse traces, and ogives, all of which have been discussed at great length in previous research (e.g. Glasser *et al*, 1998; Hambrey and Lawson, 2000; Goodsell et *al*., 2005[a]; Hambrey *et al.*, 2005).

2.5.1 Crevasses

Crevasses (Figure 2.8) can be defined as deep V-shaped clefts formed in the upper, brittle part of a glacier as a result of the fracture of ice undergoing extension (Hambrey and Alean, 2004). They are formed once critical conditions of stress and strain are reached in the surface of the ice mass (Kehle, 1964; Vaughan, 1993), at which point tensile stresses exceed the cohesive strength of the ice (Paterson, 1994). Crevasses are commonly oriented at right angles to the main stress direction (Figure 2.7). This common orientation of crevasses allows for an approximate indication of stress and strain directions within the ice (Benn and Evans, 1998). From field measurements on the White Glacier, Hambrey and Müller (1978) suggested that there is no well-defined critical strain rate associated with the presence of crevasses, whilst Hooke (2005) points out that crevassing is a result of high tensile stresses.

Spatial patterns and concentrations of crevasses can change dramatically as the stress regime of the moving ice changes over time. An excellent example of this can be seen at icefalls where ice flow typically accelerates before decelerating (Benn and Evans, 1998). As ice approaches an icefall its velocity increases as it flows over what is in effect a very slow moving waterfall. This rapid acceleration causes longitudinal extension of ice resulting in extensive fracture and crevassing. As the ice slows at the base of the icefall, compression occurs, closing crevasses. Hooke (2005) points out that the onset of fracturing occurs at lower stresses in tension than in compression.

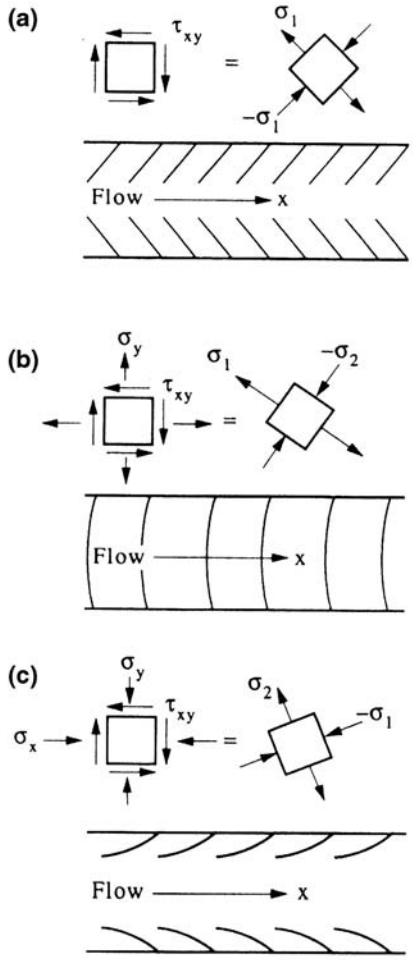

Figure 2.7: Crevasse patterns in a valley glacier. The diagrams at the top show shear stresses and longitudinal and transverse normal stresses at the glacier surface near the upper margin (left panels) and the resultant principal stresses (right panels). (a) Chevron Crevasses resulting from shear stress exerted by the walls. (b) Transverse Crevasses resulting from a combination of shear stress and longitudinal tensile stress (extending flow). (c) Splaying Crevasses due to a combination of shear stress and longitudinal compressive stress (compressive flow) (Benn & Evans, 1998).

Along with compressive and expansive flow, rotation and re-orientation of ice can influence the presence or absence of crevasses. On valley glaciers such as Fox Glacier, marginal crevasses tend to rotate because of the higher velocity near the centre caused by frictional drag of the valley walls. This rotation causes these marginal crevasses to close, unless the principal tensional stress direction also rotates (Nesje and Dahl, 2000).

Figure 2.8: Crevasses seen in the accumulation area of Fox Glacier. (Photo: M. Hambrey)

2.5.2 Crevasse Traces

Upon closing, crevasses may leave linear 'scars' (Figure 2.9) a few centimetres in width, known as crevasse traces (Hambrey, 1994). Traces usually appear as prominent blue ice layers formed by the freezing of water in the crevasse prior to closure, or as bubbly, white layers indicating a former snow-filled crevasse (Benn and Evans, 1998). Hambrey and Alean (2004) suggested crevasse traces as being veins of clear ice formed as a result of fracture and recrystallization of ice without separation of the two walls. Crevasse traces and tensional veins are usually initially close to vertical, but are rotated into other orientations by glacier flow (Benn and Evans, 1998). Usually less than 20 cm in width, traces can often be followed for tens of metres; cross-cutting other structures (Goodsell *et al.*, 2005[a]).

Figure 2.9: Crevasse traces in the lower ablation area of Fox Glacier. Field of view approximately five metres with ice flowing from right to left. (Photo: J Appleby)

2.5.3 Ogives

Ogives are one of the most enigmatic indicators of glacier flow and are of two main types: wave ogives and band ogives (Goodsell *et al.*, 2002). Ogives can be seen as arcuate bands or waves (Figure 2.10), with their apices pointing down-glacier, which develop in an icefall (Hambrey and Alean, 2004). They appear convex down-flow, with the amount of curvature increasing in each successive band, due to the greater velocity of the central part of the glacier compared with the margins (Benn and Evans, 1998). Alternating light and dark bands are called banded ogives or Forbes bands named after James Forbes who first suggested a method for their formation (Forbes, 1859). Each pair of bands (or one 'wave' and 'trough') is believed to represent a year's movement through an icefall (Nye, 1958; Hambrey and Alean, 2004), however, the reason for the observed colour difference in band ogives remains a highly contentious issue, with several hypotheses having been proposed for the genesis of both band and wave ogives by numerous authors (e.g. Washburn, 1935;

King and Lewis, 1961; Fisher, 1962; Posamentier, 1978; Waddington, 1986). Band ogive formation hypotheses include the stratification, depression, block-ridge, shearing, summer versus winter passage, and ice-type hypotheses, whilst Rhythmic compression and pressure waves, along with the ablation-plastic-stretching mechanism have been suggested to explain wave ogive formation (Goodsell *et al.*, 2002). Ice moves faster through an icefall than anywhere else, and so undergoes stretching and thinning as it accelerates into the upper part of the icefall. This stretching means a much larger surface area than equivalent volumes of ice in other parts of the glacier. As a result, ice flowing through an icefall during the summer will experience more ablation than ice else where and also collects more wind-blown and avalanched surficial debris. As the ice decelerates at the base of an icefall, it is compressed to form troughs of dark material, where the thinner, debris-rich ice forms into a narrower band. Wave crests or bands can be formed when ice travels through an icefall during the winter and collects excessive snow on the areas of increased thinning and stretching, which is then compressed as it is discharged from the icefall (Benn and Evans, 1998).

Figure 2.10: Ogives on Svinafellsjökull, southern Iceland. (Photo J. Alean)

2.5.4 Foliation

Foliation is the pervasive planar structure seen in almost all glaciers (Hambrey and Lawson, 2000) as alternating, discontinuous layers of bubble-rich and bubble-free white and blue ice (Figure 2.11). Foliation is found parallel or sub-parallel to surface ice movement (Goodsell *et al.*, 2005[a]), and alternate layers of course and fine-grained ice may also be seen (Paterson, 1994). Each layer may be only a few centimetres wide, but the pattern is repeated many times. Foliation is probably produced in regions of exceptionally high stress as a result of shear or compression (Hambrey and Alean, 2004) such as at the base of an icefall (Paterson, 1994). Banding is most prominent in englacial and supraglacial ice in ablation areas (Benn and Evans, 1998) but may also be seen deep in crevasse walls in the accumulation area (Hooke, 2005). Hooke and Huddleston (1978) suggest that most foliation develops from sedimentary stratification or crevasse traces which have undergone high strains and may have been rotated by glacier flow. Excessive rotation of this sedimentary stratification may result in folding.

Figure 2.11: Foliation observed in a crevasse wall in the ablation area of Fox Glacier. Field of view is approximately 0.5m. (Photo: J Appleby)

2.5.5 Folding

In the same way that flowing water experiences non-laminar, turbulent flow, so does glacial ice. Within this turbulent flow, layers of ice such as foliation may be deformed into curved forms known as folds (Figure 2.12) (Hambrey and Alean, 2004). Folding can occur to such an extent that in many valley glaciers, particularly if they are heavily crevassed, stratification is almost completely destroyed and may not be recognisable at all (Hambrey and Müller, 1978). Goodsell *et al.* (2005[a]) identified folds as isolated linear features which can be followed in one direction before turning through an angle (the fold hinge) and being followed in different directions. It has been suggested (Huddleston, 1976) that folding may occur when foliation has developed under a certain flow regime over a number of years, but then this regime changes causing a perturbation in flow sufficient to fold the ice. This change in regime maybe due to changes in channel geometry or differential flow (Hambrey and Lawson, 2000). As glaciers advance and retreat, and because they rest on irregular beds, folding is likely to be common (Hooke, 2005).

Figure 2.12: Fold at the base of the frontal cliff of Trapridge Glacier, Ice field Ranges, Yukon, Canada. (Photo: M. Hambrey)

2.6 Structural Mapping

Two main methods are employed to map the features and structures of a glacier surface. Remote-sensing techniques such as aerial photography or satellite imagery are often used to map areas of 10 to 1000 km^2 or greater (Hubbard and Glasser, 2005). Smaller scale areas usually less than $10km^2$ are more likely to be investigated through field surveying and field mapping. Glacial areas are often remote and may cover vast areas (e.g. Dowdeswell and Williams, 1997) and so great difficulty can be found in monitoring glaciers on a regular basis, with field observations and mapping often proving time consuming, expensive and even impossible (Hubbard and Glasser, 2005).

Remote-sensing instruments can be divided into imaging and non-imaging classes, with the imaging class including analogue and digital cameras, optical-mechanical scanners, passive microwave and active microwave sensors. The non-imaging class includes radar and laser altimetry, radio-echo sounders and gravimetres (Williams and Hall, 1998).

Platform	Instrument	Sensor/band	Spatial resolution	Swath width	Revisit period
Airplane	Camera	Photographs	Variable	Variable	Variable
Airplane	Scanner	AVIRIS			
Satellite	Landsat	RBV	79m	98km	16 days
		MSS	79m		
		TM	30m		
		ETM	15m		
Satellite	SPOT	PAN	10m	60km	26 days
		XL	20m		
Satellite	NOAA	AVHRR	1.1km	2400km	12 hours

Figure 2.13: Parametres of remote-sensing techniques commonly used in glaciological research (Gao and Liu, 2001; Hubbard and Glasser, 2005).

The method of remote sensing used is often determined by the aim of the mapping, and is limited by parametres such as spatial resolution and periodicity of repeat surveys (Figure 2.13), along with which data set or method is available for the particular study area.

2.6.1 Aerial Photography

According to Hubbard and Glasser (2005) aerial photography is a particularly powerful tool for landform identification, landform mapping, for mapping ice surface structures and for making glacier restitutions. The first known sequences of vertical aerial photographs in New Zealand were taken in 1937 and 1938 by New Zealand Aerial Mapping, Ltd. who concentrated on lowland areas until 1953 when a set of vertical aerial photographs was taken over the Franz Josef, Fox, Tasman, and Hooker glaciers (New Zealand Aerial Mapping, 2007). This was followed in 1955 by a set of oblique aerial photographs taken by the Royal New Zealand Air Force along both sides of the Southern Alps. Since these early surveys, systematic vertical aerial photographic flights have been made over the Southern Alps as part of a nationwide photogrammetric mapping program, which by the end of the 1960's had all of the glacierized areas of New Zealand photographed with many areas having been re-photographed since (Chinn, 2000). The most recent aerial photograph of Fox Glacier was taken by New Zealand Aerial Mapping in March 1985 (Figure 2.14).

Aerial photographs can be divided into two classes: vertical and oblique, as described by Dickinson (1969). Vertical aerial photographs are acquired by a camera pointing vertically downwards (usually within 2 or 3 degrees of vertical) producing a 'plan' of the ground. Oblique aerial photographs are acquired when the camera axis is pointed at an angle to the ground producing an elevation view similar to that from a high vantage point. Vertical dimensions are considerably stretched in aerial photographs, known as relief stretching, due to the exposure of stereo pairs at tens of metres apart in comparison with the average distance between the pupils of the human eyes at approximately 6 cm (Hubbard and Glasser, 2005).

Depending on resolution, aerial photographs can be used to study glacier dynamics at a variety of scales. For example, structural maps of glaciers at a valley scale can be produced using overlapping vertical aerial photographs (Hubbard and Glasser, 2005), whilst individual structures can be studied on high resolution enlargements (e.g. Hambrey and Müller, 1978). Aerial photographs have proven particularly useful for monitoring of glacial

advance and retreat in New Zealand, being used extensively for snow line surveys produced annually by the National Institute of Water and Atmosphere (NIWA).

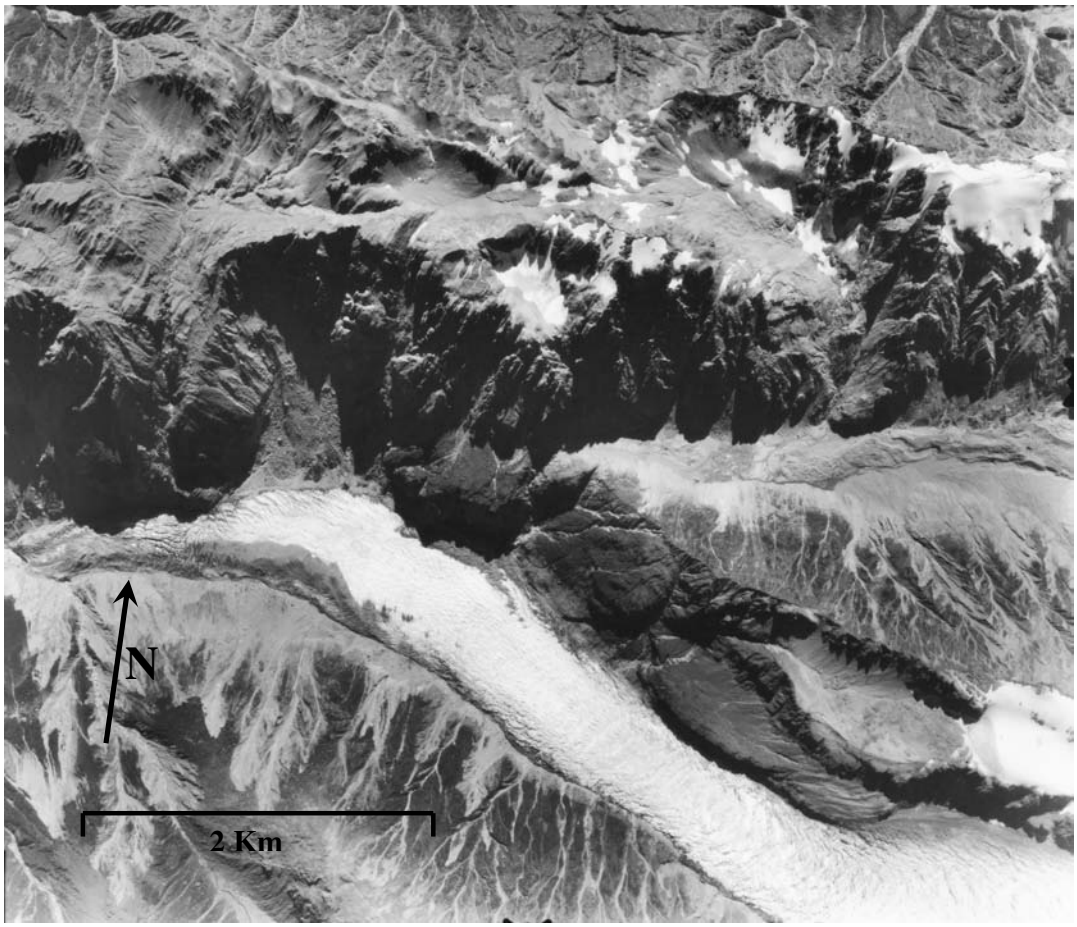

Figure 2.14: Section of aerial photograph SN8478 G13 taken by New Zealand Aerial Mapping Limited during a Cook River-Franz Josef pass on 27th March 1985.

2.6.2 Satellite Imagery

Aerial photography provides detailed visualization of surface morphology and is still used extensively for fine resolution landform mapping (Jansson, 2005). However, the analysis of landform patterns, as well as individual landforms, requires the study of large areas (e.g. Hambrey and Dowdeswell, 1994) which generates high costs, a result of flying time and photogrammetric processing. High quality field mapping and aerial photographic interpretation are relatively expensive methods. In contrast, satellite imagery has large aerial coverage, relatively low cost and enables relatively rapid rates of mapping (Punkari,

1982. Clark, 1997). It has also been suggested that along with the spatial extent of snow and ice cover which can also be determined with aerial photography, satellite imagery may be used to determine snow and ice density and moisture content (Thomas *et al.*, 1978).

All of New Zealand's glacierized areas are included in existing Landsat images (Figure 2.15), but not all of the images are usable for glacial observations. The two requisites for an optimum usable image are no cloud cover and an image acquired at the time of minimum snow cover (late summer). The major limiting factor of satellite imagery such as the Landsat image series of New Zealand for glaciological monitoring and structural analysis is the effective spatial resolution (Chinn, 2000). Along with this, many New Zealand glaciers are completely covered in debris. This is certainly true of glaciers on the eastern side of the Main Divide, upon which surface features are almost completely obscured by supraglacial material. This limiting factor also applies to the use of aerial photography mapping techniques.

Despite the large number of techniques involved and a general awareness and agreement of their benefits and limitations, there has been no direct comparison between the individual methodologies and techniques (Smith *et al.*, 2006) available to researchers interested in the remote sensing and structural mapping of glaciated and glacierized areas.

2.6.3 Field Observations

The collection of data in the field is often a major component of all glacial research projects. Field research can involve the mapping, measuring and monitoring of landforms and processes (Hubbard and Glasser, 2005). Field observation usually involves the identification of prominent features, notably primary stratification, longitudinal foliation (e.g. Carassa, 1992), crevasses and crevasse traces (e.g. Allen *et al.*, 1960; Hambrey and Müller, 1978; Lawson *et al.*, 1994) and ogives (e.g. Goodsell *et al.*, 2002).

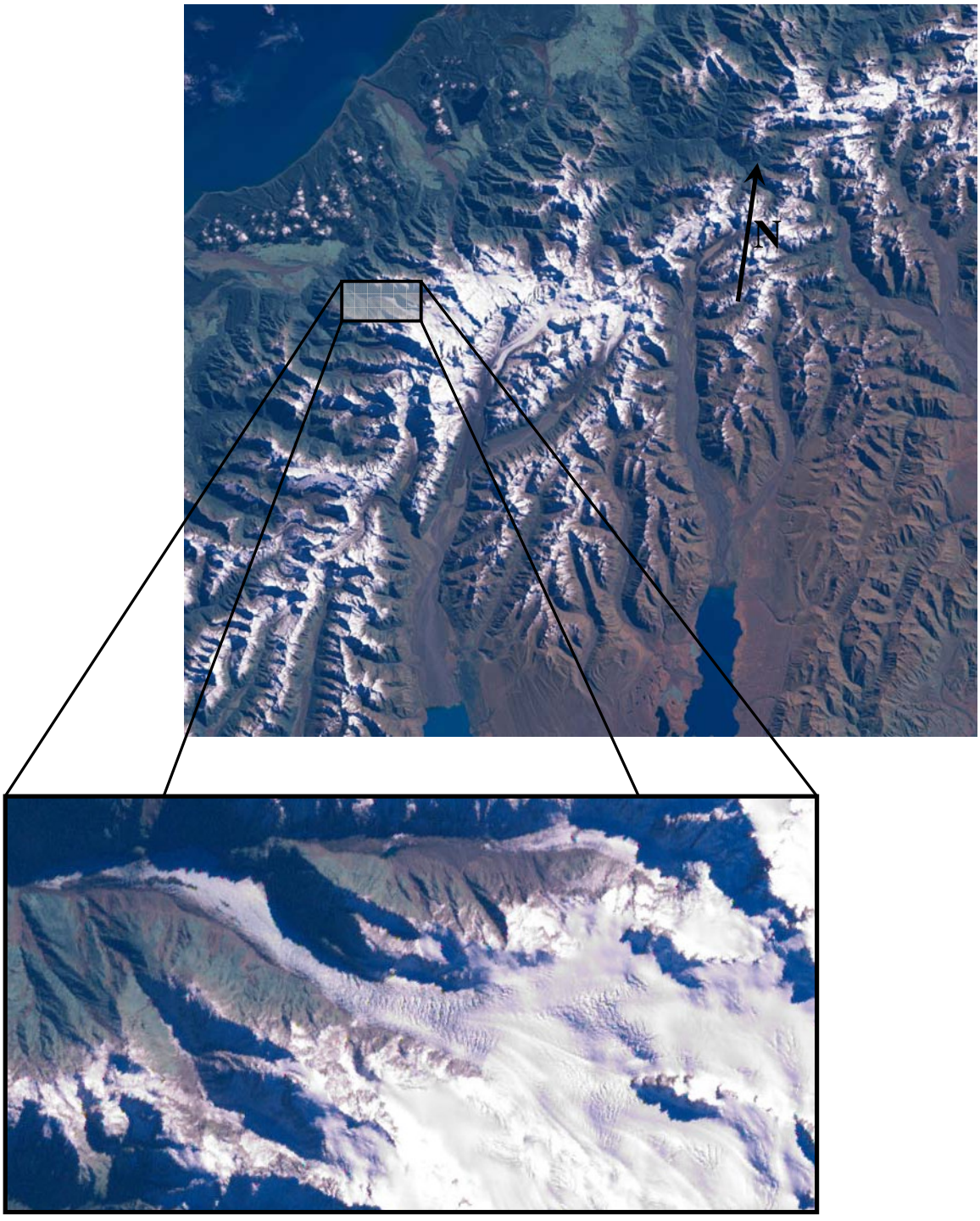

Figure 2.15: Landsat 7 image of *Aoraki*/ Mount Cook area, showing the extent of snow and ice cover during the New Zealand summer, along with an enlargement showing available detail of Fox Glacier at the spatial resolution produced by a pan sharpened ETM+ sensor, (NASA, 2001).

Landform recognition and interpretation is often a subjective process, and can depend largely on the experience of the observer in glacial environments. For this reason a good base knowledge of structure recognition should be gained prior to undertaking fieldwork from such sources as Hambrey and Müller (1978), Lawson *et al.* (1994), Glasser *et al.* (1998), Hambrey and Lawson (2000), and Goodsell *et al.* (2005[a]).

With several thousand individual structures present on the surface of a glacier, it is more convenient to take representative measurements of features along transect lines. An appropriate technique is to identify, map and record the size and orientation of structures at each sample point, with data being collected using the conventional strike dip technique used in structural geology (Goodsell *et al.*, 2005[a]). The location of each feature can be logged using a Global Positioning System, and then transposed onto a base map once back from the field.

The creation of maps from field-acquired data was discussed at length by Blachut and Müller (1966), who considered scale, contour interval, shading, delineation of the glacierized area, and symbols. Ewing and Marcus (1966) suggested the need for standardised symbols in glacial cartography. The most common method currently in use consists of a 'structural level' of S_0, S_1, S_2, etc. with primary stratification starting at the S_o level.

2.7 Aims and Objectives of Research

It is apparent that very little work has been done on New Zealand's glaciers with regard to structural mapping or stress and strain measurements. An absence of available published data suggests a lack of major studies looking at structural glaciology, stress and strain measurements, or a combination and analysis of both. Almost all structural glaciological work has been carried out in Europe, North America, and the Polar Regions, rather than temperate, mid-latitude glaciers.

Even more apparent is the dearth of research on Fox Glacier, when compared with other glaciers and glaciated areas of New Zealand. The research that has been undertaken and

published (e.g. Wilson, 1896; Speight, 1935; Gunn, 1964; Purdie, 2005) are more concerned with mass balance, velocity and ablation studies. The results of these studies suggest that Fox Glacier is highly dynamic. How this dynamism is reflected in the glaciological process mechanisms of Fox Glacier is unknown. Research (Purdie *et al.*, 2007) suggests that Fox Glacier responds rapidly (9 years) to a change in climatic input, with El Nino-Southern Oscillation (ENSO) a key factor causing its advance and retreat phases.

These observations, coupled with the previous literature review have created a number of research questions:

- What structures are present on the surface of the Fox Glacier?
- What processes are occurring to produce these structures?
- What strain rates are present on the surface of the Fox Glacier?
- How do these strain rates vary over the surface of the Fox Glacier?
- How do these strain rates relate to the observed processes and structures?

From these questions, objectives can be developed for the research that will be carried out on Fox Glacier.

The specific objectives of this study are to:

1. produce a structural map of the surface of the lower part of Fox Glacier;
2. determine the spatial variation of strain rates within the measured array on the glacier surface;
3. identify relationships between the structures observed on the surface of the glacier and the measured strain rates.

2.8 Hypothesis

In scientific study, it is important to develop a hypothesis for research that will propose an outcome based on the information gained from previous research and a knowledge of the subject area. This deductive reasoning should assert a causal relationship between the variables to be considered in the research (Johnson-Laird, 1999). Considering this

reasoning, along with the research questions and objectives proposed, the research hypothesis is:

- Strain rates will be relatively higher in areas exhibiting a more disturbed and complex ice surface, demonstrated by the presence of features such as (but not limited to) crevasses, folds and rotation of primary stratification.

This hypothesis about a possible association does not stipulate the cause and effect *per se*, but states that one variable is related to another; in this case strain is related to structure. For the purposes of this research however, it can be assumed that a cause and effect relationship does occur, in that structure is caused by strain rate, strain rate being a manifestation of the stress conditions in the ice.

Chapter 3: Methodology of Research

3.1 Structural Mapping

3.1.1 Introduction

The surface structure of the Fox Glacier was identified and mapped using two techniques; i) analysis of aerial photographs and ii) observations made in the field. Both techniques are described in this methods chapter, along with the methods of displaying this data.

3.1.2 Aerial Photography

A structural map was produced from the observation of two overlapping vertical aerial photographs (Figure 3.1) taken on 27th March 1985 by New Zealand Aerial Mapping Limited. March is near the end of the summer ablation season in New Zealand's Southern Alps, and so the maximum amount of snow-free ice was exposed.

The observed structures were recognised and recorded according to their orientation, size, relation to other structures (e.g. cross-cutting), and location on the glaciers surface, using the criteria as described by Goodsell *et al.* (2005[a]) (Table 3.2). The photographs were scanned into a digital format and then line tracings were made on the digital image to produce a line map of the glacier surface.

3.1.2.1 Use of Aerial Photographs

Aerial photograph stereo pairs were viewed through a *Wild Heerbrugg* mirror stereoscope using the standard method, overlapping two photographs covering the same area, so that features on each matched and appeared in three dimensions (Dickinson, 1969).

When using stereoscopes as highlighted by Smith *et al*. (2006), it is important to follow a few simple rules:

- The photographs must be a stereo-pair; that is to say, they must contain the same area taken from two different viewpoints. Normally they are two successive exposures from a single run;

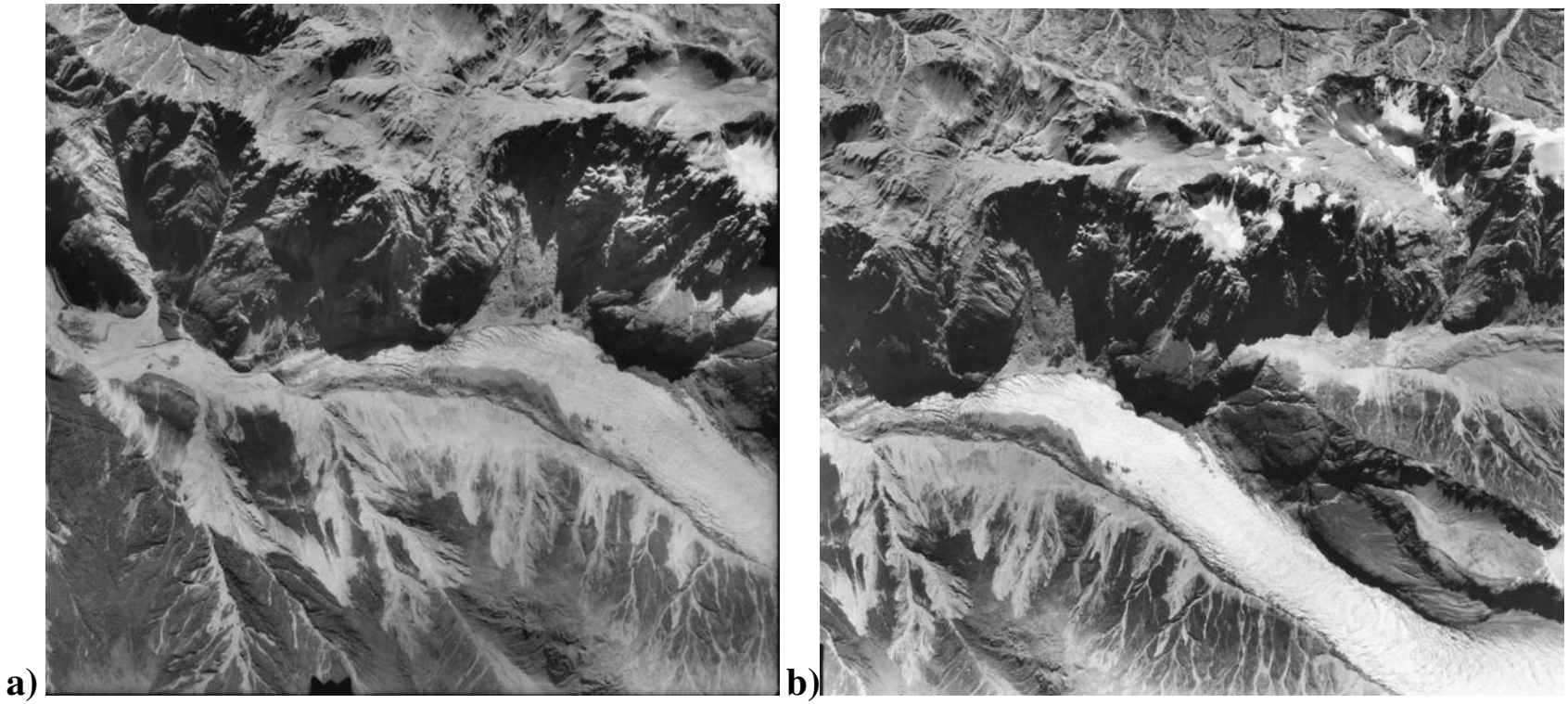

Figure 3.1: Aerial photographs SN 8478 G/12 (a), and SN 8478 G/13 (b), taken by New Zealand Aerial Mapping Limited on Wednesday 27th March 1985.

Table 3.1: The observation of structures from aerial photographs and field observations (Goodsell *et al*, 2005[a]).

Nongenetic name	Interpretation	Identification on aerial photograph	Identification in the field
Systematic layering	Primary stratification	Parallel layering usually found in the upper glacier basin, sometimes parallel to snowline.	Thin darker layers between thicker lighter layers of firn often found parallel to receding snowline in late summer.
Discontinuities in layering	Unconformity	A break in the normal systematic layering of the primary stratification.	Difficult to observe close-up. Can be identified as a break in the normal layering when viewed from a distance.
Structural discontinuity	Flow unit boundary	A junction that seperates structures rotated in one orientation from structures rotated in a different orientation.	Difficult to identify close-up, but can sometimes be recognised by structures oriented at different angles on either side of an area of intense foliation.
Crevasses	Crevasses	Either as straight white lines (snow filled) or straight dark lines (non-snow filled or water filled), with cross-cut features.	A crack with a visible opening.
Transverse/arcuate structures	Crevasse traces	First found in areas of crevassing as straight dark lines, can be followed downglacier as deforming dark lines, cross-cutting previously formed structures.	Linear or arcuate features, usually <20cm width, which can be followed lterally for tens of meters.
Steeply dipping longitudinal foliation	Longitudinal foliation	Long linear pervasive layered structure parallel to ice movement, which can be traced discontinuously for several hundred meters.	Alternating, discontinuous layers of bubble-rich and bubble-free white and blue ice, parallel or sub-parallel to surface ice movement.
Folding	Folding	Large-scale folding is identified as curves in linear features which do not follow surface topography.	Isolated folds are identified by linear features which can be followed in one direction before turning through and angle and being followed in a different direction.
Prominent arcuate structures near snout	Thrusts	Not observed on aerial photographs.	A step in the glacier surface, parallel to crevasse traces near the snout of the glacier. Displacement of marker horizons. Associated with basal derived debris.

- They must be in their correct relative positions, that is, so that the right eye looks at the photograph taken from the right-hand position;
- Shadows should always fall downwards or towards the viewer. If this is not done, the brain, which is used to 'seeing' shadows falling this way, will be deceived into 'seeing' inverted relief (Dickinson, 1969).

To correctly map features from an aerial photograph, it is important to know an approximate scale for the photograph. The scale or representative fraction (RF) of the aerial photographs has been calculated as approximately 1:25000 using the following method,

$$RF = \frac{\text{Photographic distance between two points}}{\text{Ground distance between same points}}$$

It is important to remember, when identifying features from aerial photographs that the two images are taken from a much greater distance than the distance between our eyes, giving a much exaggerated vertical scale. Fortunately this exaggeration is uniform across most of the image and so relative height difference between features remains unchanged (Dickinson, 1969; Holz, 1973; Amir, 2005).

3.1.3 Field Observation

As with the aerial photography, structures were recorded and recognised according to their orientation, size, relation to other structures, and location on the glaciers surface, using criteria as described by Goodsell *et al* (2005[a]), Barnes (1997) and McClay (1997). Transect lines were walked from one side of the glacier to the other repeatedly along the length of the study area, comprising the lower four kilometres of Fox Glacier (Figure 3.2) with large-scale features such as crevasses being recorded on a predefined outline of the Fox Glacier, produced from tracings of a topographical map. The locations of smaller features were recorded using a hand-held Garmin Global Positioning System (GPS) unit and these features were then transposed onto the base map. Transect lines were walked in approximately straight lines to ensure uniformity of ground cover, although this was not

always possible due to topographical constraints of the glacier surface including crevassing and moulins.

Features such as primary stratification, foliation, and crevasse traces are mapped using techniques adopted from structural geology, namely strike and dip orientation (Figure 3.2). Strike represents the orientation in degrees from North, across the plane of the feature, with dip perpendicular to the strike line representing the angle down-plane in degrees from the vertical (McClay, 1997). Commonly referred to as 'the right hand rule', strike and dip can be quickly identified in the field with strike following the direction in which the index finger points, whilst dip is in the direction of the thumb (Barnes, 1997).

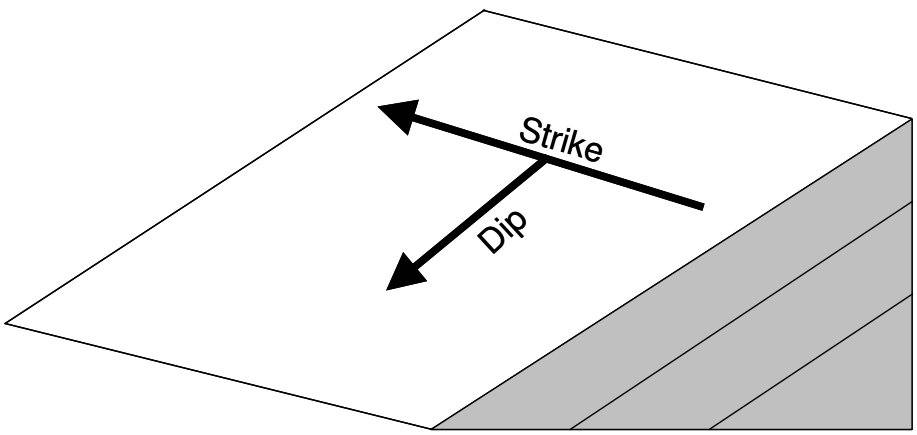

Figure 3.2: Strike and dip technique of measuring orientation of features such as foliation, primary stratification and crevasse traces. Strike measures the orientation of the across-plane direction in degrees from North, with the dip representing the down-plane direction measured in degrees from vertical.

Strike and dip data is conventionally displayed using a Schmidt equal-area stereonet polar plot (Figure 3.3). The stereonet allows data to be viewed in three dimensions by plotting strike orientation in degrees from North, shown at the top of the circle, and dip angle in degrees from horizontal, where 90° is represented by the centre of the circle, and 0° is at the outside of the circle.

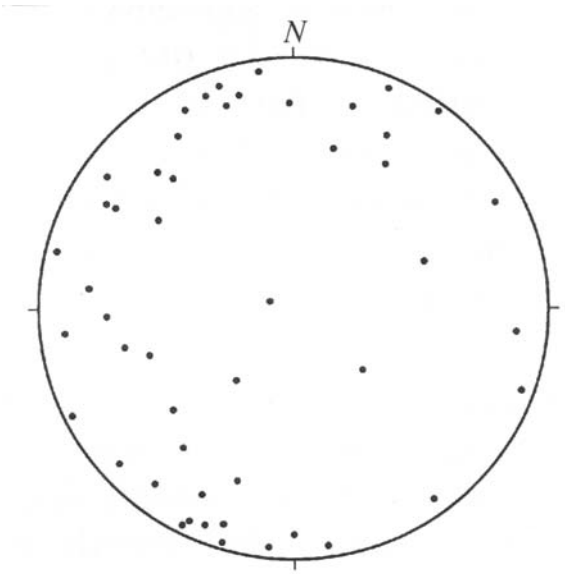

Figure 3.3: Schmidt equal-area stereonet showing three dimensional orientation of strike and dip of structural features. Each point represents a single feature. The centre of the circle represents a dip of 90° whilst the circle represents 0°. The orientation of the strike is represented as an angle of *x*° from North (Hubbard and Glasser, 2005).

3.2 Strain and Deformation

Calculation of strain rates and cumulative strain was based on the changing dimensions of polygons as described by Nye (1959), Wu and Christensen (1964), Milnes and Hambrey (1976), Vaughan (1993), and Goodsell *et al.* (2005[a]). For this research, triangles were used to avoid complexity whilst still allowing accurate measurements of strain.

Three transects A; B; and C (Figure 3.4) were positioned across the width of the glacier with one above the first icefall, one below the first icefall, and one as close to the snout as possible. The transects were constructed of 25mm Ø plastic ablation stakes (Figure 3.5), drilled into the ice surface using a Kovac ice auger (Figure 3.6). The positions of each of the stakes was recorded using a Trimble R8 Real-Time-Kinematic (RTK) Global Positioning System (Figure 3.7) at the start of the study period in January 2007, and again at the end of the study period in February 2007.

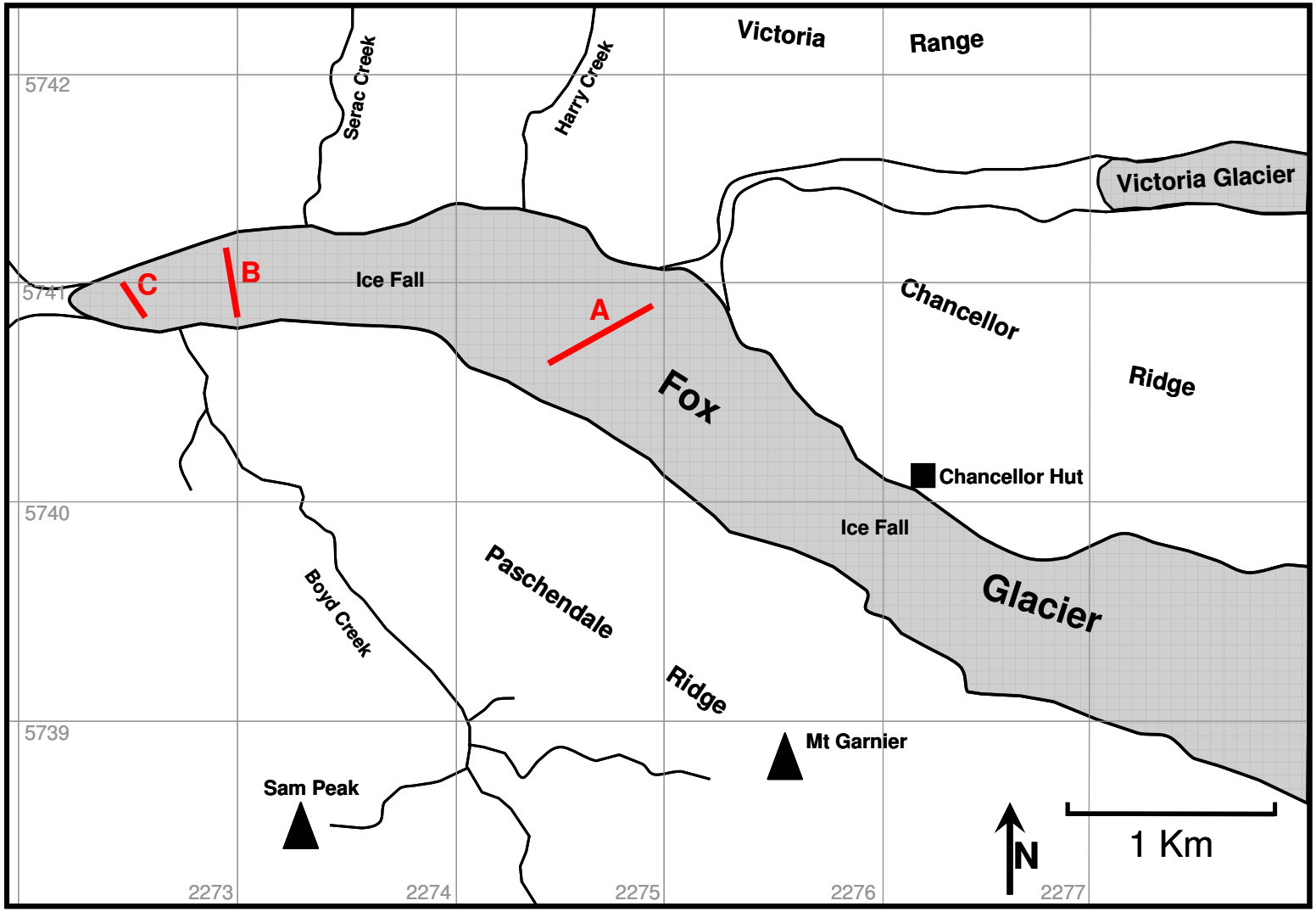

Figure 3.4: Location of stake transects on lower Fox Glacier used to measure deformation and strain rates of surface ice.

Figure 3.5: Ablation Stake used in the stake network transects. (Photo: J. Appleby)

Figure 3.6: Drilling ablation stake holes using a Kovac ice auger. (Photo: M. Brook)

Figure 3.7: Trimble R8 Differential Real-Time-Kinematic GPS rover unit being used on the lower Fox Glacier. (Photo: J. Appleby)

3.2.1 Determining Deformation of Polygons

In an ideal situation, deformation polygons should be formed by perfect squares (or diamonds depending on orientation) (Figure 3.8) with a *y*-axis representing the down-glacier direction, and an *x*-axis representing the across-glacier direction (Nye, 1959; Hambrey and Müller, 1978). A *z*-axis can be used to represent a component normal to the glaciers surface (Wu and Christensen, 1964) however, this research is only concerned with deformation measurements in two dimensions and so the z-axis has been dispensed with.

The distance *d* between two points in a plane of known co-ordinates (i.e. point A = (x_1, y_1) and point B = (x_2, y_2)) is given by

$$d = \sqrt{(x_2-x_1)^2 + (y_2-y_1)^2} \quad . \tag{3.1}$$

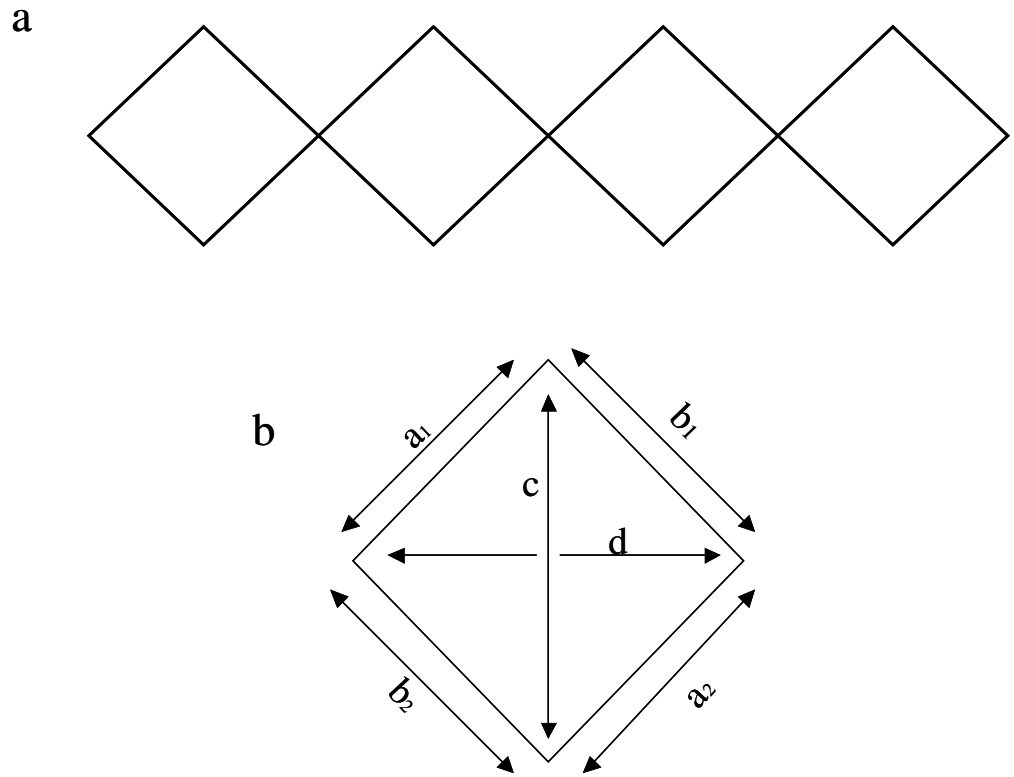

Figure 3.8: Idealised pattern of transect polygons to measure deformation of ice surface with each point of the diamonds being an ablation stake (a), and averaged components of deformation vectors (b) with *c* representing the down-valley *y*-axis.

Equation 3.1 was used to determine the initial distance between two ablation stakes at the start of the study period in early January and then again at the end of the study period in late February, allowing the deformation in shape of the triangles to be calculated.

Over greater distances, for example ice caps or ice sheets, the haversine formula can be used to determine distance between two points whilst taking into account the curvature of the Earth's surface as described by Sinnott (1984). For two points with latitudes ϕ_1 and ϕ_2 respectively and longitudinal separation $\Delta\lambda$, where angles are in radians on the surface of a sphere (e.g. the Earth) of radius *R*, the distance *d* between them is related to their locations by the formula

$$\text{haversine}\left(\frac{d}{R}\right) = \text{haversine}(\Delta\phi) + \cos(\phi_1)\cos(\phi_2)\text{haversine}\,(\Delta\lambda),$$

(3.2)

Where $\Delta\text{ø} = \text{ø}1 - \text{ø}2$. Let h denote $\text{haversine}\left(\frac{d}{R}\right)$. Distance d is given by

$$d = R\text{haversine}^{-1}(h) = 2R\arcsin\left(\sqrt{h}\right).$$

(3.3)

Although intended for greater distances, the haversine formula is still accurate for the distances involved in mountain and valley glaciology, but the curvature of the Earth will be insignificant on this scale. The localised topography of the ice will negate any influence the curvature of the plane has.

Measurements made of distance between the stakes of the diamonds will yield six values for change in distance $\acute{\varepsilon}$. Averaging the intervals a_1 & a_2, and b_1 & b_2 then reduces these six measurements into four, which give us values of έ corresponding to the directions $\theta = 0$, 45, 90, and 135° relative to the centre point of the diamond (Figure 3.9).

According to Nye (1959) an immediate check on consistency comes from the fact that theoretically

$$\acute{\varepsilon}_0 + \acute{\varepsilon}_{90} = \acute{\varepsilon}_{45} + \acute{\varepsilon}_{135}.$$

(3.4)

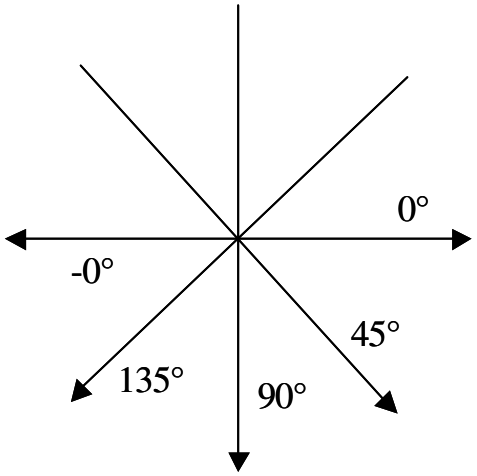

Figure 3.9: Angle θ of averaged change in distance $\acute{\varepsilon}$ relative to the centre of a diamond. The average of a_1 & a_2 produces a change in the 135° direction, b_1 & b_2 in the 45° direction and c in the 90° direction, whilst any change in d is shown in the 0° direction.

3.2.2 Determining Strain Rate of Surface Ice

The values of three strain rate components $\acute{\varepsilon}_x$, $\acute{\varepsilon}_y$, and $\acute{\varepsilon}_{xy}$ can be determined from the four distance $\acute{\varepsilon}$ measurement using the simplified equation system

$$\begin{aligned}
\acute{\varepsilon}_x &= -\frac{1}{4}\acute{\varepsilon}_0 + \frac{1}{4}\acute{\varepsilon}_{45} + \frac{1}{4}\acute{\varepsilon}_{90} + \frac{1}{4}\acute{\varepsilon}_{135} \\
\acute{\varepsilon}_{xy} &= \frac{1}{2}\acute{\varepsilon}_{45} - \frac{1}{2}\acute{\varepsilon}_{135} \\
\acute{\varepsilon}_y &= \frac{3}{4}\acute{\varepsilon}_0 + \frac{1}{4}\acute{\varepsilon}_{45} - \frac{1}{4}\acute{\varepsilon}_{90} + \frac{1}{4}\acute{\varepsilon}_{135} .
\end{aligned} \tag{3.5}$$

The full method of reaching this system using four simultaneous linear equations is described by Nye (1957), and need not be repeated in this methods section.

The measured strain rates are simply determined by comparing these $\acute{\varepsilon}$ values with a certain unit of time, in this case the study period from January to February, 2007. Once these strain

components are known, the magnitude and direction of the principal strain rate can be graphed using Mohr's Circles, discussed further in 3.2.4. The major principle strains can be denoted by $\acute{\varepsilon}_1$ and $\acute{\varepsilon}_3$, with the angle between the y-axis and the $\acute{\varepsilon}_1$ vector being denoted by θ. Assuming there has been no area change of the diamond, an intermediate strain $\acute{\varepsilon}_2$ can be determined by means of the relationship

$$\acute{\varepsilon}_1 + \acute{\varepsilon}_2 + \acute{\varepsilon}_3 = 0 \ . \tag{3.6}$$

3.2.3 Determining Stress of Surface Ice

An averaged strain rate can be derived from the principal strains, and then used to determine the stresses acting on the surface ice. Stresses can be calculated from the averaged strain rate by using the stress and strain-rate relationship obtained by Glen (1955), as discussed in 2.2.4, namely

$$\acute{\varepsilon} = B\tau^n \ . \tag{3.7}$$

Where $\acute{\varepsilon}$ and τ are given by

$$\acute{\varepsilon}^2 = \frac{1}{2}\acute{\varepsilon}_{ij}\acute{\varepsilon}_{ij}$$

and

$$\tau^2 = \frac{1}{2}\sigma'_{ij}\sigma'_{ij} \quad , \tag{3.8}$$

as defined by Nye (1959), whilst n = 4.2 and B = 0.148 yr^{-1} bar^{-n}. Here $\acute{\varepsilon}_{ij}$ and σ'_{ij} are the components of the strain-rate and stress deviator tensors (Wu and Christensen, 1964).

A stress deviator can then be obtained from the relationship

$$\sigma'_1 = \frac{\tau}{\varepsilon}\acute{\varepsilon}_1 \quad \sigma'_2 = \frac{\tau}{\varepsilon}\acute{\varepsilon}_2 \quad \sigma'_3 = \frac{\tau}{\varepsilon}\acute{\varepsilon}_3 \quad , \tag{3.9}$$

and the principal stresses are given by

$$\sigma_1 = 2\sigma'_1 + \sigma'_3 \qquad \sigma_2 = 0 \qquad \sigma_3 = \sigma'_1 + 2\sigma'_3 \quad . \tag{3.10}$$

If the principal stresses calculated are not in the *x* and *y* directions, the stresses σ_x, σ_y, and τ_{xy} can be calculated graphically using a Mohr's Circle.

3.2.4 Graphical Representation of Stress, Strain & Deformation

The relative positions of the stakes in each transect at the beginning of the study period and the end can be graphed by simply inputting the co-ordinates to an Excel file. This produces a transect pattern as for part *a*, Figure 3.9. Any change in geometry between the primary and secondary transects can then easily be seen.

Stress data is plotted on two-dimensional stereonet rose diagrams (Figure 3.10), which are effectively circular histograms, summarising stress orientation experienced by a single point, in groups or intervals. The stereonet plots are produced using Georient, a graphical software package available for download on the Internet (Appendix 2).

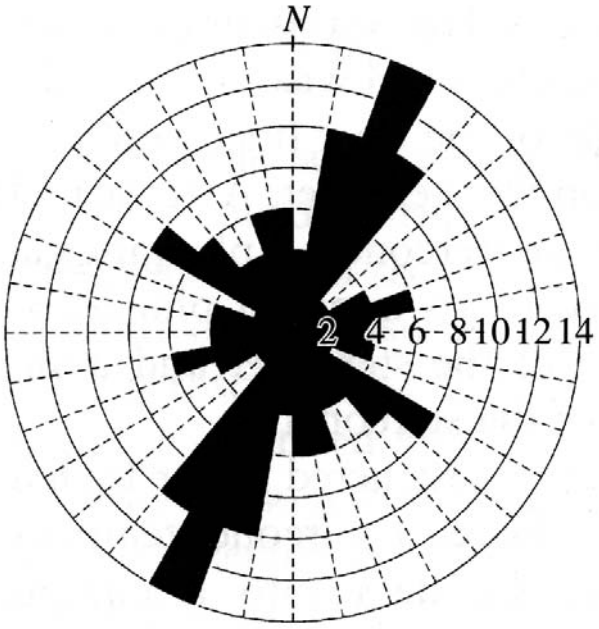

Figure 3.10: Example of a stereonet rose diagram showing two-dimensional magnitude and orientation of stresses experienced on a plane (Hubbard and Glasser, 2005).

In addition to rose diagrams, the stress across a specified plane (in this case the surface of the ice) can be represented by a stress vector which can be resolved into two individual stresses; σ_n, the normal stress acting perpendicular to the plane, and τ, the shear stress acting parallel to the plane. Given these principal stresses, along with the angle θ of the plane, a Mohr's Circle (Figure 3.11) can be plotted showing the stress vector acting across that plane (Engelder and Marshak, 1998). Since Mohr's circle represents the stress-transformation equations graphically; it can be used to determine the normal and shear stress components acting on an arbitrary plane (Hibbeler, 1997). Mohr's Circles can also be used to determine the magnitude and direction of the principle strain rates experienced on an *x-y* plane.

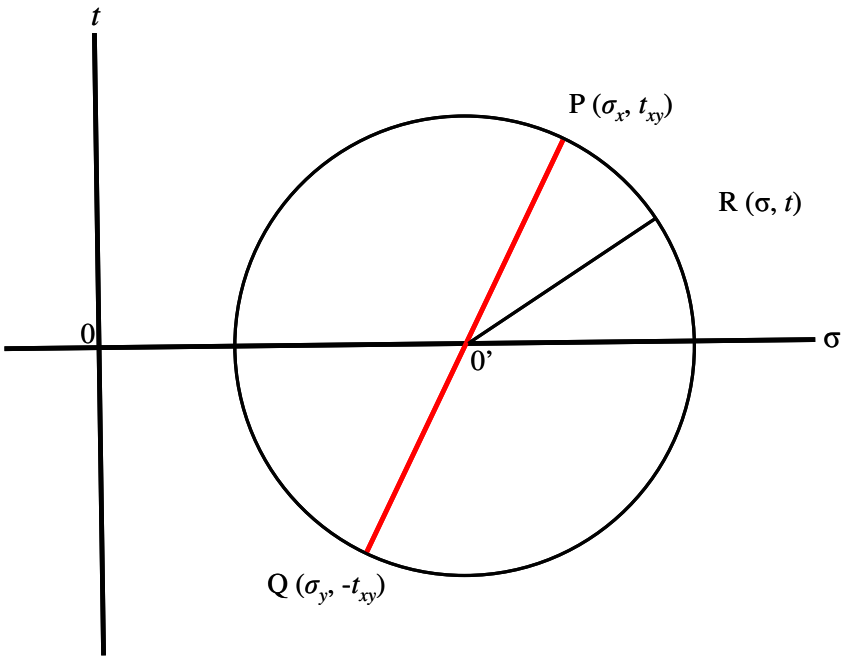

Figure 3.11: Example of a Mohr's Circle of stress; points P and Q correspond to the stress states (σ_x, τ_{xy}) and (σ_y, $-\tau_{xy}$) respectively, and are diametrically opposite. The state of stress on a plane inclined at an angle θ to 0_y is given by point *R*, with maximum stress denoted by the radius of the circle (Case *et al.*, 1999).

Most research uses strain rate as a standard method of quantifying the deformation of ice. For this reason, and for the ease of comparison between this study and previous research, this study will determine strain rate and omit measurements of stress.

3.3 Surficial Debris Clast Analysis

Transport of material through the glacial system imparts characteristic signals on the morphology or form of individual clasts which give information about the likely mode of transport of the material (Boulton, 1978; Benn and Ballantyne, 1994). According to Boulton (1978), transport of material can be divided into active or passive transport. Active transport takes place at the glacier sole, and involves the interaction between particles or between particles and immobile objects, resulting in progressive debris modification through abrasion and crushing. Debris carried in an englacial or supraglacial position can be considered as undergoing passive transport.

Research (e.g. Vere and Benn, 1989; Benn and Ballantyne, 1994; Kirkbride and Spedding, 1996) has suggested that it is possible to determine the type of transport a clast of material has undergone. Surficial material has been classified on Fox Glacier according to C_{40} index (percentage of clasts with a c:a ratio ≤0.4) (Figure 3.12) and RA index (percentage of angular and very angular clasts) (Table 3.2) according to Benn and Ballantyne (1994).

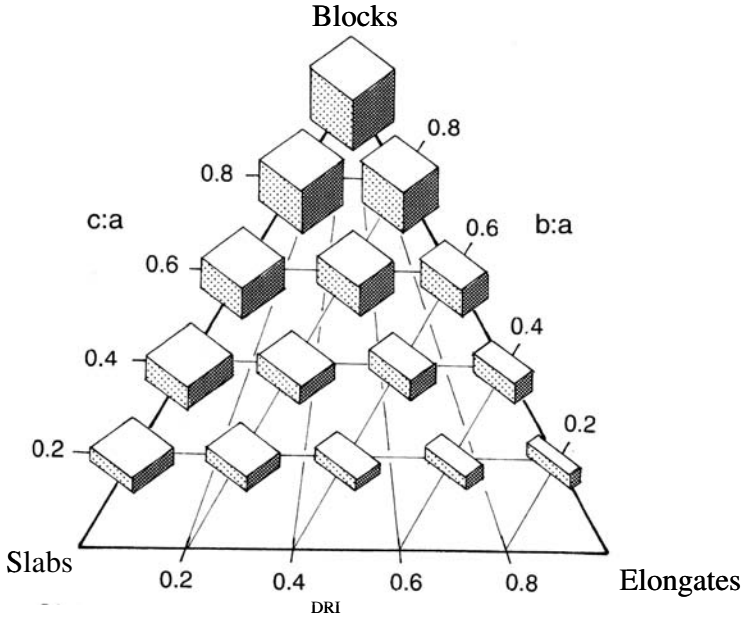

Figure 3.12: The continuum of particle shape, showing variation between blocks, elongates and slabs. The diagram is scaled using ratios between the long (a), intermediate (b), and short (c) axes. DRI is the 'disk-rod index', equal to (a-b)/(a-c) (Benn and Ballantyne, 1994).

Table 3.2: Classification of clast roundness. The percentage of angular and very angular clasts in a sample gives an RA index value, identifying the proportion of a sample that has not been edge-rounded by transport (Benn and Ballantyne, 1994).

Class	Description
Very Angular (VA)	Edges and faces unworn; sharp, delicate protuberances
Angular (A)	Edges and faces worn
Sub Angular (SA)	Faces unworn, edges worn
Sub Rounded (SR)	Edges and faces worn but clearly distinguishable
Rounded (R)	Edges and faces worn and barely distinguishable
Well Rounded (WR)	No edges or faces distinguishable

Chapter 4: Results

4.1 Glacier Structure

Aerial photography and field observations have been used to identify, quantify and map surface structures of the lower Fox Glacier. Field observations were undertaken by walking transects across the surface of the glacier (Figure 4.1), in approximately straight lines, where surface topography would allow it.

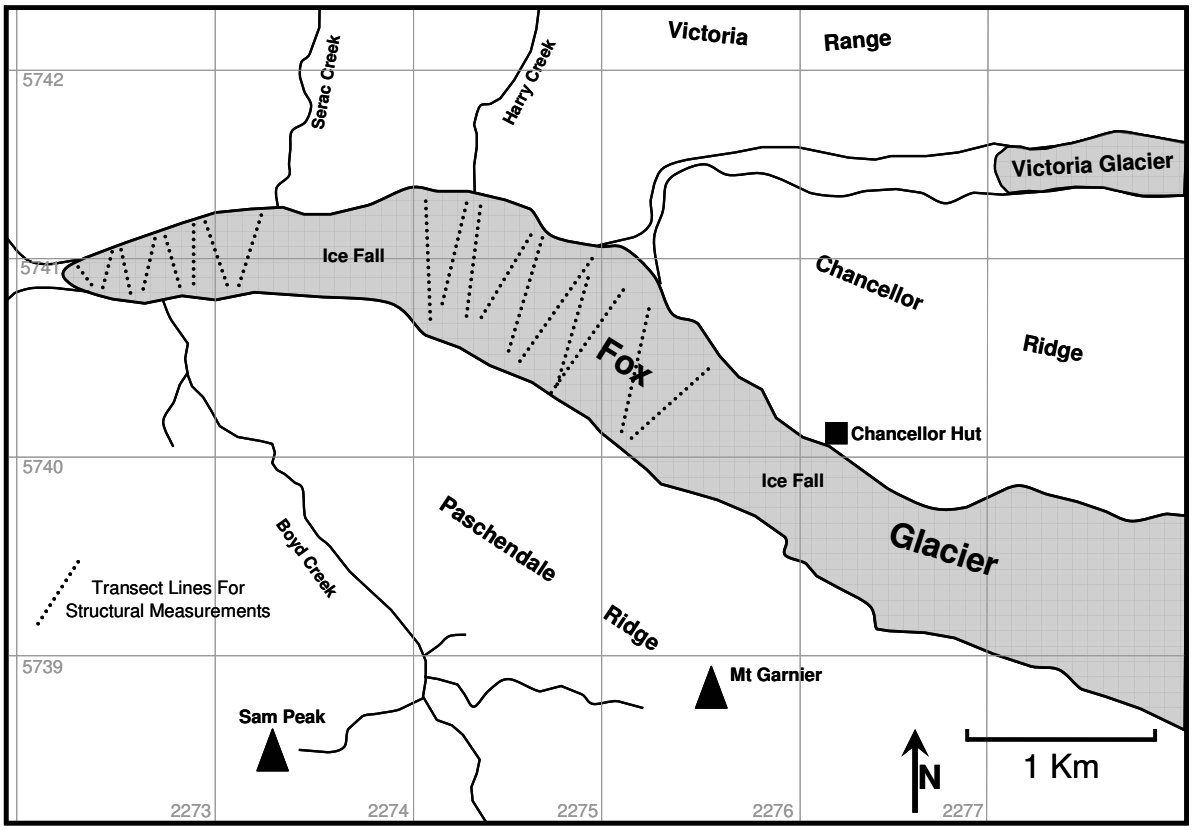

Figure 4.1: Location map of Fox Glacier showing the region used for structural mapping. Approximate transect lines along which structural measurements were taken are denoted by the dashed lines.

4.1.1 Aerial Photography

Using stereo-aerial photographs SN 8478 G/12 and G/13 (Figure 4.2) it has been possible to create a structural map of the surface of Fox Glacier from 1985 (Figure 4.3), following the criteria outlined in Table 3.1. Large-scale structures such as crevasses have been identified using a three dimensional image produced from a stereoscope in the areas not obscured by shadow. However, the spatial resolution of the aerial photograph is not sufficient to identify smaller-scale features, such as foliation and folding, and so field observations have also been used.

Figure 4.2: Composite of stereo-aerial photographs SN 8478 G/12 & G/13. Scale of photograph 1:25000 (New Zealand Aerial Mapping Limited, 1985).

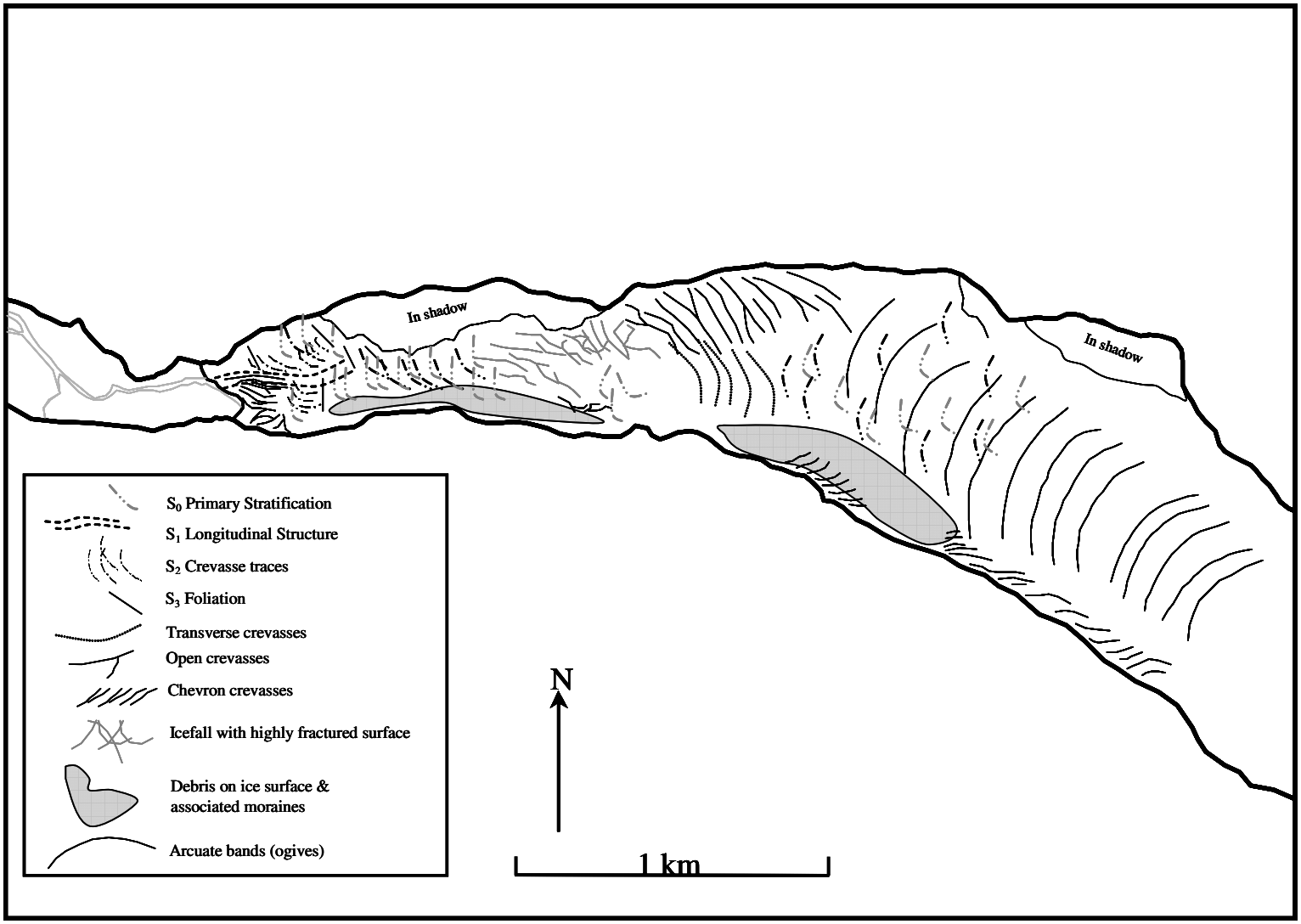

Figure 4.3: Structural glaciological interpretation of the glacier surface features visible on aerial photographs.

4.1.2 Field Observation

4.1.2.1 Introduction

Field observations have identified many of the features typical of a valley glacier (Figure 4.4) (Table, including structures composed of the glacial ice and some composed of a combination of ice and rock material such as supraglacial moraine or englacial debris. It is possible to identify trends in the field observations where certain structures appear more often in certain areas than other structures.

Structurally, it appears the study area can be divided into two distinct domains. The upper part of the study area above the first icefall has a low gradient (<5°), continuously gentle topography (Figure 4.5), with the surface occasionally broken by crevasses, moulins and 'slushy swamp' areas of accumulating supraglacial meltwater. The lower study area between the first icefall and the snout is of a much steeper gradient (15-20°), with a more complex surface topography (Figure 4.6). Generally this area is characterized by a 'ridge and trough' pattern, which can be seen across the whole width of the glacier. A summary of the features found in each of the two domains is presented in Table 4.1.

Table 4.1: Summary of features found in upper and lower parts of the study area.

Feature	Upper Domain	Lower Domain
Primary Stratification	●	●
Crevasse Traces	●	●
Foliation	●	●
Crevasses	●	●
Folding	●	
Ridge & Trough		●
Moulins	●	●
Supraglacial Water Storage	●	
Surficial Debris		●
Ogives	●	

Separating the two domains is the first (lower) icefall (Figure 4.7), where the ice flows over and down a large step in the valley profile and falls approximately 200 metres from the upper part of the study area to the lower, after a lateral distance of approximately 700m. Field observations of this area are not possible due to the highly unstable conditions within the fall, but deep crevasses, fractured ice, and serács are clearly visible from aerial photographs, and aerial observations.

Figure 4.4: Topographically constrained ice of the Fox Glacier, demonstrating many of the typical features of a valley glacier. (Photo: J. Appleby)

Figure 4.5: Subdued topography of Victoria Flat, looking down-valley from above the first icefall. (Photo: J. Appleby)

Figure 4.6: Characteristic ‘ridge & trough’ pattern of the lower study area between the first icefall and snout of Fox Glacier. (Photo: J. Appleby)

Figure 4.7: Heavily crevassed ice of the lower icefall. Flow is from left to right. (Photo: J. Appleby)

Structures were identified using the criteria outlined in Table 3.1. Prominent features such as primary stratification, longitudinal structures, crevasses and crevasse traces were measured according to orientation, or strike and dip, as used in structural geology. The location of these features was recorded using a handheld Garmin Global Positioning System, before being transposed onto an outline base map of Fox Glacier. Schmidt equal-area stereographic projection was used to plot the three dimensional orientation of some of the features, using Georient equal angle stereographic projection software, available to download from the internet (Appendix 2). Data was collected in January and February 2007, when the maximum amount of snow-free ice was exposed, and is presented in Appendix 3.

4.1.2.2 Primary Stratification S_0

Primary stratification is difficult to define from the aerial photograph, but very apparent in the field. In the walls of deeper crevasses, such as in the lower icefall, it is possible to see distinct layering dipping at almost 90° (Figure 4.8). Stratification is more apparent in the

lower study area around transects B and C due to the increased occurrence of fractured and crevassed ice, and is identified as fairly regular layers of white ice broken by thinner dirty dark layers. The orientation of the layering varies considerably throughout the surface of the glacier with some layers undergoing complete rotation from horizontal to vertical, and most experiencing a high angle of dip. The location, strike and dip of primary stratification, along with the location of a longitudinal structure identified close to the snout, are mapped in Figure 4.9.

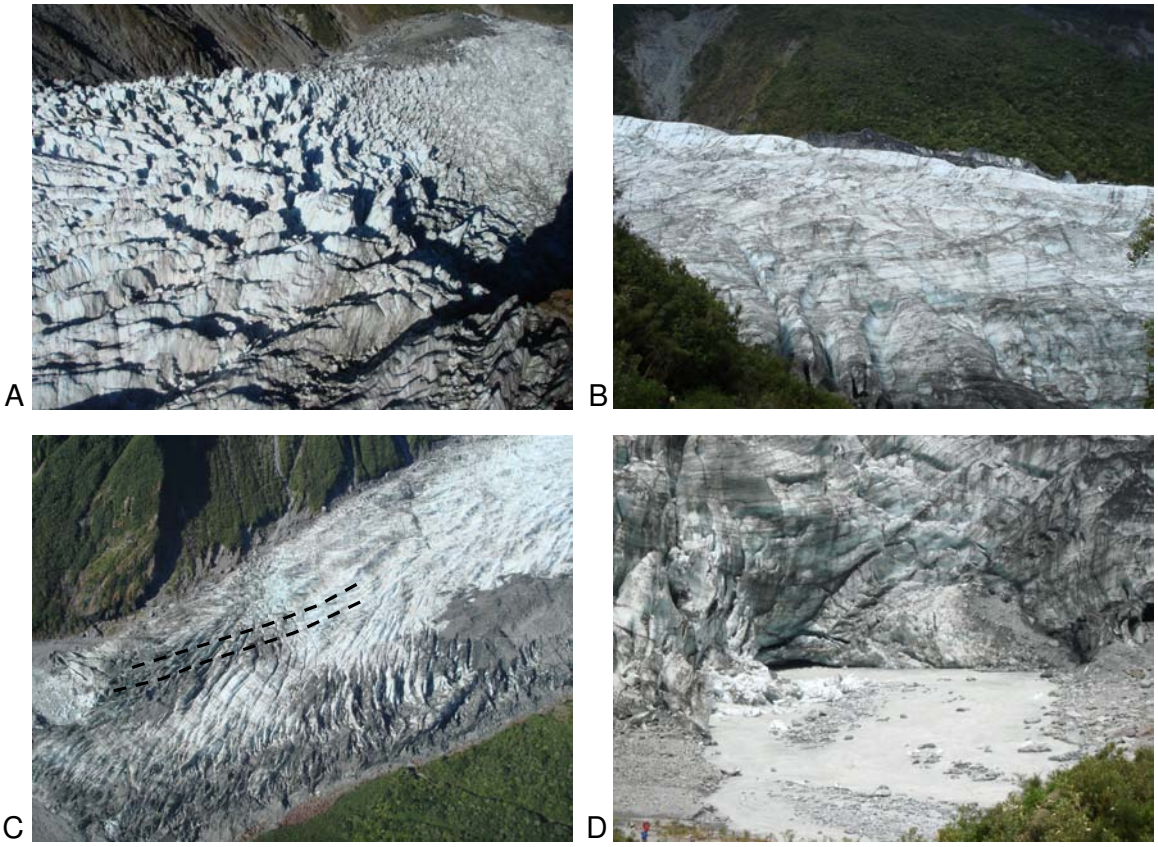

Figure 4.8: Primary stratification seen throughout the study area: (A) Shows almost vertically dipping stratification in the lower icefall: The angle of dip can be seen to change in the lower glacier (B), and the snout seen from above in (C), and from the front in (D). A longitudinal structure is denoted by the dashed lines in (C). (Photos: J. Appleby)

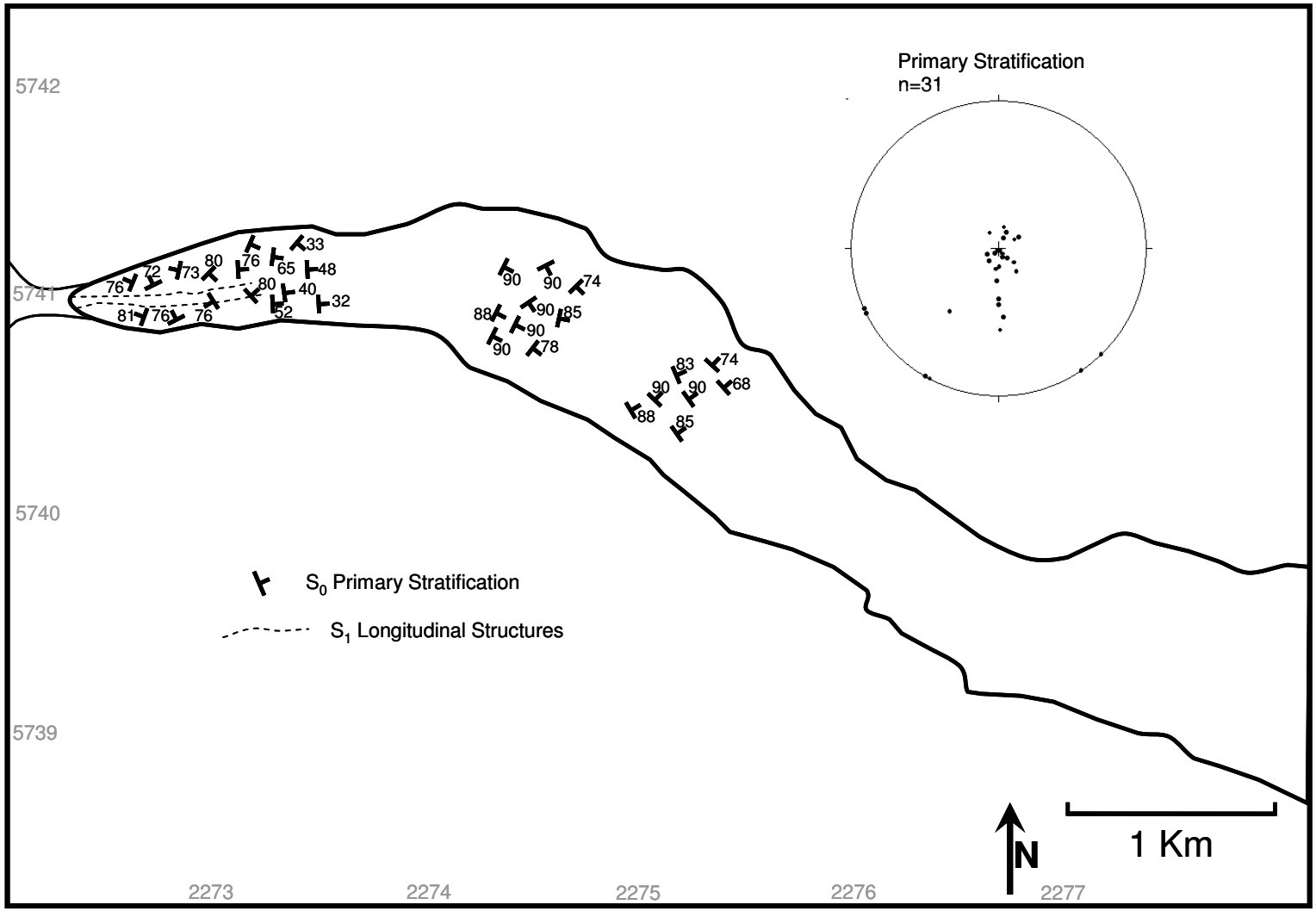

Figure 4.9: Field measurements of primary stratification and longitudinal structures presented as a structural field map. Strike and dip of 31 primary stratification measurements is represented by a 3-D equal area stereographic projection, with 90° at the centre of the circle, and 0° at the outside.

4.1.2.3 Crevasses

Various types of crevasses have been identified throughout the study area (Figure 4.10). The upper study area is characterized by transverse crevasses immediately below the upper icefall, and directly above the lower icefall, with evidence of their formation in the lower half of Victoria Flat. Both the true left and true right of the upper part of the study area show chevron crevasses, which then continue down-valley past the lower icefall into the lower part of the study area.

Towards the snout of the glacier in the area around transect C, very steep-sided (approx. 85°), deep crevasses (>10m) are found (Figure 4.10) where the ice is fracturing and expanding as the glacier terminates, and is less constrained. This area also experiences rapid ablation (Purdie, 2005). These crevasses are found across the width of the glacier snout but are deeper (>15m) and more pronounced towards the true left of the terminus. Immediately above the first icefall, these crevasses take on more of a splaying crevasse appearance as the glacier turns and flows over the icefall. Approximately half of the crevasses on the true left of Fox Glacier are filled or covered by supraglacial material transported passively across the glacier surface (Figure 4.3). This material appears to have originated on the true left valley wall, below Paschendale Ridge. Loose material falls directly from the valley side (a drop of approximately 800m), whilst some is transported to the ice down the numerous gullies and streams, such as Boyd Creek, flowing from Sam Peak and Mount Garnier. The location and orientation of a selection of crevasses identified by field observation has been mapped on Figure 4.11.

A number of structures demonstrating similar characteristics to open crevasses and fractures can be identified from both aerial photographs and field observations. These transverse arcuate structures are the remnant of former open crevasses, and can be termed crevasse traces.

Figure 4.10: Crevasses identified from field observations in both the upper and lower parts of the study area: (A) Chevron crevasses on the true left of the glacier above the lower icefall at the lower end of Victoria Flat; (B) Splaying crevasses at the snout of Fox Glacier, looking down to the Fox River below; (C) Opening Crevasse on Victoria Flat (flow right to left); and (D) transverse crevasses above the lower icefall, looking down-valley. (Photos: J. Appleby)

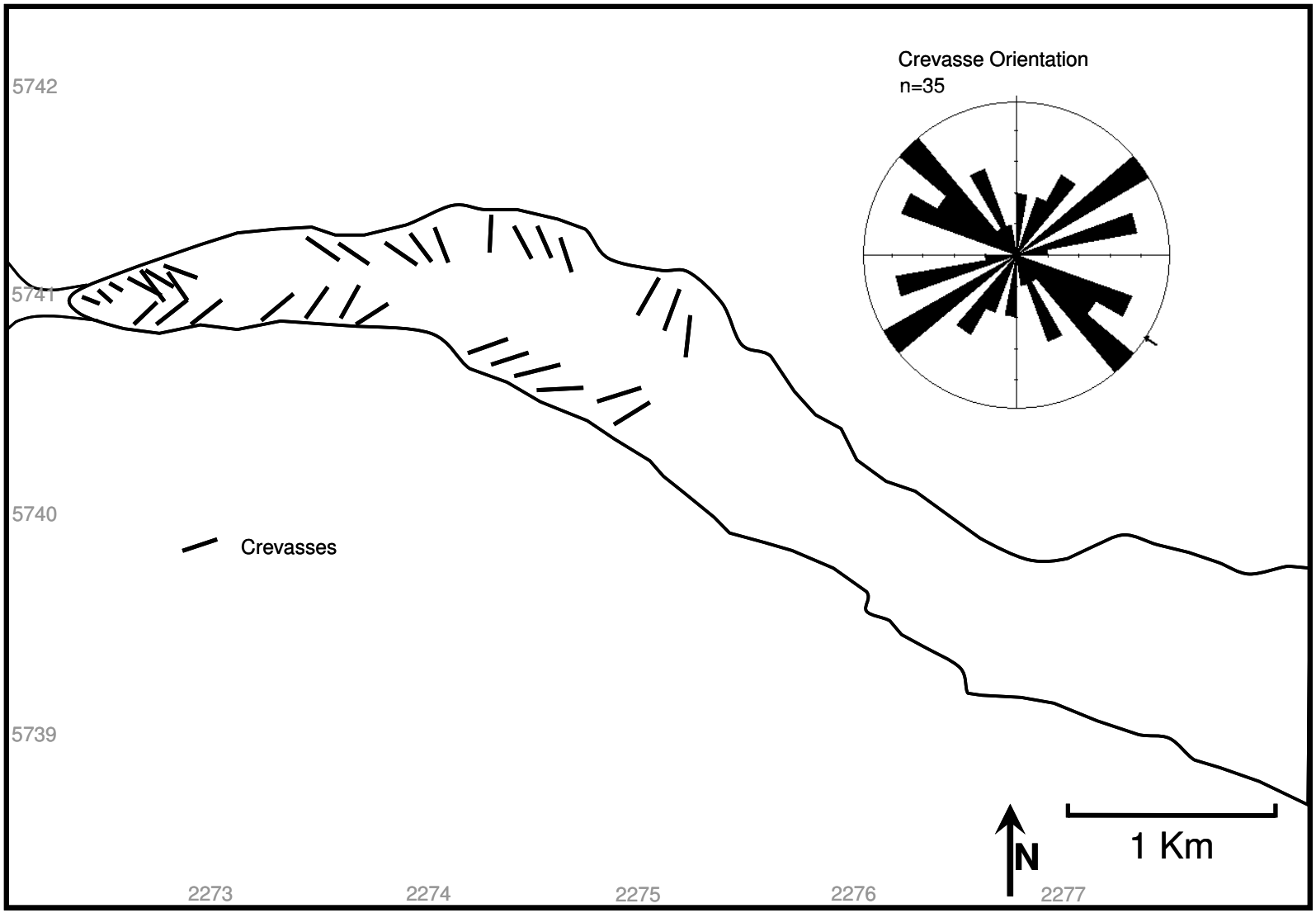

Figure 4.11: Field measurements of crevasses presented as a structural field map. Orientation and frequency of 35 crevasse measurements are represented by a rose diagram.

4.1.2.4 Transverse Arcuate Structures (Crevasse Traces) S_2

Crevasse Traces have been identified over most of the surface of Fox Glacier, from both aerial photographs and field observations (Figure 4.12). They are recognised as linear features cross-cutting other structural features, typically persisting for almost the whole width of the glacier. These features typically display up-glacier dips at very high angles, as can be seen in Figure 4.12 and Figure 4.13.

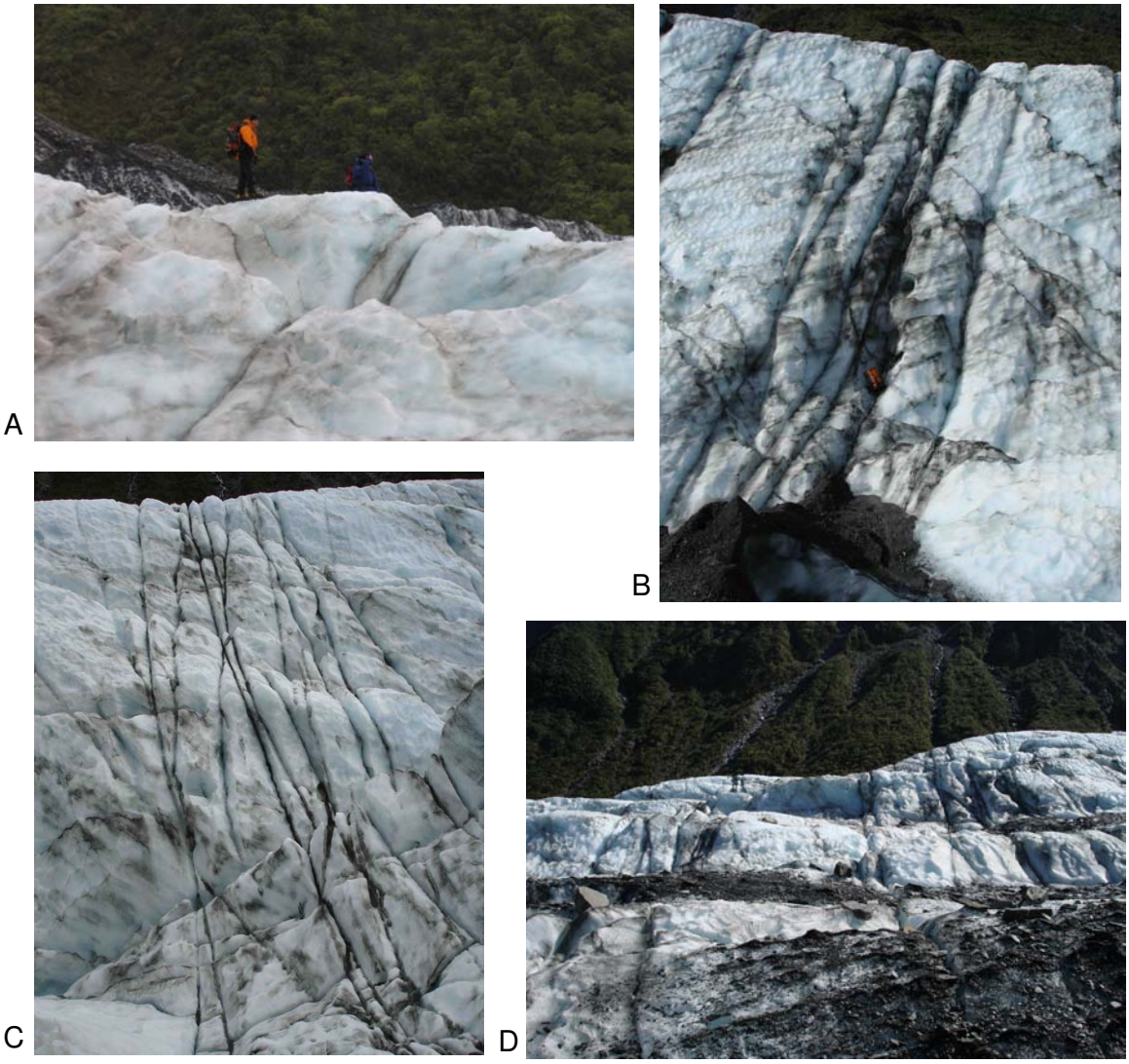

Figure 4.12: Transverse arcuate structures (crevasse traces) in the lower part of the study area: (A) Typical 'stepped pattern' of crevasse traces; (B) Steeply dipping crevasse traces cross-cutting primary stratification (rucksack approximately 80cm in length); (C) Crevasse traces cross-cutting other crevasse traces; (D) Transverse arcuate structures running the width of Fox Glacier. (Photos: J. Appleby)

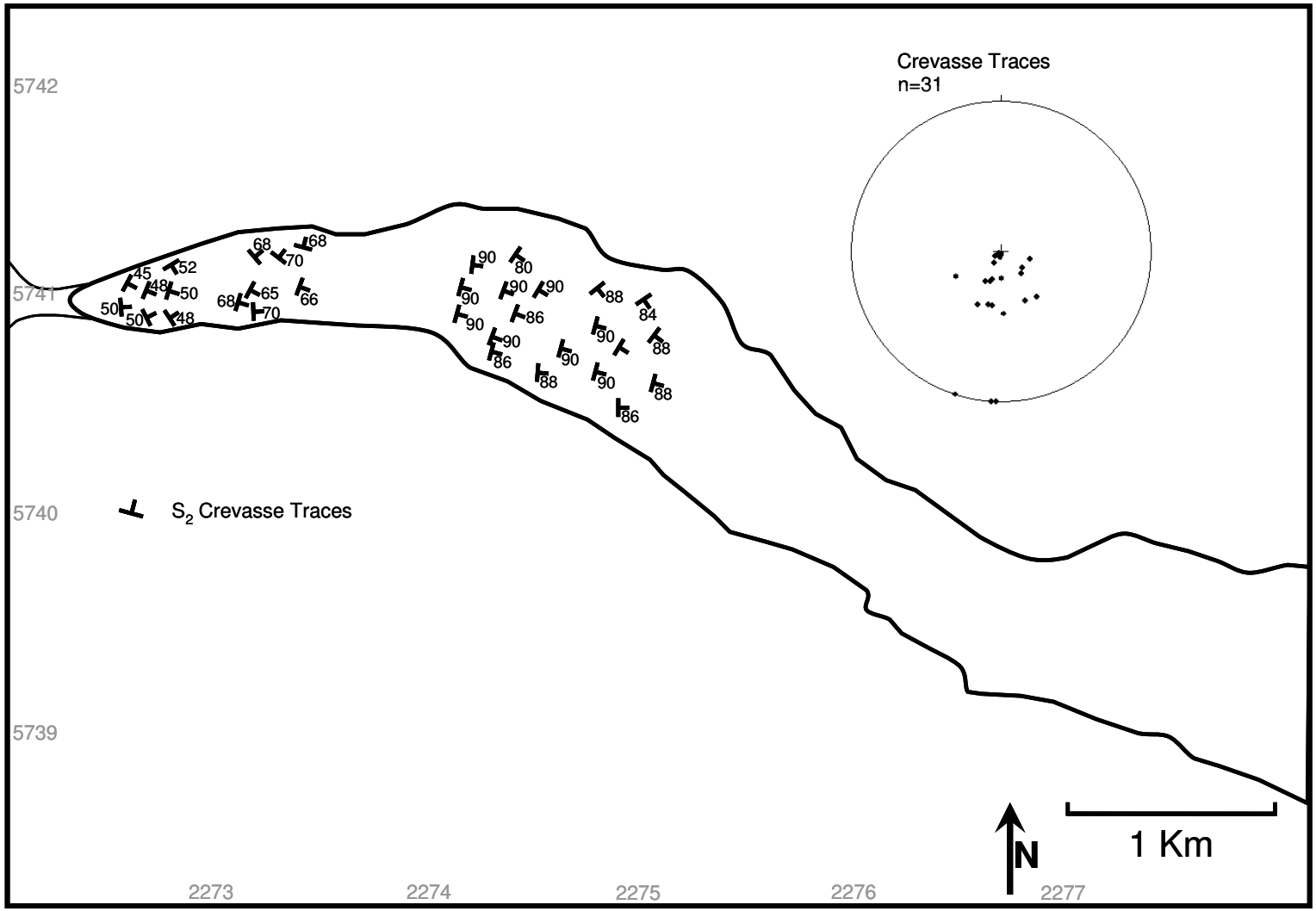

Figure 4.13: Field measurements of transverse arcuate structures (crevasse traces) presented as a structural field map. Strike and dip of 31 crevasse trace measurements are represented by a 3-D equal area stereographic projection, with 90° at the centre of the circle, and 0° at the outside.

Some of the crevasse traces are constructed of different densities and colours of ice, with some being constructed of very white, course ice, and others being of hard, blue ice, whilst others contain no dirt or debris. This may suggest these traces have never actually opened; rather they have been created in an area of expanding ice which has then compressed before reaching the threshold of fracture. Crevasse traces filled with dirt and debris may represent once open crevasses that have since closed due to compressive flow, or relict crevasse from a period of more active ice movement.

Crevasse traces measured in the upper part of the study area generally have a very steep up-valley dip (80 to 90°). More variation in strike orientation is evident in the lower part of the study area. Dip angles in this area appear lower than those further up the glacier (45 to 70°). The number of transverse arcuate structures observed in the field appears to increase with distance down glacier.

4.1.2.5 Foliation S_3

Foliation is evident in the lower part of the study area (Figure 4. 14), but is not obviously apparent in the upper part of the study area on Victoria Flat. The majority of foliation layers identified in the lower part of the study area were of a longitudinal orientation, dipping to the true right of the glacier, with a medium to high dip angle. Orientation and dip angle of foliation layers observed in the field are mapped in Figure 4.15.

The foliation layers consist of course bubbly white ice, layered with hard, fine grained blue ice. The hard blue ice layers were generally less than 5cm in width, with the rest consisting of the less-dense white ice. The layers were occasionally interspersed with layers of fine dirt and debris.

These layers may have been produced from primary stratification that has undergone high strain and has been rotated by glacier flow. An alternative explanation may be that they are a uniquely metamorphic structure produced entirely from high strain rates and ice flow, and do not originate from primary stratification.

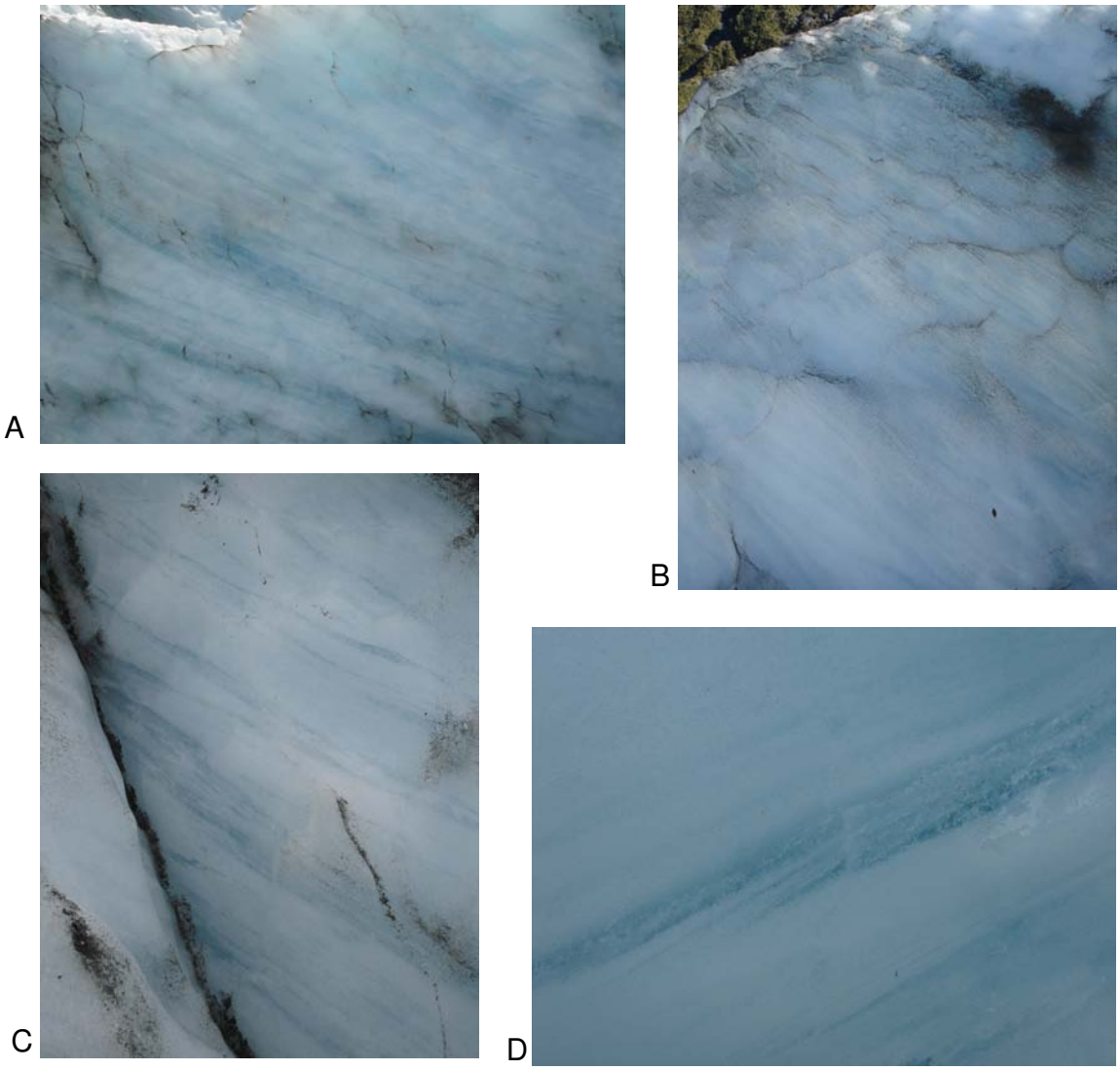

Figure 4.14: Foliation observed as course-grained, white bubbly ice, layered with much harder, smaller-grained blue ice. These medium to steeply dipping foliation layers were recorded in deep crevasse walls in the lower part of the study area. (Photo: J. Appleby)

Gunn (1964) associated transverse foliation in Fox Glacier with a high strain-rate in ice under compression, and noted a markedly decreasing rate of flow being found down the length of the glacier.

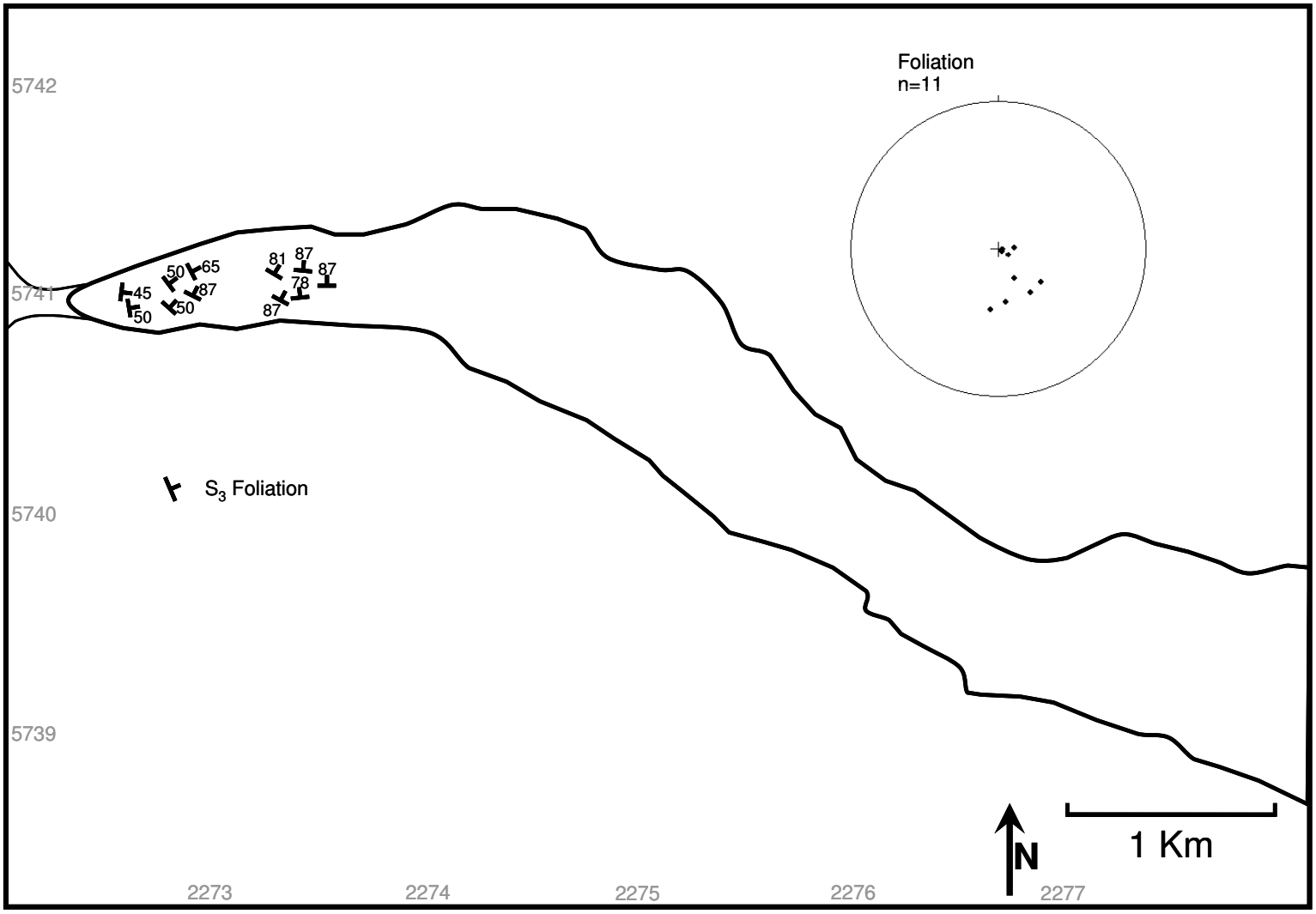

Figure 4.15: Field measurements of foliation presented as a structural field map. Strike and dip of 11 foliation layer measurements are represented by a 3-D equal area stereographic projection, with 90° at the centre of the circle, and 0° at the outside.

4.1.2.6 Folding

Intact fold structures have only been identified in the upper study area (Figure 4.16). The walls of chevron crevasses on the true left of the glacier immediately above the second icefall show limited folding of the surface ice. Less pronounced folding can be seen closer to the centre of the glacier, and further up valley towards the base of the second icefall. Most folds were found in isolation whilst some were found in a repeating pattern along the length of a crevasse wall, with the folds having a wavelength of approximately three metres.

Figure 4.16: Folding of dirt layers observed in the wall of a chevron crevasse above the lower icefall, at the lower end of Victoria Flat. The Wavelength of the fold is approximately 3 metres, with its shape being classified as Fourier 3 E (Appendix 4. The fold could be followed for approximately 10 metres along the wall of the crevasse. (Photo: J. Appleby)

4.1.2.7 Moulins

Moulins are found in both the upper and lower domains of the study area (Figure 4.18). The largest and most well developed moulins are found in the upper study area (Figure 4.17) between the first and second icefalls, and are fed by extensive supra-glacial channel patterns. Some of these channels can be followed for distances in excess of fifty metres before disappearing into the ice. The majority of moulins in the lower part of the study area had a diameter of less than 20cm, with all of those measured having a diameter of less than 80cm. The moulins of the upper study area had a much larger range of diametres, although most were greater than 50cm in diameter. Most moulins had a continuous flow of melt water whilst some only became active after periods of rainfall. Some initially round moulins have been deformed by ice movement so that they now demonstrate an elliptical shape.

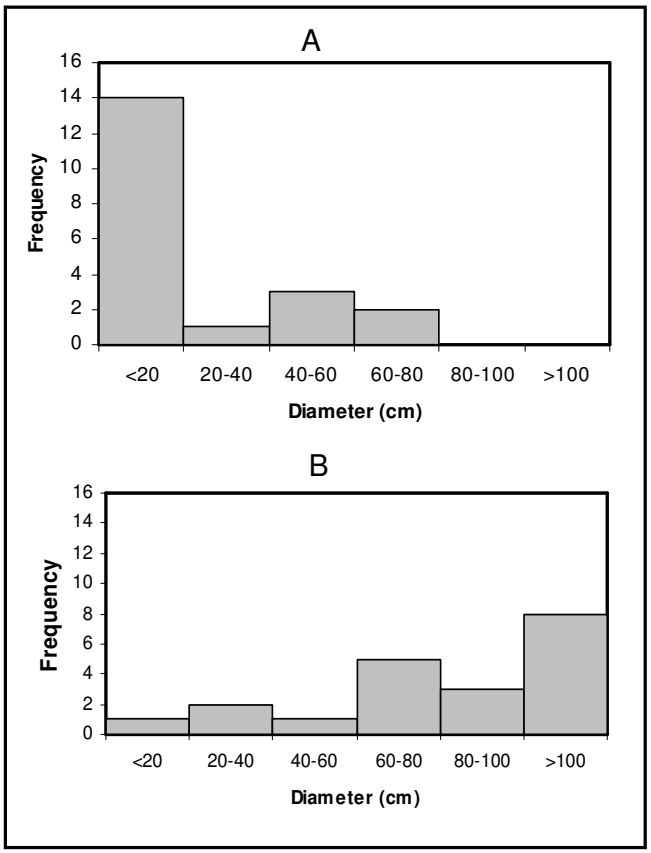

Figure 4.17: Frequency of moulin diameter in (A) the lower part of the study area between the lower icefall and the snout, and (B) the upper part of the study area on Victoria Flat above the lower icefall.

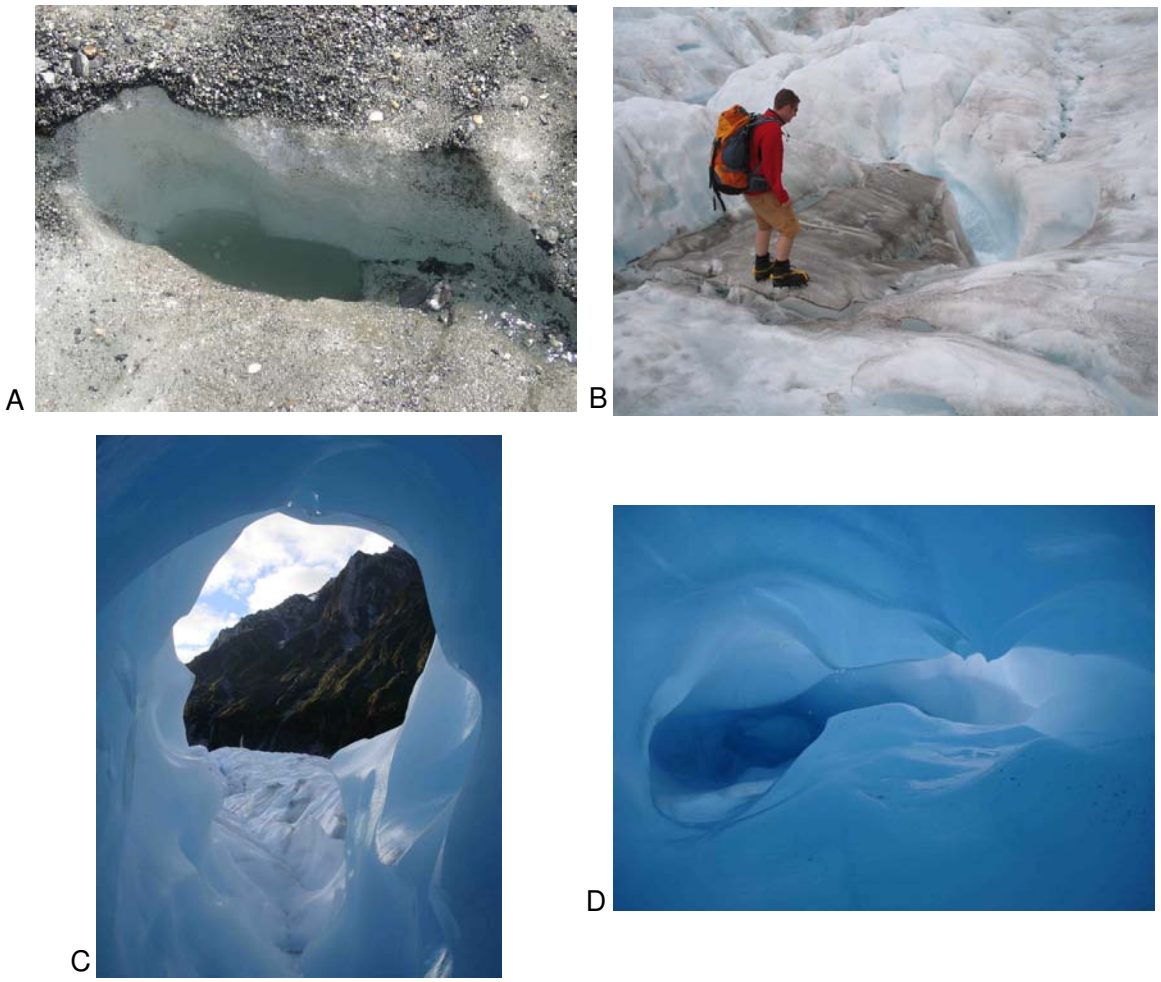

Figure 4.18: (A) Elliptical moulin deformed from a round shape by ice movement and deformation; (B) Large moulin and supraglacial channel observed in the upper part of the study area on Victoria Flat; (C) and D) exposed englacial conduits seen in the upper part of the study area, immediately below the upper icefall. (Photos: J. Appleby)

4.1.2.8 Englacial Conduits

Some englacial conduits associated with moulins have been exposed in the upper part of the study area (Figure 4.18) between the first and second icefalls. They can be seen towards the centre of the glacier and are mainly found exposed in the walls of crevasses below the upper icefall. The conduits have a maximum diameter of 2 metres and range in shape from almost circular, to an ellipse deformed so that one axis is more than twice the length of the

other. The conduits dip into the ice at angles of less than 30° down glacier, and are generally aligned longitudinally.

4.1.2.9 Surficial Debris

Although not a glacial structure, surficial debris (Figure 4.19) can have considerable impacts on surface ablation (Nicholson and Benn, 2006) and meltwater quantity and routing, and therefore stress and strain of valley glacier ice. Supraglacial debris has been identified as forming a moraine on the true left of the glacier above the first icefall, which then continues below the first icefall and develops an area of medial moraine as the glacier flows left down the Fox valley. The material in the moraine on the true left is passively transported to the snout of the glacier where material is dumped and gravitationally re-worked into the proglacial zone from the ice surface above the snout.

Passive transport allows debris to be transported through the glacier system with little or no modification. Even where debris concentrations are high, such as in glacier ablation zones in alpine environments like Fox Glacier, inter-particle contact forces are generally small, unlike those at glacier beds (Kirkbride and Spedding, 2006).

Localised patches of small size debris and very fine rock flour can be seen at random intervals on the surface towards the centre of the glacier, and are found in conjunction with areas of disturbed ice and rapid ablation. These deposits are more common in the lower study area than the upper. The material has been measured and recorded according to clast roundness and morphology (Figure 4.20).

The true left and true right surficial debris deposits have high C_{40} values of 90 and 74 respectively. This indicates flat slabby material; passively transported and relatively unworked. The surficial material at the centre of the glacier has a much lower C_{40} value of 32. The majority of clasts in all three of the sample areas demonstrate an angular or very angular shape, but the material towards the centre of the glacier also demonstrated some sub-rounded clasts. The proportion of clasts with an angular or very angular shape is represented by RA values of 64 for the true left material, 86 for the true right material, and

56 for the material on the surface of the centre of the glacier. C_{40} and RA values can be plotted against each other in a covariance plot (Figure 4.21). The covariance plot produces a number of facies envelopes identifying different clast types (e.g. Scree/supraglacial debris; subglacial debris; valley moraines; and glaciofluvial material). Clasts of each type should be plotted in there respective envelope when RA and C_{40} index values are compared (Glasser *et al*. 2006).

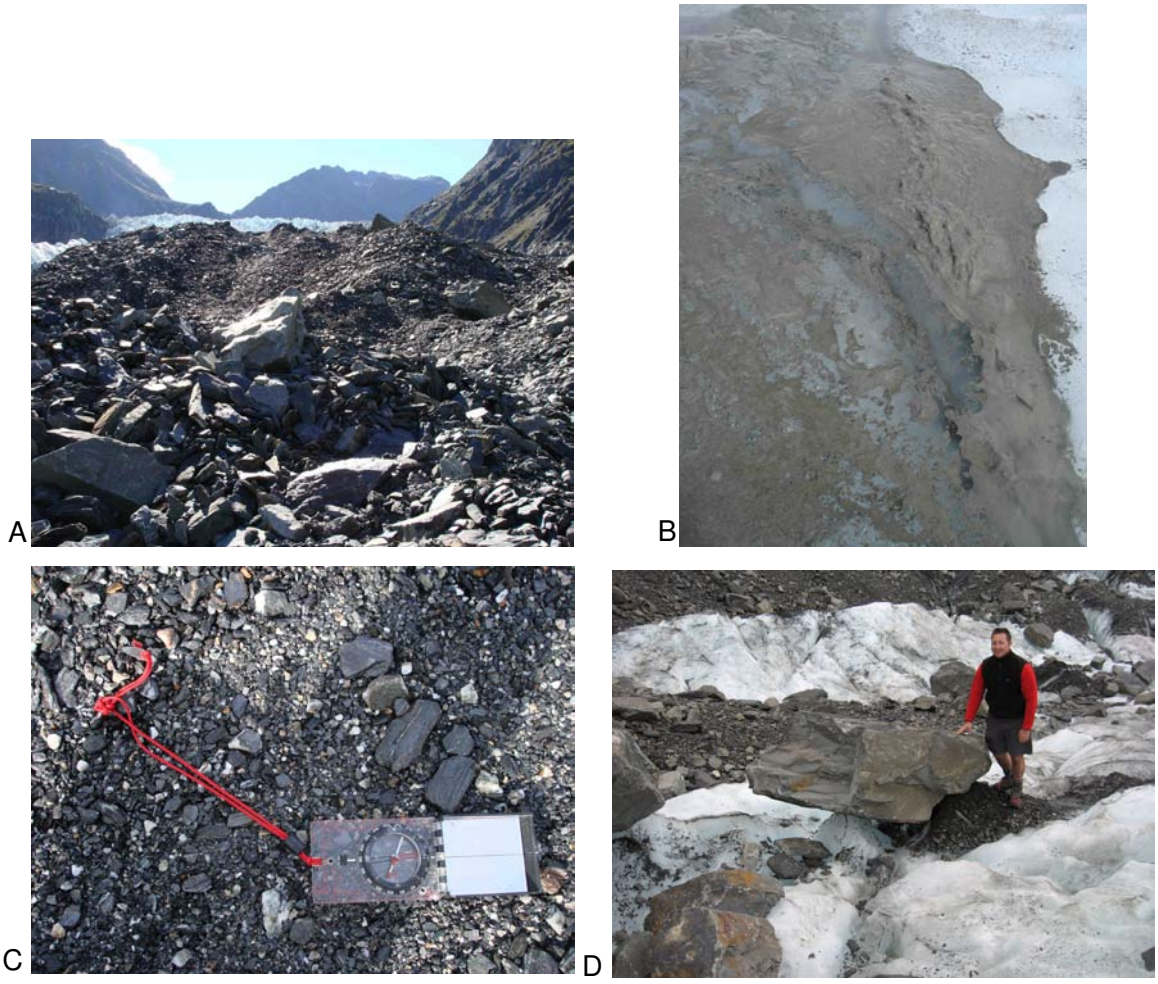

Figure 4.19: Surficial debris observed in the lower part of the study area, between the lower icefall and the snout of Fox Glacier. (A) Cones of material forming a lateral moraine on the true left of the lower glacier; (B) Very fine (<1mm) water-saturated rock flour found towards the centre of the lower part of the study area; (C) Small sized material found in a small deposit at the centre of the lower part of the study area; and (D) Large-scale material found on the true left and true right of the lower study area, with axes often greater than 1m in length. This clast has formed a glacier table, protecting the ice below from ablation and weathering. (Photos: J. Appleby)

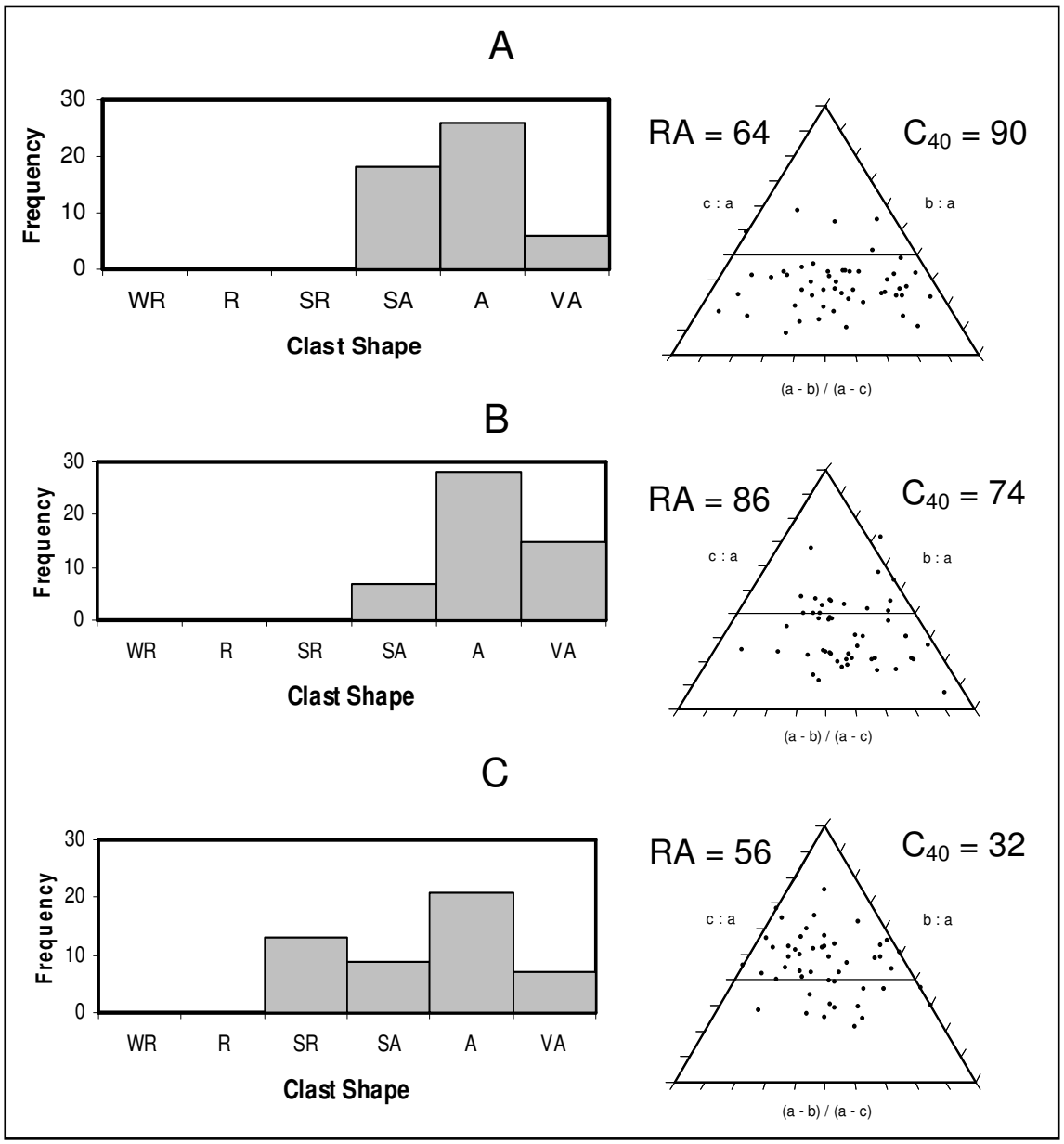

Figure 4.20: Clast shape and morphology of surficial debris measured on (A) the true left; (B) the true right; and (C) centre of the glacier. Frequency histograms show the frequency of clast shape (well rounded, rounded, sub-rounded, sub-angular, angular, and very angular), with the proportion of angular and very angular clasts represented by RA (%) values. Clast morphology is represented by ternary diagrams and C_{40} values.

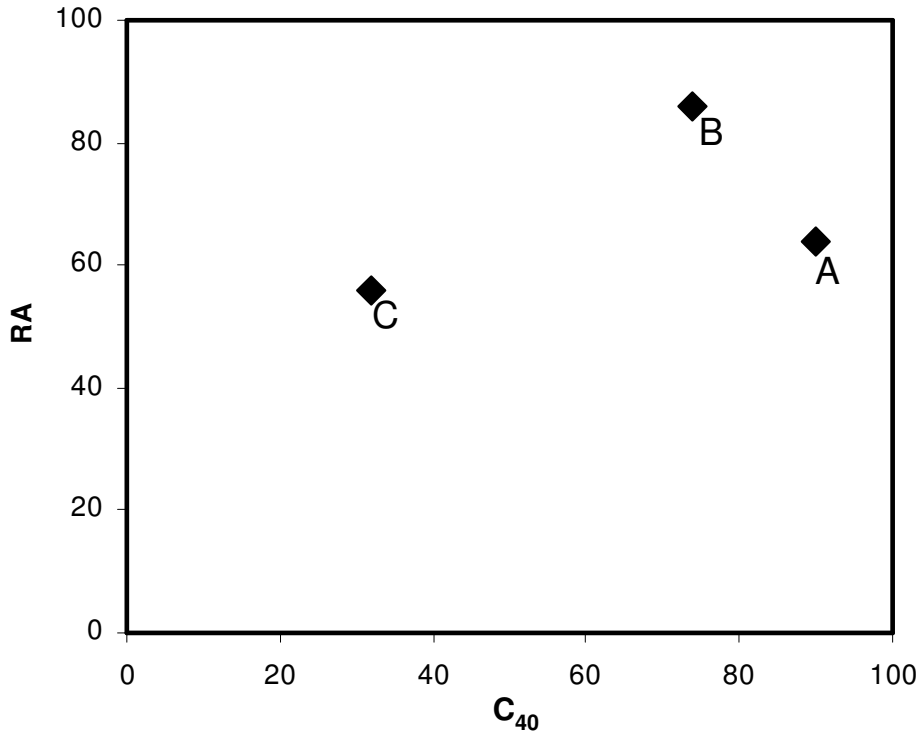

Figure 4.21: Covariance plot of C_{40} index (percentage of clasts with c/a axial ratio $\leqq$ 0.4) against RA index (percentage of angular and very angular clasts) for surficial debris measured; (A) on the true left of the glacier; (B) on the true right of the glacier; and (C) at the centre of the glacier.

4.1.2.10Arcuate Bands (Ogives)

Along the length of the study area, arcuate bands (ogives) can be seen (Figure 4.21), with convex bands being evident as both 'light and dark' ice, and 'ridge and troughs'. Ridge and troughs are more evident in the upper part of the study area as the ice is much flatter and less disturbed than below the first icefall, whilst light and dark bands are more prominent between the first icefall and the snout.

Assuming one set of ogives (either 'light and dark' or 'ridge and trough' unit) represents one years ice passage through an icefall, an approximate transfer rate of ice from the accumulation area to the terminus can be calculated by counting the number of bands along the length of the glacier.

Figure 4.21: Ogives seen on the true right of chevron crevasses above the lower icefall denoted by dashed lines. Flow is from right to left, with the field of view approximately 1km. (Photo: J. Appleby)

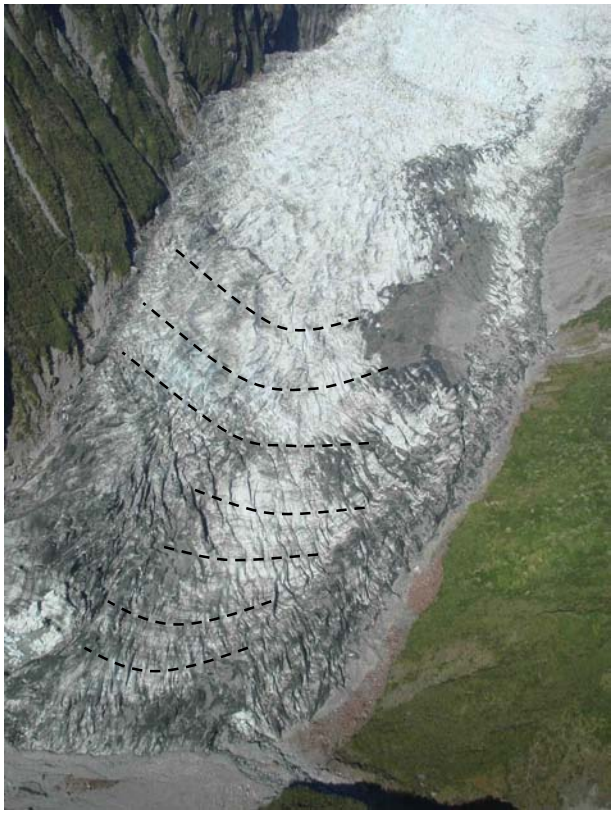

Figure 4.22: Light and dark ogives at the snout of Fox Glacier denoted by dashed lines Ogives on the true right are heavily disturbed by crevassing and longitudinal structures. (Photo: J. Appleby)

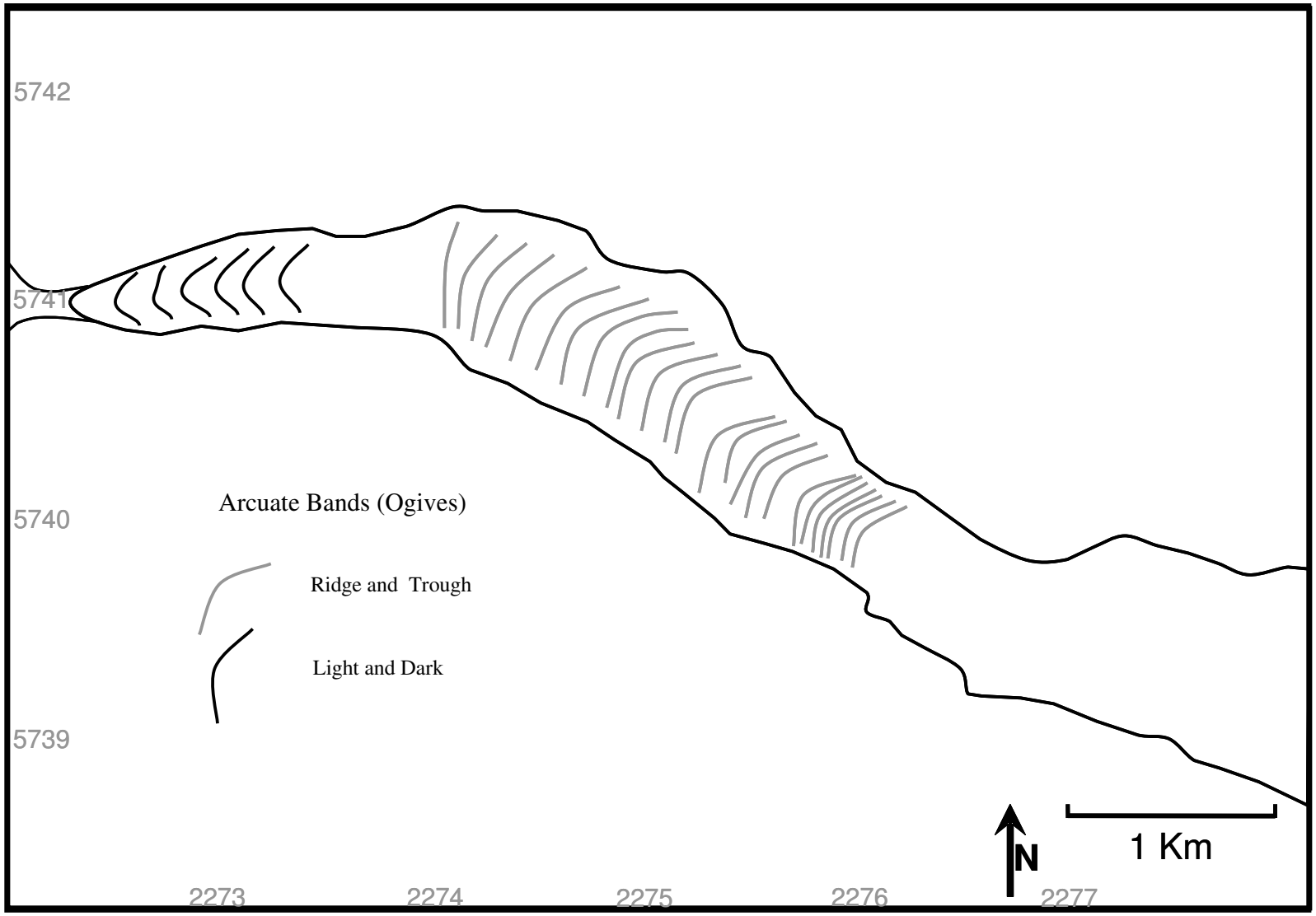

Figure 4.23: Field measurements of arcuate bands (ogives) presented as a structural field map.

4.2 Strain & Deformation

Data were collected and analysed according to the methods described in Chapter 3: Methodology of Research. To re-iterate, calculation of strain rates and cumulative strain is based on the changing dimensions of polygons as described by Nye (1959), Wu and Christensen (1964), Milnes and Hambrey (1976), Vaughan (1993), and Goodsell *et a.l* (2005[a]). Strain caused by an applied stress is fundamental to the behaviour and deformation of glacier ice, and so the features and landforms we associate with glacial and periglacial landscapes.

Transects A, B and C were located above and below the lower icefall, and at the snout of the glaciers respectively, as can be seen from the map in Figure 4.24. The study period ran from the 12th of January to the 21st of February 2007, giving a total of 40 days. The two metre ablation stakes used to construct the diamond arrays in the three transects required re-drilling every three to four days of the study, suggesting a summer ablation rate of between 60mm and 90mm per day.

Deformation of the three transects over the study period can be expressed visually by graphing the location of each stake at the start of the study period and again at the end. This gives an indication of velocity and deformation along and across the glacier. The amount of deformation varies considerably between each transect as can be seen in Figures 4.25, 4.26, and 4.27. Transect A (Figure 4.25) appears to have experienced relatively little deformation, compared to transect B (Figure 4.26) and transect C (Figure 4.27). The greatest deformation appears to have occurred in transect C, close to the snout, where some of the diamond arrays are almost completely changed in size and shape. The second measurements for diamond 4 in transect C are incomplete as the end stake was lost due to ice disturbance and crevassing. Down-valley movement is evident on each of the transects.

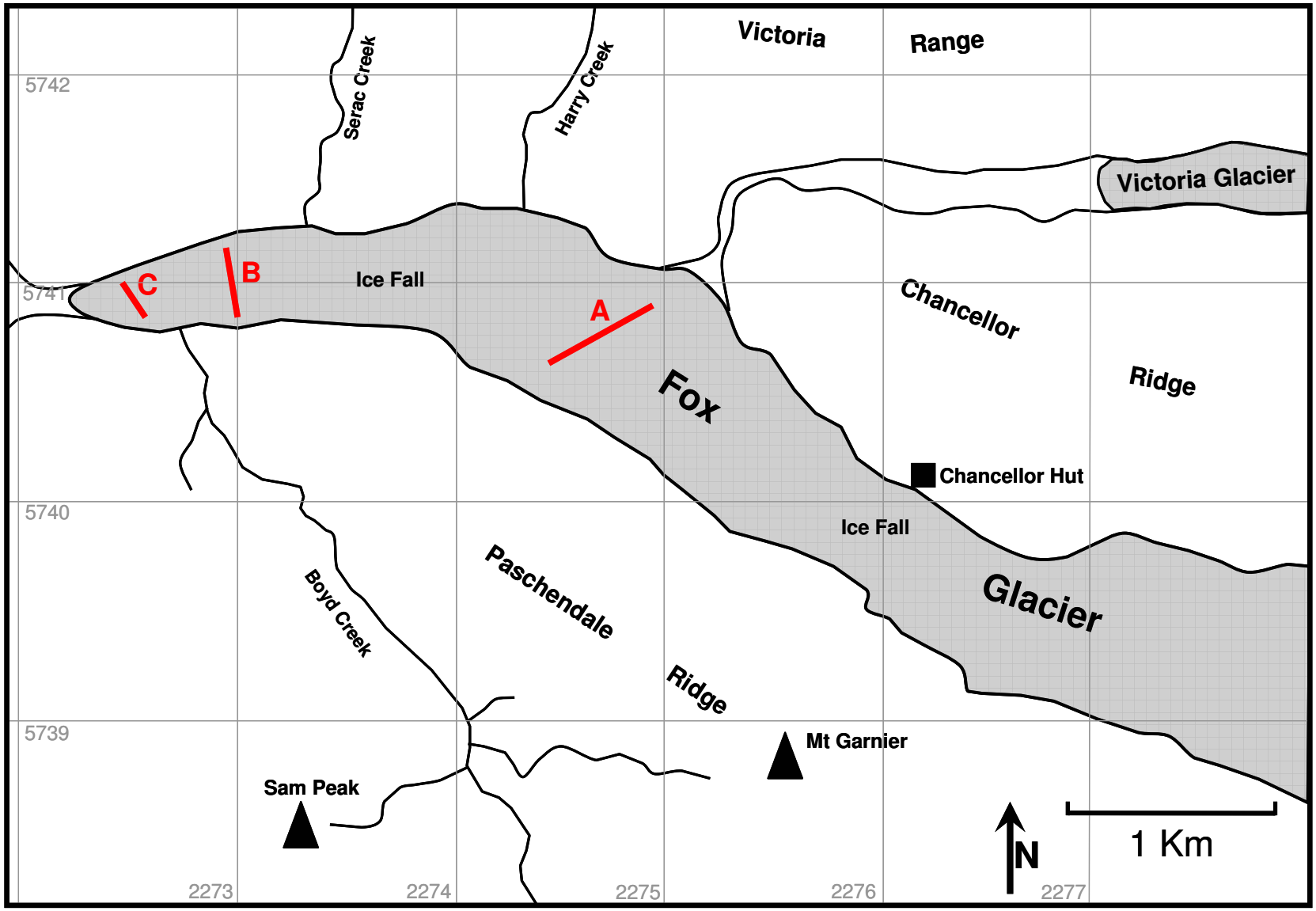

Figure 4.24: Location of transects A, B, and C above and below the lower icefall on Fox Glacier.

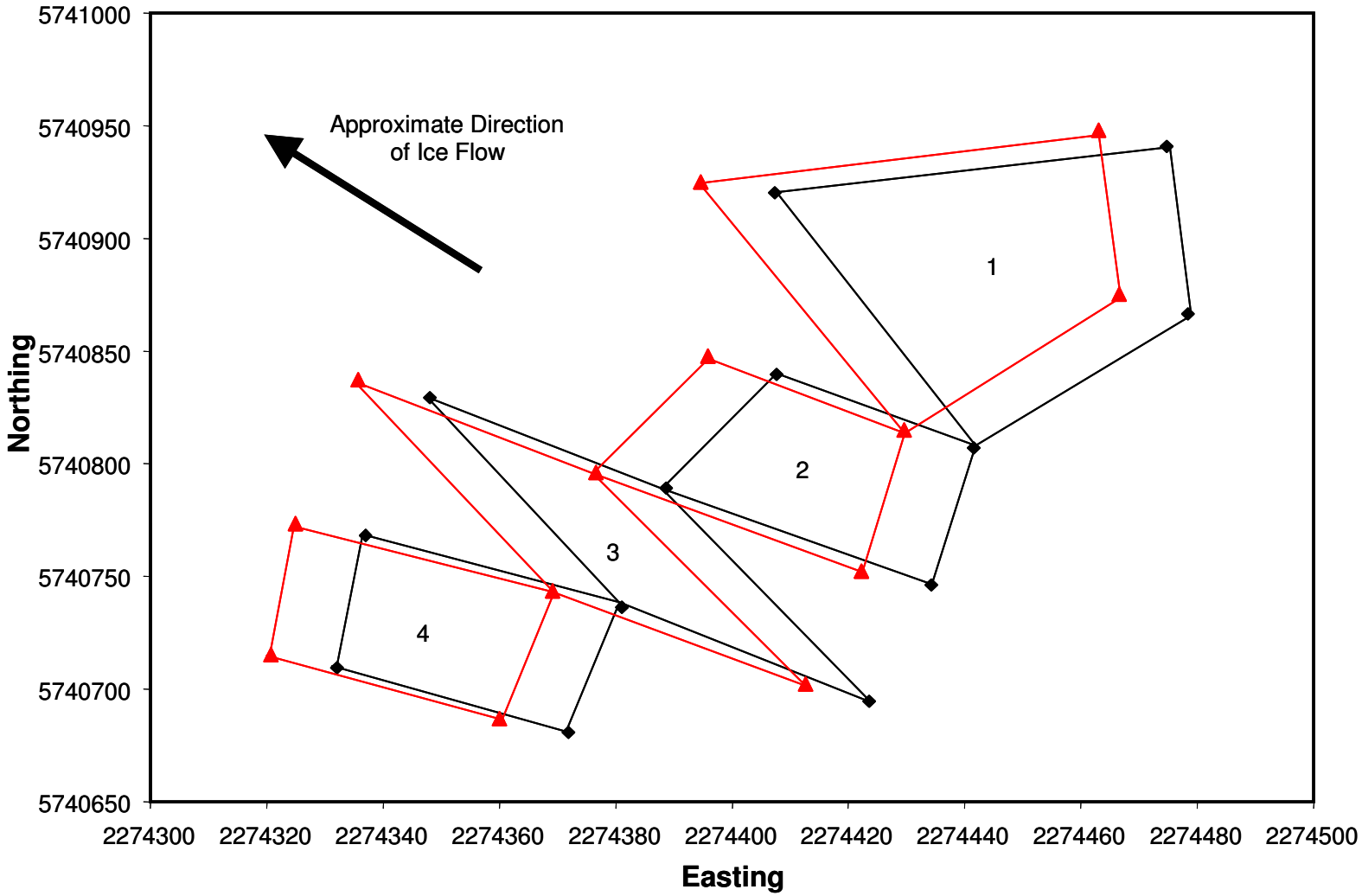

Figure 4.25: Graphical representation of deformation for Transect A above the lower icefall. Primary measurements taken at the start of the study period are represented by black points and lines, whilst secondary measurements taken at the end of the study period are represented by red triangles and lines.

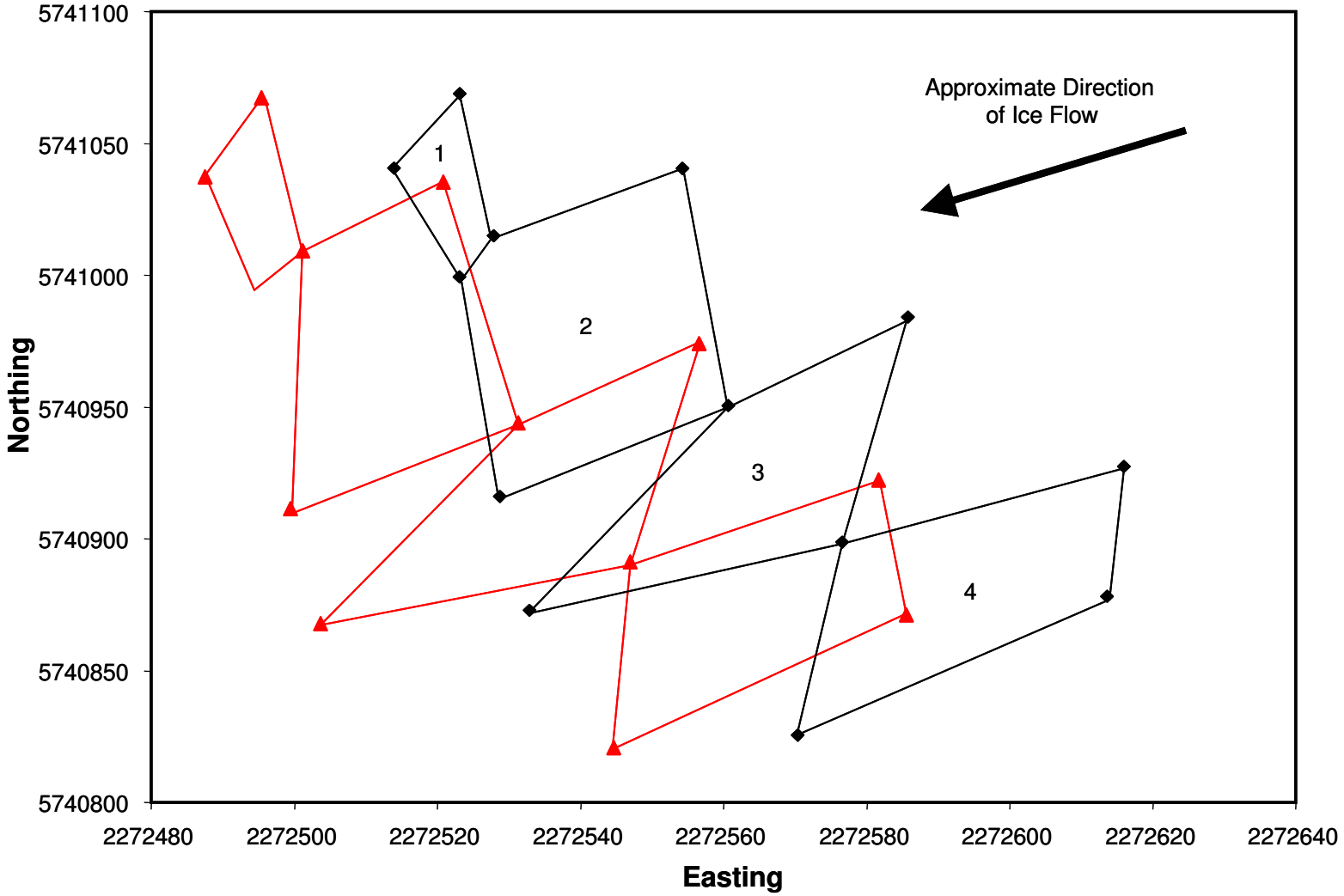

Figure 4.26: Graphical representation of deformation for Transect B below the lower icefall. Primary measurements taken at the start of the study period are represented by black points and lines, whilst secondary measurements taken at the end of the study period are represented by red triangles and lines.

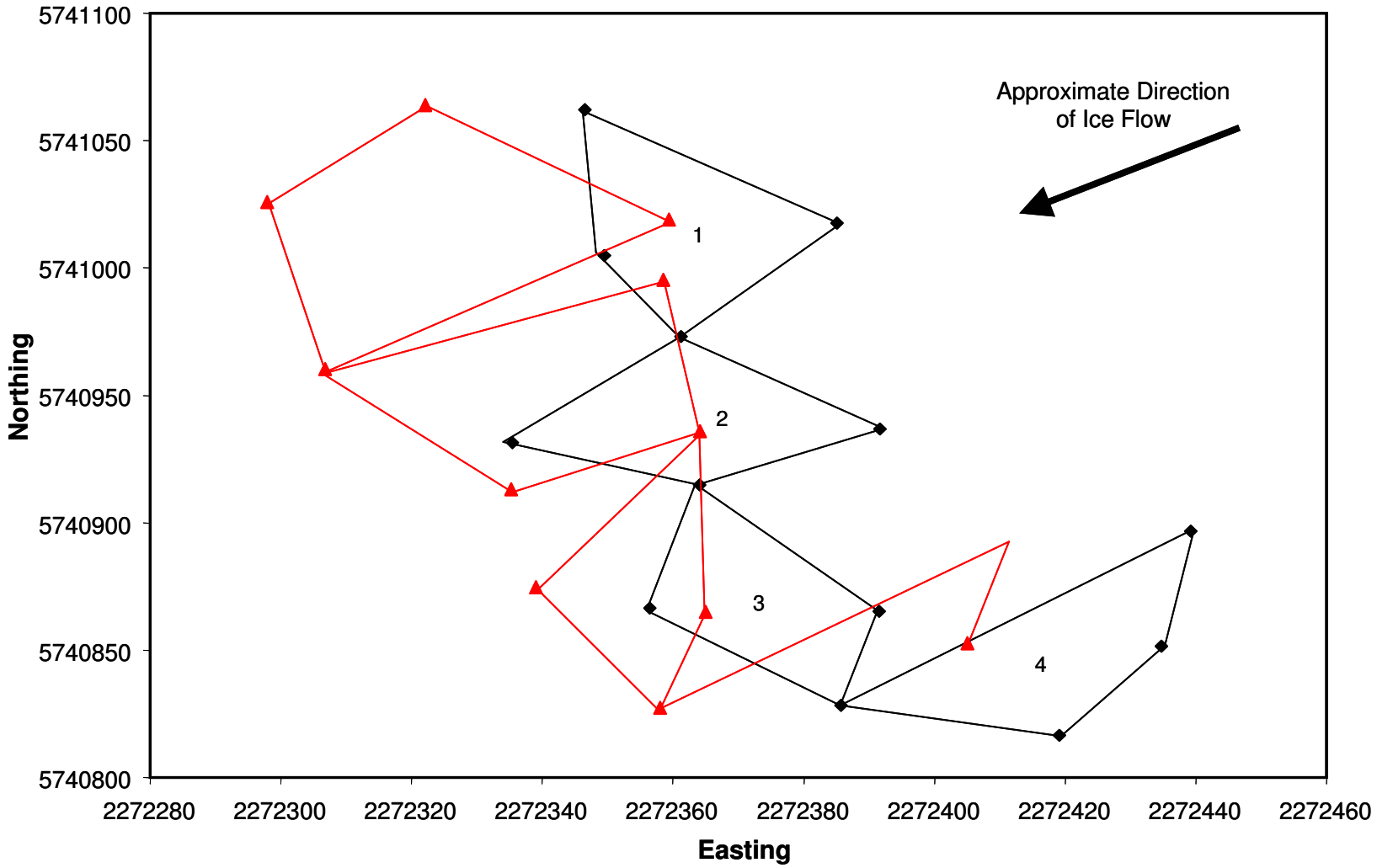

Figure 4.27: Graphical representation of deformation for Transect C at the snout of the glacier. Primary measurements taken at the start of the study period are represented by black points and lines, whilst secondary measurements taken at the end of the study period are represented by red triangles and lines.

4.2.1 Cumulative Strain

The total strain or deformation of each of the diamonds occurring over the whole of the study period has been measured, and can be expressed as total cumulative strain ε. The cumulative strain is a measure of the extensional or compressive change in length of the diamond relative to its un-strained state. The numbers alone represent strain, as strain is considered a unit-less value.

Transect A (Table 4.1) was measured over a 25 day period in January and February 2007. The cumulative strains ε measured ranged from -0.01 in the 45° direction for diamond 4 to 0.48 in the 135° direction for diamond 3. Eleven of the sixteen directions experienced a positive strain.

Table 4.1: Cumulative strain ε measured in the 0, 45, 90 and 135° directions for diamonds 1-4 in Transect A.

Diamond	ε0	ε45	ε90	ε135
1	0.08	0.23	-0.02	-0.26
2	0.15	0.04	0.05	-0.07
3	0.09	0.07	0.52	0.48
4	0.22	-0.01	0.222	0.32

Transect B (Table 4.2) was measured over a 40 day period in January and February 2007. The cumulative strains ε measured range from -0.04 in the 135° direction for diamond 2 to -9.64 in the 135° direction for diamond 4. Only four of the sixteen directions experienced a positive cumulative strain.

Table 4.2: Cumulative strain ε measured in the 0, 45, 90 and 135° directions for diamonds 1-4 in Transect B.

Diamond	ε0	ε45	ε90	ε135
1	2.73	-1.15	-6.60	-0.95
2	1.17	0.63	-0.56	-0.04
3	0.37	-1.85	-5.25	-2.50
4	-3.12	-2.42	-0.14	-9.65

Transect C (Table 4.3) was also measured over a 40 day period in January and February 2007. The cumulative strains ε measured ranged from 0.26 in the 0° direction for diamond 3 to 23.44 in the 90° direction for diamond 1. Eight of the sixteen directions experienced a positive strain. The cumulative strains ε recorded in transect C are considerably higher than those measured in transects A or B. No data is available for cumulative strain in the 0° direction for diamond 4 as the stake was lost on the glacier due to disturbance and crevassing of the ice.

Table 4.3: Cumulative strain ε measured in the 0, 45, 90 and 135° directions for diamonds 1-4 in transect C.

Diamond	ε0	ε45	ε90	ε135
1	-13.18	-19.49	23.45	16.07
2	27.37	7.65	5.18	16.90
3	0.26	-5.82	-13.64	-3.71
4		0.52	-0.53	-3.44

4.2.2 Strain Rate

Cumulative strains for each of the diamond arrays in the three transects were measured over slightly different study periods, due to constraints in fieldwork. For this reason the rate at which the strain occurred (strain rate) is a more appropriate measure to compare the different transects and diamonds. In this research strain rates are displayed (Figures 4.4, 4.5, and 4.6) as strain per day d^{-1}, and strain per year y^{-1}. Most previous research has shown strain rate as strain per year y^{-1} due to the small strain rates experienced. However, the rapid movement of Fox Glacier, coupled with the relatively short study period has made strain per day d^{-1} more appropriate. Strain per year y^{-1} is displayed for comparison with previous research. Being closely related to climatic fluctuations, Fox Glacier experiences considerable intra-annual variation in velocity (e.g. Purdie *et al*., 2007; Purdie et *al*., 2008) and so surface strain rates over the year y^{-1} must be viewed critically without a more long-term study.

Measured cumulative strains were divided over the 25 day study period for Transect A (Table 4.4) to give strain rates that ranged from less than 0.01 d^{-1} for the $\acute{\varepsilon}_y$ axis of diamond 1 to -0.09 d^{-1} for the $\acute{\varepsilon}_{xy}$ axis of diamond 3. All four diamonds of transect A had a positive strain rate in the down-valley *y* axis, whereas three of the four diamonds had a negative strain rate in the across-valley *x* axis.

Table 4.4: Strain rates per day (d^{-1}) and per year (y^{-1}) in the *x*, *xy* and *y* axes for diamonds 1-4 in Transect A.

Diamond	d^{-1}			y^{-1}		
	ἐx	ἐxy	ἐy	ἐx	ἐxy	ἐy
1	-0.02	0.01	0.00	-5.84	4.02	0.73
2	-0.01	0.02	0.04	-5.11	8.40	13.87
3	0.01	-0.10	0.00	4.02	-35.77	1.10
4	0.00	-0.08	0.00	-1.10	-29.20	1.46

The measured strain rates can be displayed graphically using idealised diamonds (Figures 4.28, 4.29, and 4.30). The diagrams graphically display magnitude and direction of the strain rates measured for the four diamonds of each transect.

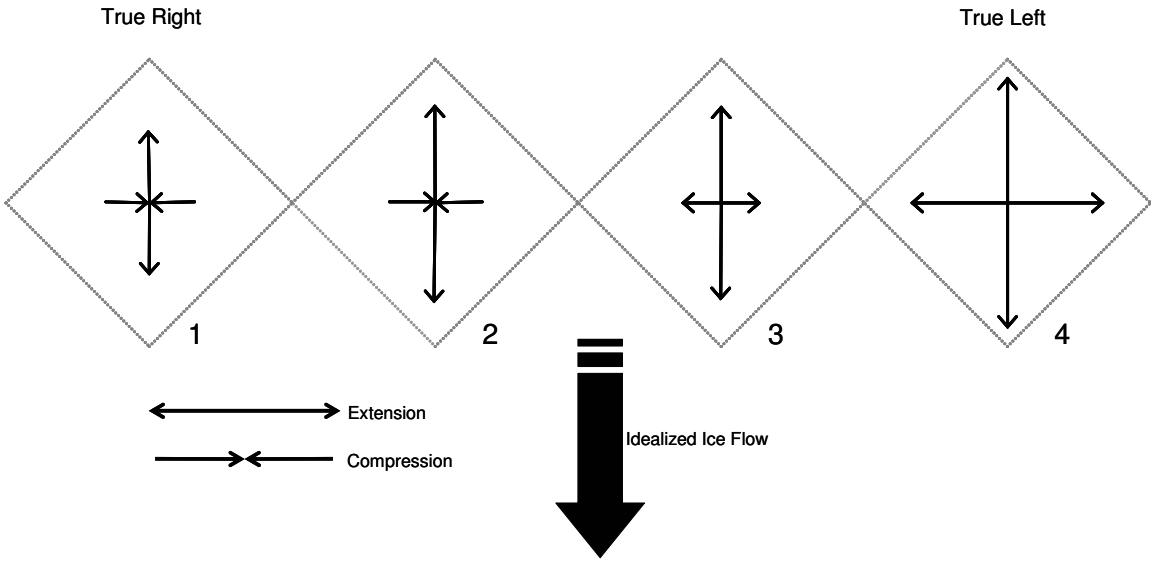

Figure 4.28: Graphical representation of strain rate magnitude in the *x* and *y* directions for diamonds 1-4 in Transect A. Arrows towards the centre represent a compressive strain whilst arrows away from the centre represent extension.

Measured cumulative strains were divided over the 40 day study period for Transect B (Table 4.5) giving strain rates that ranged from 0.03 d^{-1} for the $\acute{\varepsilon}_y$ axis of diamond 2 to -0.13 d^{-1} for the $\acute{\varepsilon}_y$ axis of diamond 4. All four diamonds of transect B had a negative strain rate in the cross-valley *x* axis, with two of the four having a positive strain rate on the *y* axis.

Table 4.5: Strain rates per day (d^{-1}) and per year (y^{-1}) in the *x*, *xy* and *y* axes for diamonds 1-4 in Transect B.

Diamond	d^{-1}			y^{-1}		
	ἐx	ἐxy	ἐy	ἐx	ἐxy	ἐy
1	-0.07	0.05	0.07	-25.92	17.16	26.65
2	-0.07	0.04	0.03	-25.92	14.24	9.49
3	-0.06	0.08	-0.05	-22.63	29.57	-16.79
4	-0.06	0.09	-0.13	-20.44	32.85	-45.99

The relative magnitude of the largest strain rate measured, in diamond 4 of Transect B, is apparent from the strain rate diagram (Figure 4.29). The diagram also suggests that diamonds 3 and 4 on the true left of the glacier experienced an over all compression.

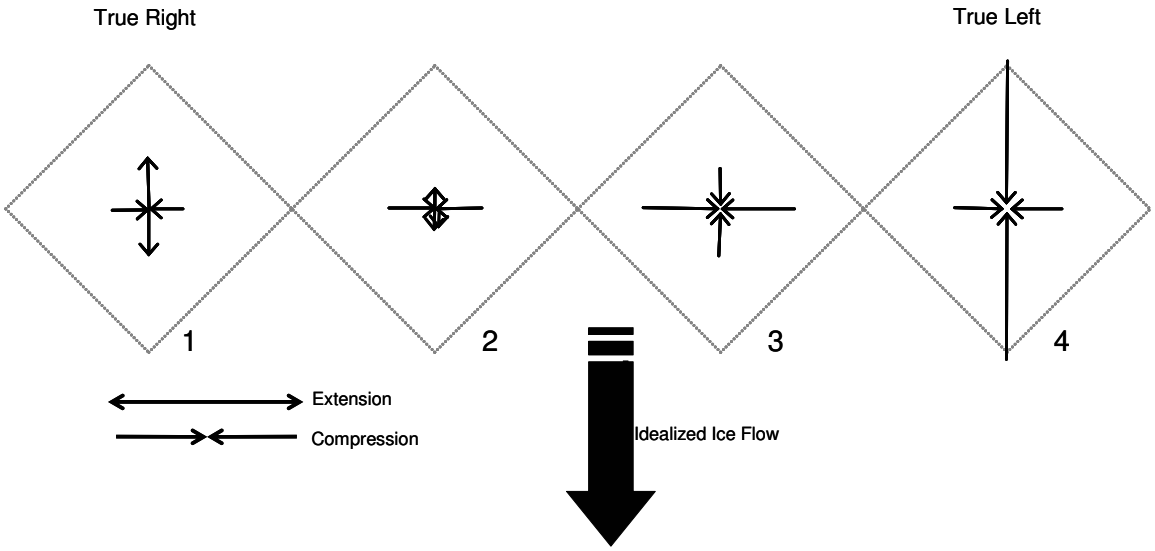

Figure 4.29: Graphical representation of strain rate magnitude in the *x* and *y* directions for diamonds 1-4 in Transect B. Arrows towards the centre represent a compressive strain whilst arrows away from the centre represent expansion.

Measured cumulative strains for Transect C were also divided over a 40 day study period (Table 4.5) giving strain rates ranging from 0.01 d^{-1} for the $\dot{\varepsilon}_x$ axis of diamond 2 to 0.57 d^{-1} for the $\dot{\varepsilon}_y$ axis of diamond 2. Diamond 2 had a positive strain rate in both the *x* and *y* axes, whilst diamond 4 had a negative strain rate in both the *x* and *y* axes.

Relatively low strain rates are apparent in diamonds C and D of transect C on the true left of the glacier (Figure 4.30), compared to the magnitudes seen in diamonds A and B on the true right.

Table 4.6: Strain rates per day (d^{-1}) and per year (y^{-1}) in the *x*, *xy* and *y* axes for diamonds 1-4 in Transect C.

Diamond	d^{-1}			y^{-1}		
	ἐx	ἐxy	ἐy	ἐx	ἐxy	ἐy
1	0.21	-0.44	-0.39	75.56	-162.06	-140.53
2	0.01	-0.12	0.57	5.11	-41.98	208.78
3	-0.15	-0.03	0.03	-53.29	-9.49	10.59
4	-0.02	0.05	-0.02	-7.67	17.89	-5.48

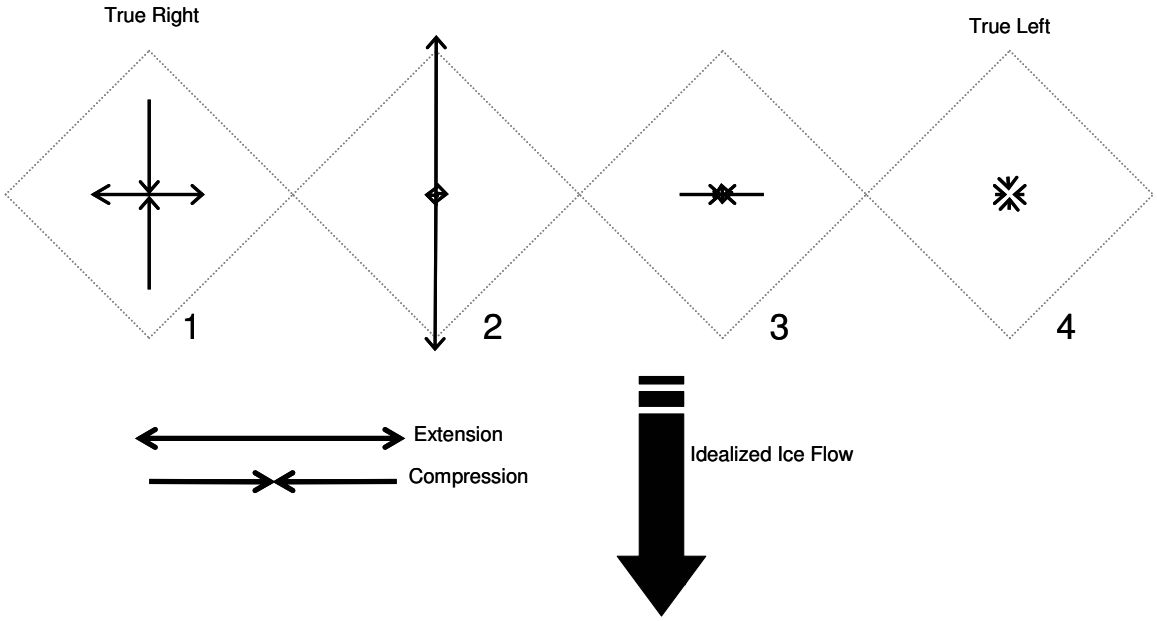

Figure 4.30: Graphical representation of strain rate magnitude in the *x* and *y* directions for diamonds A-D in Transect C. Arrows towards the centre represent a compressive strain whilst arrows away from the centre represent an expansive strain.

4.2.3 Principal Strains

Principal strains are the maximum and minimum strain experienced by a point on a plain when no rotation or shear occurs, and are usually referred to as the major and minor principle strain respectively. Principal strains measured in Transect A (Table 4.7) range from 0.05 (major) in diamond 3, to -0.02 (minor) in diamonds 1 and 2. All major principal strains for diamonds 1 to 4 in Transect A had a positive value, whilst all of the minor principal strains had a negative value, indicating the most dominant strains were causing an extension rather than compression of the ice surface.

Table 4.7: Major and minor principle strain rates for diamonds 1-4 in Transect A. Major strain rates are denoted ɛi, whilst minor strain rates are denoted ɛiii.

Diamond	ɛi	ɛiii
1	0.00	-0.02
2	0.04	-0.02
3	0.06	-0.04
4	0.04	-0.05

The major and minor principle strains can be graphed using Mohr diagrams (Figure 4.31), which represent the magnitude and direction of these strains. The maximum strain is equal to the radius of the circle, whilst the circumference of the circle represents a strain 'envelope' or threshold of failure; which in the case of glacier ice would result in brittle fracture. The major and minor normal strains in a plane such as the surface of the ice are always perpendicular to one another and oriented in a direction at which shear strains due to rotation are zero.

Diamonds 3 and 4 of transect B (Table 4.8) have negative values for both major and minor principal strains rather than a positive major strain and a negative minor strain as measured at the centre of diamonds 1 and 2. Smaller magnitude strains were measured towards the centre of the glacier as shown by the relatively smaller diameter of the

Mohr Diagrams for diamonds 2 and 3 (Figure 4.32). The major and minor principal strains measured in diamond 4 had a different orientation than diamonds 1, 2, and 3.

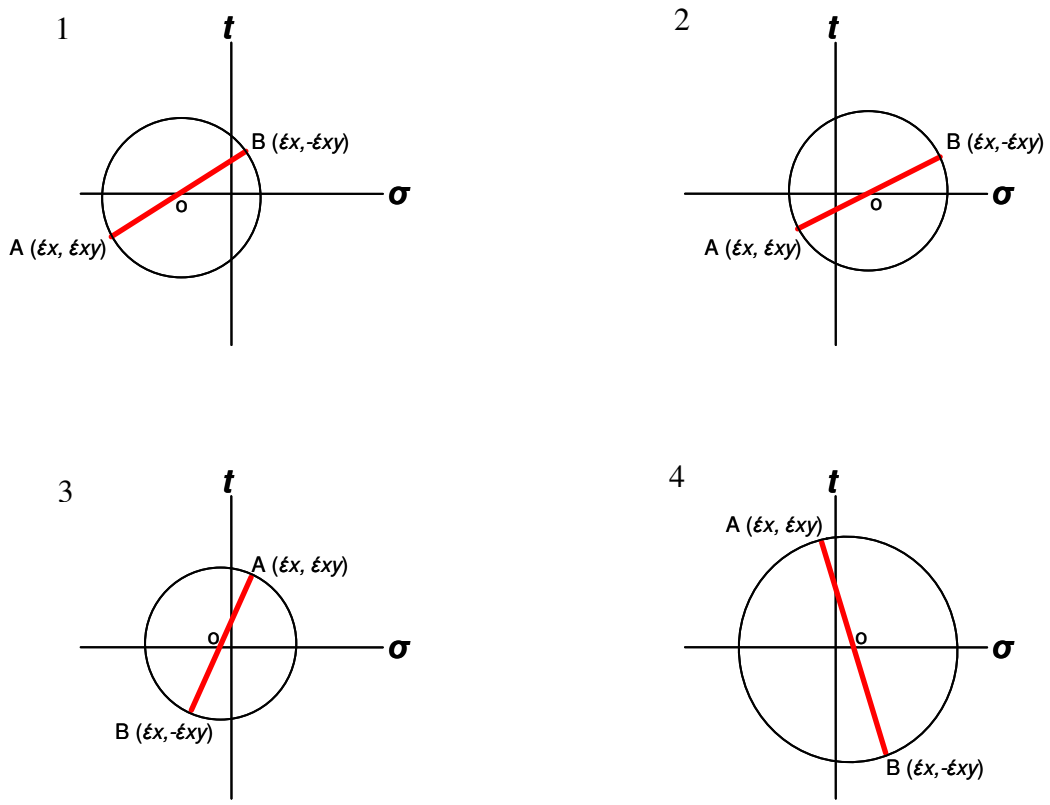

Figure 4.31: Mohr diagrams representing major (A) and minor (B) principal strains measured at the centre of each diamond in transect A. *x* and *y* axes are conventionally represented as *σ* and *t* respectively, with each diagram graphed to the same scale. The centre of the circle is represented by *o* as it intercepts the *σ* (*x*) axis.

Table 4.8: Major and minor principle strain rates for diamonds 1-4 in Transect B. Major strain rates are denoted *ɛ̇i*, whilst minor strain rates are denoted *ɛ̇iii*.

Diamond	ɛ̇i	ɛ̇iii
1	0.08	-0.07
2	0.03	-0.08
3	-0.01	-0.10
4	-0.03	-0.15

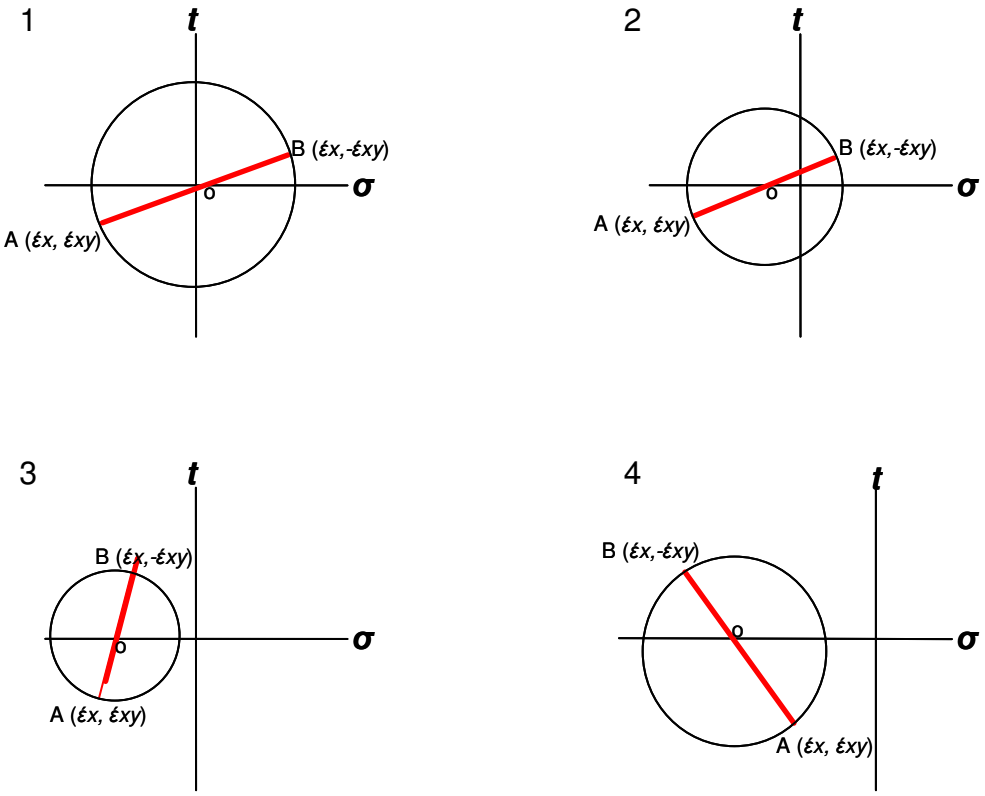

Figure 4.32: Mohr diagrams representing major (A) and minor (B) principal strains measured at the centre of each diamond in transect B. *x* and *y* axes are conventionally represented as *σ* and *t* respectively, with each diagram graphed to the same scale. The centre of the circle is represented by *o* as it intercepts the *σ* (*x*) axis.

Principle strains measured in transect C (Table 4.9) range from 0.53 (major) in diamond 2, to less than 0.01 (minor) in diamond 2. Great variation occurs between diamonds 1 & 2, and diamonds 3 & 4, with diamond 2 having a major principal strain (0.53) more than 80 times greater in magnitude than the major principal strain of diamond C (<0.01). This is reflected by the relative sizes of the Mohr Diagrams in Figure 4.33, which are all graphed at the same scale. The principal strains measured at the centre of diamond 3 are oriented in a different direction to those measured in diamonds 1, 2, and 4.

Table 4.9: Major and minor principle strain rates for diamonds 1-4 in Transect C. Major strain rates are denoted *έi*, whilst minor strain rates are denoted *έiii*.

Diamond	έi	έiii
1	0.28	-0.46
2	0.53	0.01
3	0.03	-0.15
4	0.01	-0.04

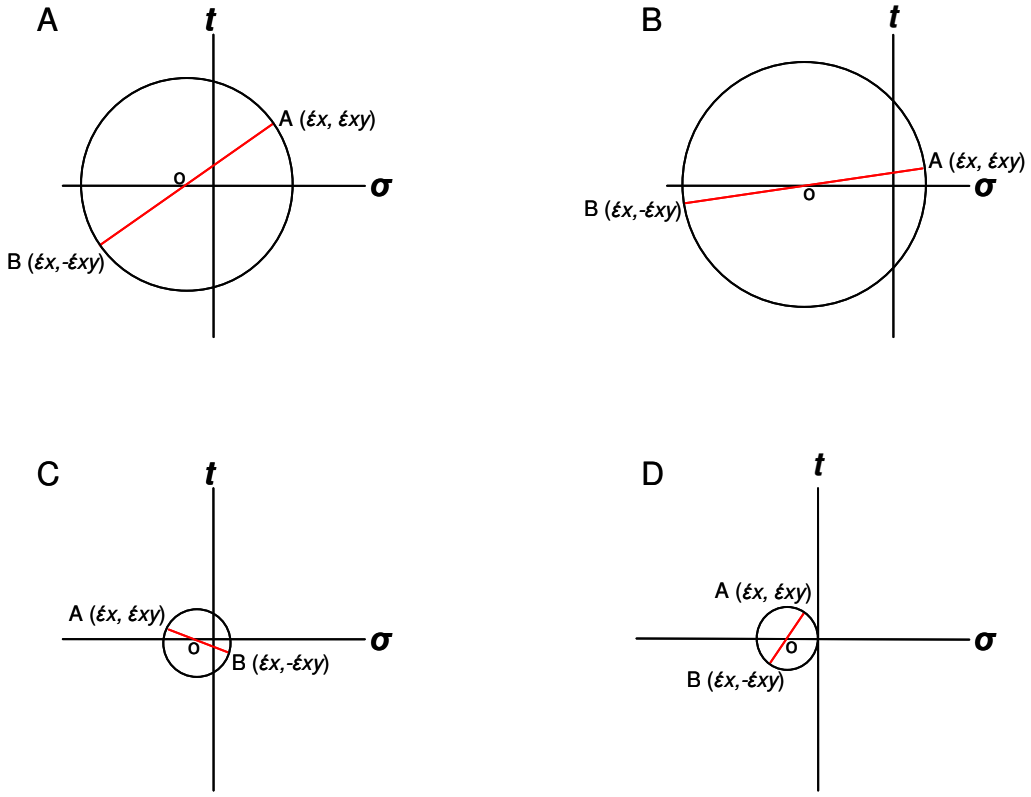

Figure 4.33: Mohr diagrams representing major (A) and minor (B) principal strains measured at the centre of each diamond in transect C. *x* and *y* axes are conventionally represented as *σ* and *t* respectively, with each diagram graphed to the same scale. The centre of the circle is represented by *o* as it intercepts the *σ* (*x*) axis.

4.2.4 Comparisons with Previous Research

The maximum extensional and compressive strain rates ε recorded on Fox Glacier can be compared with results obtained by researchers undertaking studies on other glaciers and ice sheets (Table 5.1). As can be seen from Table 5.1, most previous research has been undertaken on glaciers in Polar Regions such as Antarctica, northern Canada and Alaska, and Svalbard (Spitzbergen) in the high Arctic. The maximum extensional strain rate, ε, recorded at Fox Glacier (208.78 y^{-1}) is more than 650 times as large as the next highest (0.32 y^{-1}) recorded at Austerdalsbreen, in Norway. The maximum compressive strain rate ε recorded at Fox Glacier (-162.06 y^{-1}) is almost 168 times as large as the next highest (-0.97 y^{-1}), again recorded at Austerdalsbreen. These figures suggest Fox Glacier as being highly dynamic, experiencing considerably higher strain rates than glaciers in similar topographic and climatic settings. The results should be considered critically, however, due to the limited study period (<40 days) and the time of year (January/February maximum ablation season) in which the fieldwork was undertaken.

Chapter 5: Discussion

5.1 Structural Mapping

5.1.1 Aerial Photography

At a macro-scale, a great deal of structural detail has been extracted from the aerial photographs of Fox Glacier to produce a structural base map of the study area. The large number of individual features present on the ice surface means mapping each structure would be almost impossible, and produce a very cluttered and confusing structural map. For this reason, general trends of structural type have been recorded for each area of the study site.

Although the structural map is a representation of the aerial photographs, the aerial photographs date from a 1985 survey. Hence, it may be difficult to relate these features with the present-day structure and strain rates found on Fox Glacier. The terminal position is approximately 0.7km further up valley than it was in the mid 1980s (Purdie *et al.*, 2008), suggesting a considerable difference in the volume of ice in the glacier. As discussed in Chapter 2: Literature Review, this will have influences on mass balance and surface gradient, the corollary being that stress distributions within the glacier may have changed.

Despite this, a number of advantages can be gained from using aerial photographic techniques of mapping glaciological structure, rather than relying on ground based observations, such as:

- aerial photography offers an improved vantage point;
- it provides a permanent recording;
- it has broader spectral sensitivity than the human eye;
- it has better spatial resolution and geometric fidelity than many ground-based sensing methods;
- and, it may be easier to measure direction and orientation of features from above (Dickinson, 1969; Amir, 2005).

Aerial photos, on the other hand, display a high degree of topographical distortion, and until corrections are made for the distortion, measurements made from a photograph are not accurate. Notwithstanding this, aerial photographs are a powerful tool for studying the earth's environment (Dickinson, 1969; Goodsell *et al*., 2005[a]; Glasser *et al*., 2006).

5.1.2 Field Observation

The general structure of Fox Glacier is typical of most temperate valley glaciers, but with perhaps a steeper gradient (5-10°) than usually seen. The upper part of the study area on Victoria Flat has a largely subdued topography due to a lower gradient of valley profile and ice surface of less than 5° compared to the lower part of the study area between the first icefall and the snout with typically an approximately 10° surface gradient. Victoria Flat is also much wider (>1km) than the glacier surface width above and below (<0.6km), which are highly constricted by the valley walls. Beneath the lower icefall in the lower part of the study area, the valley is much narrower causing a lateral compression of the ice after it descends the first icefall. More crevassing and broken ice is evident in the lower study area, which may be explained by the steep gradient. The wider valley around Victoria Flat suggests that transverse and splaying crevasses should dominate above the first icefall as tensile stresses cause the glacier to expand. In contrast, below the icefall, chevron crevasses will dominate as ice is compressed and flow at the glacier margins is retarded by valley wall friction (Mair *et al*., 2003).

The most visually striking features of Fox Glacier are the lower and upper icefalls. These are found in steep zones where ice flows rapidly over a step in the valley profile. Acceleration of ice due to this rapid flow down the rock step creates extending flow where ice stretches and thins under tensile stresses, opening up the ice surface into crevasses and serács. The ice is so broken up into serács in the icefalls that access is extremely hazardous. From above, it is sometimes possible to see the subglacial topography at the base of the crevasses in the lower icefall, demonstrating how deep into the glacier these fractures penetrate. In addition, the upper icefall above Victoria Flat is tightly constrained by the steep valley sides of Paschendale Ridge (true left) and Chancellor Ridge (true right), the ice surface being only o.5km wide at this point. Hence, rapid ice flow and deformation in the

upper icefall can be attributed as much to the step subglacial bedrock profile, as well as the narrow valley cross-profile. The corollary is that ice is already considerably deformed by the time it reaches Victoria Flat, the upper part of the study area.

As the valley profile becomes less severe after the icefall the ice slows to a much lower velocity. This deceleration of the ice creates a zone of compressive flow where the crevasses formed through tension within the icefall close and ice thickness increases.

5.1.2.1 Systematic Layering

Systematic layering can be seen in crevasse walls and areas of exposed ice throughout the study site. Systematic layering is characteristic of deeply buried, englacial ice. Some areas of layering observed in the upper part of the study area are identifiable as extending across the full width of the glacier. This indicates the layers formed in the large ($25km^2$) Fox névé before flowing down into the more confined, upper Fox valley.

Formed in a similar process to sedimentary stratification, systematic layering forms from annual accumulation layers in the névé area of Fox Glacier. Each year's accumulation undergoes the transformation cycle from fresh snow to firn and then to glacier ice, giving the compressed layers seen throughout the glacier. The layers are of two main types: course-grained bubbly white ice, and hard blue smooth ice. The course ice is likely to have formed from winter snowfall accumulation in the upper part of the accumulation area, whilst the harder blue ice is characteristic of summer ablation ice and superimposed ice caused by the refreezing of melt water (c.f. Paterson, 1994). Debris suspended in the blue ice supports this, as it suggests wind blown debris entrainment, as occurs during the formation of ogives (Yamaguchi *et al*., 2007).

Initially horizontal, as the glacier flows down-valley, the layers are slowly deformed and rotated producing the high angles of strike and dip seen in the lower part of the study area and in the lower icefall. Unconformities in the layers seen in the study area may have been caused by the truncation of layers by excessive ablation or fracturing of ice into crevasses.

5.1.2.2 Crevasses

Crevasses are the most obvious structural feature on the surface of Fox Glacier, both from aerial photographs and field observations. The type and spatial distribution of the crevasses varies considerably throughout both the upper and lower parts of the study area.

The upper part of the study area between the lower and upper icefalls is characterised by transverse crevasses. These crevasses are the product of shear stress and longitudinal tensile stress. As ice flows down and over the first icefall, its velocity increases causing a longitudinal extension of the ice immediately up-glacier on Victoria Flat. This rapid extension causes the fracture of the ice seen in the glacier-wide fractures. Figure 4.25 demonstrates this with the expansion or stretching of the deformation diamonds in the down-valley direction, parallel to ice flow.

At the snout of the glacier in the lower part of the study area longitudinal crevasses are dominant. Due to rapid surface ablation, and a widening of the valley, pressure is unloaded from the glacier tongue causing a lateral expansion of the ice. In the process of the ice expanding and widening, the ice fractures and produces very deep (>20m), broken crevasses that can be followed from the surface of the glacier to the subglacial zone close to the terminus. The rapid loss of ice volume and subsequent loss of lateral confining pressures has also resulted in the formation of splaying crevasse at the snout of the glacier. Hence, in the lower study area, above the snout, the glacier surface topography is deeply-entrenched. Figure 2.27 shows a lateral expansion of the deformation diamonds as the transect becomes wider.

Along both the true left and true right of the glacier in the upper and lower study area, chevron crevasses can be seen. These are symptomatic of drag, friction and shear stress exerted by the valley walls. As the glacier flows more rapidly at the centre than at the margins, tensile stresses pull the ice down-valley away from these margins and in towards the centre, opening up the ice surface at approximately 45° (Benn and Evans, 1998). Splaying crevasses appear more characteristic of the true left of the glacier. It would appear that this is because of shear stress produced by frictional resistance of the valley wall below

Paschendale Ridge. This is in conjunction with a longitudinal compressive stress produced by a 45° re-orientation of the glacier following the valley topography (the valley axis changes from a northwest orientation to a westerly orientation). Together, these two factors appear to have produced crevasses approximately parallel to the flow of the ice towards the centre, but which curve outwards towards the ice margin down-valley. Where there is limited or no longitudinal compressive stress such as on the true right of the glacier in the upper study area, splaying crevasses are replaced by chevron crevasses, which are the product of frictional resistance of the valley walls, and form obliquely up-valley from the ice margin, running towards the centre of the ice.

5.1.2.3 Crevasse Traces

As some of these crevasses formed by tensile stress have closed due to compressive flow or rotation, crevasse traces have been formed. These linear scars are seen over almost all of the study area, and show the location of relict crevasses. Most of the crevasse traces seen in the lower part of the study area are apparent by the dirt and debris trapped in them as the crevasse has allowed fine debris to be deposited whilst the crevasse is subaerially exposed before closing. This material has been collected in the ablation area and ice fall probably during the summer when the concentration of wind blown material is at its greatest. During this time, material in the glacial environment becomes dried by reduced precipitation and increasing sunshine and temperatures. This dry material is much less cohesive and much more easily entrained by the wind to be moved across the glacier via Aeolian transport and saltation.

Higher up the study area, crevasse traces have a cleaner appearance. They are constructed of layered white, course bubbly ice most probably the result of crevasses that were snow filled at the time of closing. Crevasse traces in the upper part of the study area also formed as crevasses closed before they reached the zone of the glacier that received the maximum amount of surficial debris from Paschendale ridge, and the numerous creeks on both the true left and true right of the valley. This would have prevented dirt and debris from falling into crevasses prior to closing.

The cross cutting of some crevasse traces into others in the lower study area, suggests ice containing crevasse traces has undergone at least two cycles of deformation. Tensile stress, as ice expands, forms crevasses in ice which has already experienced the compressive stress that closed up the crevasses originally, once again. These newer crevasses then close due to later compression. Some of these traces may never have been open crevasses, and rather created by the stretching of ice below the threshold of fracture, producing narrow tensional veins, as are often seen in rock. Hence, the cross-cutting crevasse traces indicate two cycles of deformation which may relate to ice in the lower part of the study area having passed through both the upper and lower icefalls.

Initially sub-vertical, the crevasse traces in both the upper and lower parts of the study site have been rotated so that most now have an up-glacier dip.

5.1.2.4 Foliation

The foliation identified is mainly of a transverse nature. The layers of course-grained bubbly ice make up arcs similar in appearance to ogives, with a convex, down-valley morphology in plan-form. Some longitudinal foliation can be observed crosscutting the transverse features in the lower study area.

The orientation of foliation suggests high strain rates in the ice. Originally formed approximately parallel to the ice surface as depositional systematic layers during accumulation, as crevasses traces or tensional veins, the layers show high angles of dip by the time ice has flowed into the study area. The sequence of deformation experienced as the ice has flowed from the névé and through the two icefalls has rotated and folded the layers.

5.1.2.5 Folding

Observed folding is likely to have been created by the compressive flow of ice below the two icefalls within the study area. After flowing through the icefall at a relatively high velocity, the ice will decelerate rapidly and begin to compress, causing sections of ice to compress into ice ahead that has already decelerated. As the two sections of ice merge, ice is deformed and folded.

Folding was more obvious below the second icefall in the upper part of the study area in Victoria Flat, than in the lower part of the study area between the first icefall and the glacier snout. This may be explained by the ice in the much more subdued topography of the Victoria Flat area being less disturbed by the processes that have created the steeper, more broken topography of the lower study area. This has allowed the developed fold axes and fold trains to survive as they are transported down-glacier from their formation below the upper icefall. Folds are more obvious on the true left of Victoria Flat, as flow slows and the glacier flows left over the lower icefall.

Nevertheless, it should be concluded that it has been difficult to identify all areas in which folding has taken place. Folds are only obvious in areas characterised by layering, or foliation, where the individual layers make the fold axis and limbs more obvious than in clean ice. Further, the walls of open crevasses provide an opportunity to recognise folded ice but such surfaces are difficult to analyse without descending into the crevasse.

5.1.2.6 Moulins

Moulins are present in both the upper and lower parts of the study area. Below the first and second icefalls, closed crevasses and crevasse traces provide structural weakness which supraglacial meltwater has exploited. Moulins in the upper study area are much more developed than those in the lower study area, where meltwater and rainfall flows into cracks and crevasses rather than well formed cylindrical drainage holes, due to moulins being more highly deformed in the lower study area. The difference in development is apparent from the range of Moulin diametres recorded in Chapter 4: Results.

There is also an apparent disparity between the frequency of moulins in the upper study area compared to the lower study area. Large volumes of water flow into a relatively small number of large moulins in the upper area, whilst a smaller volume of water flows into a larger number of relatively smaller moulins in the lower study area. This is due to the development of a well-developed dendritic supraglacial stream network, which has formed on the relatively level surface of Victoria Flat, concentrating water into channels. Surface

topography is too broken up and steep for the development of such a network in the lower study area.

The drainage networks supplying water to moulins on the glacier surface are highly dynamic, and in some situations, diurnally ephemeral. The drainage patterns are constantly changing with some channels becoming inactive due to ablation creating a highly dynamic surface topography, which diverts and re-routes supraglacial water. Some moulins only appear to become active when sufficient supraglacial water is present, such as following a major rainfall event. Indeed, increasing volumes of supraglacial water after heavy rainfall events often means that more water enters the system than can be discharged through the englacial and subglacial drainage network. Because the conduit network cannot adjust rapidly enough by melting to cope with high discharges, water 'backs up' the system (e.g. Nienow et al., 2005). The internal diameter and volume of drainage conduits may be insufficient to transport the extra water, causing the development of slush swamps and supraglacial 'perched' ponds (e.g. Higuchi and Tanaka, 1982; Benn *et al*., 2001). These are more common in the upper study area, due to the gentle topography, but also occur in the lower study area. However, the supraglacial pools in the lower study area tend to be water-filled crevasses, the outlet of which has been blocked, possibly as a result of deformation of the ice. The strong influence exerted by crevasse distribution of the location of moulins means that englacial drainage can be routed in directions very different from those predicted by theory (e.g. Stenborg, 1973; Fountain, 1993; Campbell *et al*., 2006).

5.1.2.7 Exposed Englacial Conduits

Within areas of disturbed ice and often in the walls of crevasses it is possible to observe exposed englacial conduits. These conduits make up part of the englacial drainage system developed to transport supraglacially derived meltwater from moulins and crevasses via discrete channels often to the ice-bed interface at the glacier bed. These conduits are identifiable by their smooth internal surface indicating the dissipation of sensible heat and mechanical energy.

The conduits have been exposed at the surface due to disturbance of the ice by fracturing and crevassing, but are also seen due to melt out of the ice surface (e.g. Holmlund, 1988) due to summer ablation, typically 60mm to 90mm/day at Fox Glacier (Purdie *et al*., 2007). The internal appearance and diameter of exposed englacial conduits suggests they represent elements of a distributed drainage network within Fox Glacier. Distributed drainage systems are inefficient as water follows more tortuous routes through a poorly connected network. This is supported by the observation of water backed-up from moulins onto the glacier surface following heavy precipitation events.

5.1.2.8 Surficial Debris

The expansive area of supraglacial debris seen on the true left of the lower part of the glacier is a product of rock falls and rock slides from Paschendale ridge and the gullies incising the true left valley side. That supraglacial debris is confluent with scree within the gullies suggests a 'coupling' between debris and transport by the glacier, analogous to fluvial systems (e.g. Harvey, 2001). The Fox valley is of very high relief, with steep valley walls, particularly on the true left of the valley. The steep terrain and close proximity of the ice to the valley sides allows for a coupling of slope and glacier processes. As the glacier flows down-valley at the base of Paschendale Ridge it undercuts and over-steepens the valley side. This causes instability and mass wasting of the valley wall supplying large quantities of material to the ice surface.

In some areas, the ice has separated from the valley wall forming areas of bergschrund or randkluft allowing access between the upper and lower study areas, bypassing the first icefall. This area is known locally to climbers as "Suicide Alley", giving an indication as to how unstable the rock of the valley side is! These areas probably form partly because of the preferential ablation adjacent to warm rock surfaces, which have a northern aspect. These fissures may also reflect movement of ice away from the rock wall (Mair and Kuhn, 1994). Ice movement such as this from the true left to the true right of Fox valley can be seen in Figure 4.26.

As the ice turns left after the first icefall, some of the material in the lateral moraine seen down true left is forced towards the centre of the glacier. The concentration of material on the surface increases lower down the glacier as ablation increases. More material is melted out and deposited at the glacier snout. The surficial debris seen in the cone deposits on the true left and true right appear to have undergone passive transport at the glacier surface as is suggested by the C_{40} and RA values recorded in Chapter 4: Results. These values can be plotted on a covariance plot displaying facies envelopes thought to represent the process-origin of the material (Figure 5.1). Indeed, data from the present study is reasonably consistent with the facies envelopes of Glasser *et al*. (2006). Material from the true right of the glacier (Point B) plots towards the centre of the scree/supraglacial debris envelope, with material from the true left (Point A) just outside. This suggests that with careful sampling, C_{40} and RA index is a powerful discriminator of transport pathways through glaciers, as suggested by Goodsell *et al*. (2002) and Hambrey and Ehrmann, 2004. The very fine-grained material seen in some areas of the lower study area (Point C, Figure 5.1) directly below the lower icefall, may originate from the subglacial zone. As the ice is squeezed and laterally compressed as it enters the narrower lower glacier, fines can be thrust upwards along thrust planes or crevasse traces that permeate to the glacier bed, deposited material onto the glacier surface. Such material can form debris-charged ridges, if enough material is deposited; implying compressional glaciotectonics toward the glacier snout (e.g. Glasser *et al*., 2003). Previous research (Goodsell *et al*, 2005[b]) has also suggested outburst events as a cause for the surficial deposition of material displaying the characteristics of more active transport (Figure 5.2).

Supraglacial debris is not usually considered a glacial structure, but it has important influences on rates of ablation, formation and routing of meltwater, hence flow and behaviour of the glacier. Movement of ice is, as we have seen, fundamental to the production of strain and stress, and so the formation of structures.

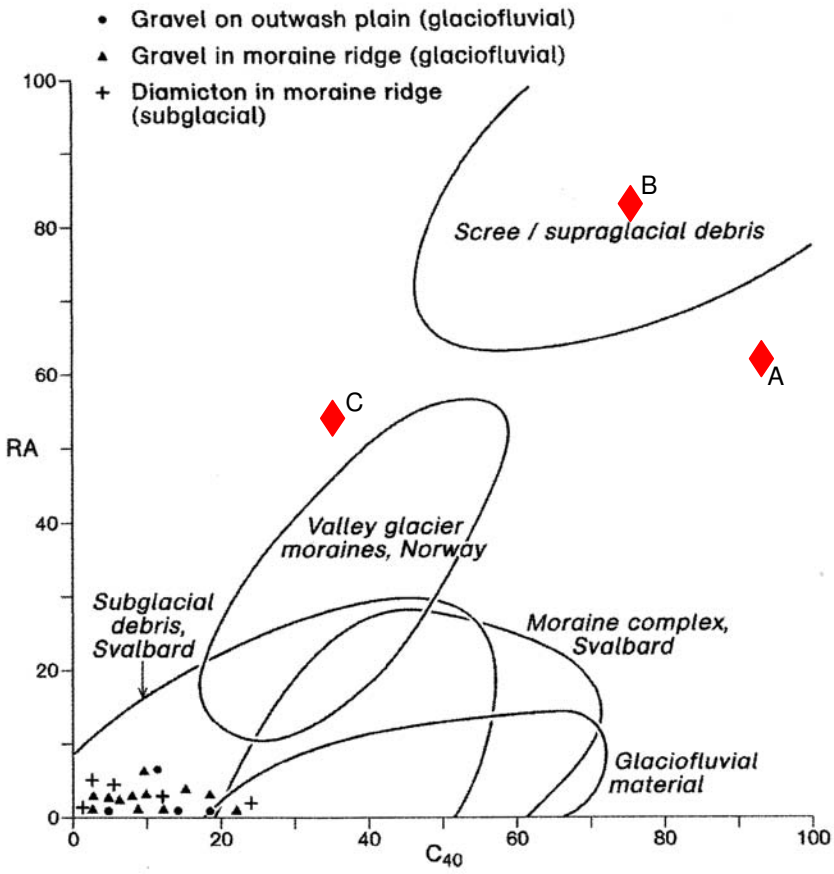

Figure 5.1: Covariant plot of RA index (percentage of angular and very angular clasts) against the C_{40} index (percentage of clasts with c/a axial ratio ≤0.4) reproduced from Glasser *et al.*, 2006. The superimposed points A, B and C represent the surficial debris samples from the true left, true right and centre of Fox Glacier, respectively.

5.1.2.9 Arcuate Bands (Ogives)

Strictly speaking, a topographic rather than structural feature, ogives are found in both the upper and lower study area and can be seen displaying a convex down-valley planform morphology, representing a greater velocity at the centre of the ice compared to the ice margins where flow is retarded by the frictional resistance of the valley walls. The ogives have probably been formed annually, with each light-dark or ridge-trough pair representing one year of ice movement (Benn and Evans, 1998). They reflect seasonal variation in the

passage of ice through icefalls (Nye, 1958), and as such, the upper part of the study area contains a different ogive formation to those in the lower part of the study area.

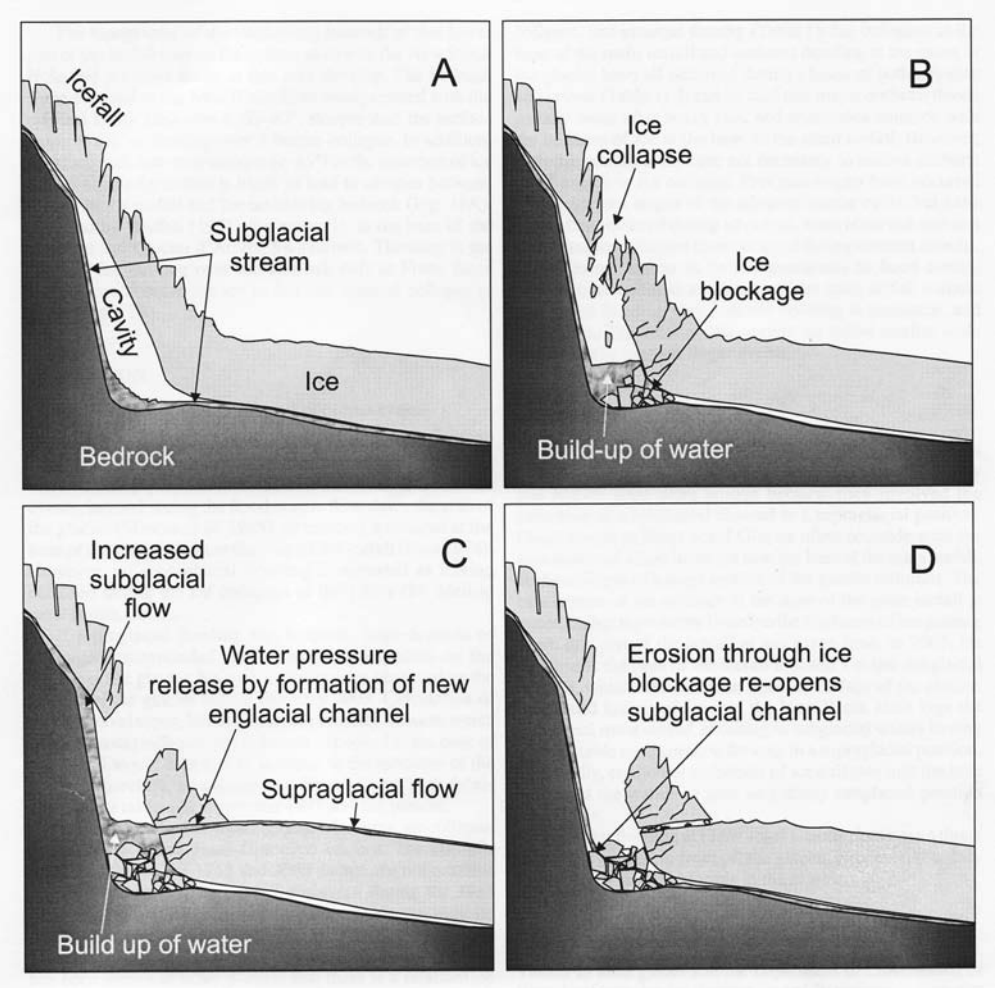

Figure 5.2: Schematic interpretation of an outburst event below an icefall causing the surficial deposition of englacially and subglacially derived material; (A) Normal configuration with steep bedrock beneath the base of an icefall, with the ice detached from the wall, and a subglacial stream beneath the ice; (B) Increased subglacial flow in response to rainfall and collapse of thinner ice, blocking flow of the subglacial stream; (C) Pressure of water build-up forces routing of the subglacial stream over the ice surface, depositing englacial material on the surface; (D) Subglacial stream erodes down to subglacial position through blockage (Goodsell *et al.*, 2005[b]).

Ogives in the upper part of the study area on Victoria Flat, are of the wave or 'swell and swale' type, and have the appearance of a repeating pattern of ridges and troughs. This ridge-trough pattern reflects winter passage through the upper icefall. As ice velocity

increases as ice flows down the icefall, the ice undergoes longitudinal expansion and becomes thinner. As the upper icefall is close to the equilibrium line altitude (ELA) and accumulation area, winter snowfall settles on this longitudinally extended, thin ice. Upon decelerating below the icefall, the material is compressed, but there is now the added mass of the winter snowfall. This extra material builds up to form a ridge (Hambrey and Alean, 2004).

In the lower part of the study area between the snout and lower icefall, the ogives are banded, and show alternating bands of light and dark ice. The dark bands consist of highly foliated dirty ice, which holds a large amount of debris (Ragan, 1969). The first icefall is much further down the valley than the second icefall, and so is further below the ELA, into the ablation area. Ice passing through the icefall during the summer will therefore lose a great deal more mass through ablation, than during the winter. The dirt and debris already contained in the ice will become concentrated as the ice melts, and will give the remaining ice a much darker and dirtier appearance. The thinner, longitudinally extended ice will also have an increased surface area, giving a larger area for wind blown and superficial debris to collect. Once again, the ice will slow at the base of the icefall then become compressed, forming dark bands (Benn and Evans, 1998; Goodsell *et al*., 2005[a]).

5.1.3 Conceptual Model of the Structural Evolution of Fox Glacier

To understand the structural evolution of the Fox Glacier, it is possible to distinguish between phases of deformation (Figure 5.3) as highlighted by Hambrey and Milnes (1977), and Goodsell *et al* (2005[a]). The first phase (A) involves the systematic layering of accumulation deposits that produces the primary stratification that pervades most of the glacier along its length. As the ice is funnelled into the narrow valley from the wide névé, individual flow lines converge and the ice undergoes a transverse compression.

Secondly B) sees the ice rapidly accelerate as it flows down the upper icefall. The steep profile allows tensile stresses to cause longitudinal expansion and stretching of the ice, producing the highly fractured surface seen within the icefall.

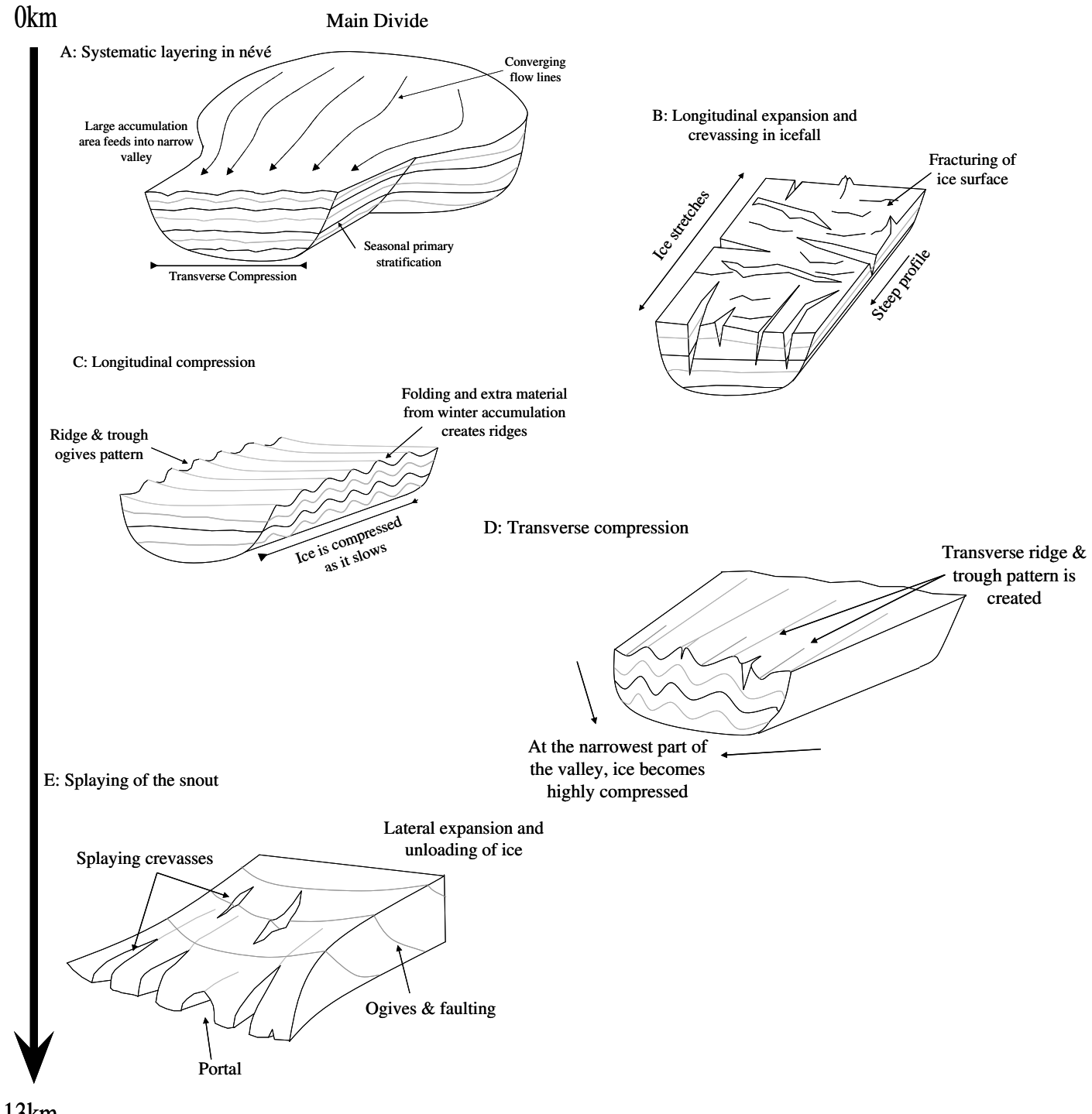

Figure 5.3: Modelled schematic diagram of the structural evolution of Fox Glacier; A) Systematic layering in névé produces S_0 Primary Stratification, with a narrowing valley causing convergence of flow lines; (B) Longitudinal expansion and crevassing of ice flowing over upper icefall; (C) Longitudinal compression creating ridge & trough ogives as ice slows on Victoria Flat; (D) Transverse compression as ice enters narrowest part of valley creating characteristic cross-glacier ridge & trough; (E) Rapid unloading, ablation and expansion causes splaying crevasses to develop at the snout.

As the glacier decelerates as it reaches the much more subdued Victoria Flat (C), the ice is longitudinally compressed, creating a 'ridge and trough' ogive pattern, and folding of primary stratification, as units of ice catch up and low into units of ice that are ahead and decelerating.

This longitudinal ridge and trough pattern in (C) is replaced by a transverse ridge and trough pattern in (D) as the ice becomes transversely compressed and squeezed as the glacier flows into the narrowest part of the valley. This compression causes fracturing at the valley sides as friction between the valley sides and ice margins is rapidly increased. Finally, unloading and ablation (E) allows for the formation of splaying crevasses at the snout.

5.1.4 Accurate Identification of Structural Features

The identification of structural features, both in the field and from remotely-sensed images is highly subjective. Individual researchers may view the same feature differently, and conclude varying processes of formation. Recent discussion in the scientific literature (Woodward *et al*., 2002; Woodward *et al*., 2003; Glasser *et al*., 2003; Woodward *et al*., 2003) has highlighted the varying 'schools of thought' on the appearance and formation of glaciological structural features. Experience and a sound knowledge of structural feature identification is required to gain consistent results, and derive accurate conclusions from fieldwork and aerial photography derived glaciological data

5.2 Strain & Deformation

5.2.1 Strain in the Fox Glacier

Measured strain varies considerably across the surface of Fox Glacier, both longitudinally and transversely. The highest cumulative strains έ (27.37 and -19.49) were recorded in the lowest transect, Transect C, close to the glacier's snout, whereas the lowest cumulative strains έ (0.04 and -0.01) were recorded in Transect A on Victoria Flat. The highest cumulative extensional strain έ was measured as 27.37 in the 0° direction for Diamond 2 of Transect C, with the highest cumulative compressive strain έ measured at -13.64 in the 90°

direction for Diamond 3 of Transect C. The areas experiencing the highest cumulative strains έ are also the areas that have the most deformed and broken ice surface. For example, Transect C is in an area of highly crevassed and deformed ice in which most features including primary stratification, foliation and crevasse traces are highly rotated from their original orientation.

The lowest cumulative strains έ were recorded in Transect A at the lower end of Victoria Flat. The lowest extensional cumulative strain έ was measured as 0.04 in the 45° direction for Diamond 2 of Transect A, whilst the lowest compressive cumulative strain έ was measured as -0.02 in the 90° direction for Diamond 1 of Transect A. Transect A was in the area of most subdued ice surface topography. The glacier surface is at its lowest gradient in this part of the valley (<5°), with the ice being less transversely compressed than in the areas above or below Victoria Flat.

This trend is supported by the strain rates calculated from the cumulative strains recorded over the various study period lengths. The highest strain rates were, again, measured in Transect C, with the highest extensional strain rate being recorded as 208.78 y^{-1}, in the $\dot{\varepsilon}_y$ direction for Diamond 2 of Transect C, and the highest compressive strain rate of -162.06 y^{-1} in the $\dot{\varepsilon}_{xy}$ direction for Diamond 1 of Transect C.

As with cumulative strains, the lowest strain rates were recorded in Transect A on Victoria Flat, with the lowest extensional strain rate of 0.73 y^{-1} being measured in the $\dot{\varepsilon}_{xy}$ direction of Diamond 1 in Transect A, and the lowest compressive strain rate of -1.10 y^{-1} being measured in the $\dot{\varepsilon}_x$ direction of Diamond four in Transect A.

In summary, it is difficult to determine the precise significance of two-dimensional stress and strain measurements, as glacial surface ice also reflects the strain history of ice as it has been rotated towards the surface during its transport down-valley. Nevertheless, findings do indicate that structures do correspond somewhat to calculated strain rates.

5.2.2 Comparison with Previous Research

Data from a number of other studies (Table 5.1) can be compared to the strain rates recorded at Fox Glacier, to relatively quantify how strained and deformed the ice of Fox Glacier is compared to other glaciers.

Compared to the recorded strain rates on other glaciers, the strain rates recorded on Fox Glacier are exceptionally high at 208.8 y^{-1} and -162.06 y^{-1}, with the next highest being recorded at Austerdalsbreen in Norway, also a temperate valley glacier, with strain rates of 0.32 and -0.97, more than 650 times smaller than Fox. Blue Glacier, Washington, and Griegletscher, Switzerland (two more temperate alpine glaciers) experienced stresses of approximately 0.1 y^{-1} and -0.1 y^{-1}, considerably lower than Austerdalsbreen. The lowest strain rates have been recorded on cold based Polar glaciers such as Shirase Glacier, East Antarctica, and Hiorthfjellet Glacier, Svalbard, experiencing strain rates of $5x10^{-4}$ y^{-1} and $8x10^{-5}$ y^{-1} respectively. These vast differences suggest Fox Glacier is much more dynamic than other glaciers where strain rates have been calculated.

Considering the size of the Fox Glacier névé, the narrow width of the Fox Valley, and the high rates of accumulation and ablation, this is quite possible. However, it must be remembered that measurements were taken at the most active time of year for glaciers on the West Coast of New Zealand's South Island. Relatively high temperatures (up to 22.5°C) (Purdie, 2005) during the ablation season create large quantities of melt water which increase ice velocity (0.5 to 1.4m/day) (Purdie, 2005) and strain. It should also be remembered that this study was undertaken over a short period and so it may be difficult to extrapolate these results to the entire year, without undertaking the same study during the autumn, winter and spring seasons. There is a huge seasonal variation in velocity (Purdie *et al*., 2007), and so the recorded strain rates give a 'snap-shot' of the summer melt season. If the study period was extended to include the entire year, strain rates would almost certainly be much lower.

5.3 Relating Strain and Structure

Structures in ice form in response to deformation usually operating over several decades in valley glaciers (Goodsell *et al.*, 2005[a]), but more likely a few years at Fox Glacier, due to the very high strain rates occurring, and the rapid response time of 9 years (Purdie *et al*., 2007). The results suggest a relationship between the observed structures on the surface of Fox Glacier and the measured cumulative strain and strain rates.

It should be noted though, that the variation in tensile strength of ice and so the strain rate at which it fractures and produces the features reported could be ascribed to differences in crystal structure, impurity content, density profiles or other local variables (Vaughan, 1993). Vaughan (1993) found that the critical strain rate for failure of ice varied by a factor of 500 over the sites compared during the study. This suggests that the relationship between strain and structure is not a simple one.

Strain ellipses have been used in other studies (e.g. Hubbard and Hubbard, 2000; Goodsell *et al*., 2005[a]) to show how measured strain rates relate spatially to observed structures. A similar approach is taken here and is represented by Figure 5.4. There is a notable similarity between the deformation of the strain ellipses and the deformation of structures observed on the surface of the Fox Glacier. Indeed, as the strain ellipses (having descended the upper icefall) are transported down valley, representing ice flow,

- The three ellipses remain unchanged in shape as they move through Victoria Flat but spread out transversely and longitudinally as the valley widens, and the middle ellipse has a greater velocity at the centre of the glacier than the two ellipses closer to the glacier margins.
- The ellipses extend longitudinally on the true right as the ice velocity increases as it flows over the lower ice fall. The ellipses on the true right remain unchanged and may even undergo small amounts of compression as the valley turns to the true left.
- All three ellipses are compressed as ice velocity decreases at the base of the lower icefall.

- The ellipses extend longitudinal as they undergo transverse compression from the narrowing valley walls, as they get closer to the snout. The ellipses also become orientated with the features observed in the lower part of the study area.

It should be noted that this is a very simplified simulation, as in reality, ice begins to be deformed as it is flowing toward, and down, the upper icefall prior to reaching the upper–most part of the study area.

5.4 Future Research

This study has by no means been exhaustive, though some interesting questions can be raised from the results and observations made. For this reason, a number of possible future studies can be suggested to further investigate the structural glaciology and related features of Fox Glacier.

5.4.1 Ground Penetrating Radar of Structure

Ground penetrating Radar (GPR) may be employed to determine characteristics of the basal environment and englacial structure. Using electromagnetic energy GPR can be used to determined basal topography by means of a digital elevation model (DEM) (e.g. Langley *et al*., 2007; Yamamoto *et al*., 2004) and ice-bed interface material. The surface topography of the bed may alter the characteristics of the ice as it flows down-valley, influencing the types and location of structures seen at the glaciers surface. For example, obstructions or areas of bed unconformity may cause an increase in friction at the ice-bed interface and so cause brittle fracture at the ice surface in an area that may not otherwise experience crevassing.

Ground penetrating Radar may also be used to determined internal structures such as crevasses (e.g. Woodward and Burke, 2007) and thrust faults (e.g. Irvine-Flynn *et al*., 1997). Identifying the englacial structure in addition to the surface structure of the Fox Glacier will allow for an understanding of what internal processes are occurring, and where.

Table 5.1: Previous research measuring strain rate of various types of glaciers in a variety of locations.

Location	Type of Glacier	Maximum Extentional Strain Rate y^{-1}	Maximum Compressive Strain Rate y^{-1}	
Austerdalsbreen, Norway	Temperate, Alpine Valley	0.32	-0.97	Nye (1959)
Saskatchewan Glacier, Alaska	Polar, Icefield Outlet	0.15	-0.19	Meier (1960)
Taku Glacier, Alaska	Polar, Tidewater	0.11	-0.13	Wu & Christensen (1964)
Mendenhall Glacier, Alaska	Polar, Calving, Icefield Outlet	0.31	-0.18	Higashi (1967)
Hintereisferner, Austria	Temperate, Alpine Valley	0.08	-0.15	Ambach (1968)
Athabasca Glacier, Canada	Polar, Icefield Outlet	0.16	-0.12	Raymond (1969)
Meserve Glacier, Wright Valley, Antarctica	Polar, Icecap Outlet	0.02	*	Holdsworth (1969)
Kaskawulsh Glacier, Alaska	Polar, Icefield Outlet	0.29	-0.29	Anderton (1973)
Blue Glacier, Washington	Temperate, Alpine Valley	0.12	-0.1	Meier *et al* (1974)
Griegletscher, Switzerland	Temperate, Alpine Valley	0.1	-0.16	Hambrey (1978)
White Glacier, Canada	Polar, Outlet	0.16	-0.43	Hambrey (1978)
Urumqi Glacier Number 1, China	Cold Based, Alpine	0.06	*	Echelmeyer & Wang (1987)
Storglaciaren, Sweden	Polythermal, Alpine	0.02	*	Hooke et al (1989)
Jutulstraumen, Antarctica	Polar, Outlet	0.05	*	Hoydal (1996)
Unteraargletscher, Switzerland	Temperate, Alpine Valley	0.05	*	Guddmundsson et al (1997)
Haut Glacier d'Arolla	Temperate, Alpine Valley	0.015	*	Hubbard et al (1998)
Glaciar Upsala, Patagonia	Mountain, Calving Outlet	0.22	*	Naruse & Skvarca (2000)
Amery Ice Shelf, East Antarctica	Polar, Calving Ice Shelf	0.1	*	Young & Hyland (2002)
Hiorthfjellet Glacier, Svalbard	Polar, Valley	$8x10^{-5}$	*	Ødegård *et al* (2003)
Shirase Glacier, East Antarctica	Polar, Calving Icecap Outlet	$5x10^{-4}$	*	Pattyn & Naruse (2003)
Koryto Glacier, Russia	Polar, Valley	*	-0.36	Sugiyama *et al* (2005)
Fox Glacier, New Zealand	Temperate, Maritime, Valley	208.78	-162.06	This Study

*No data

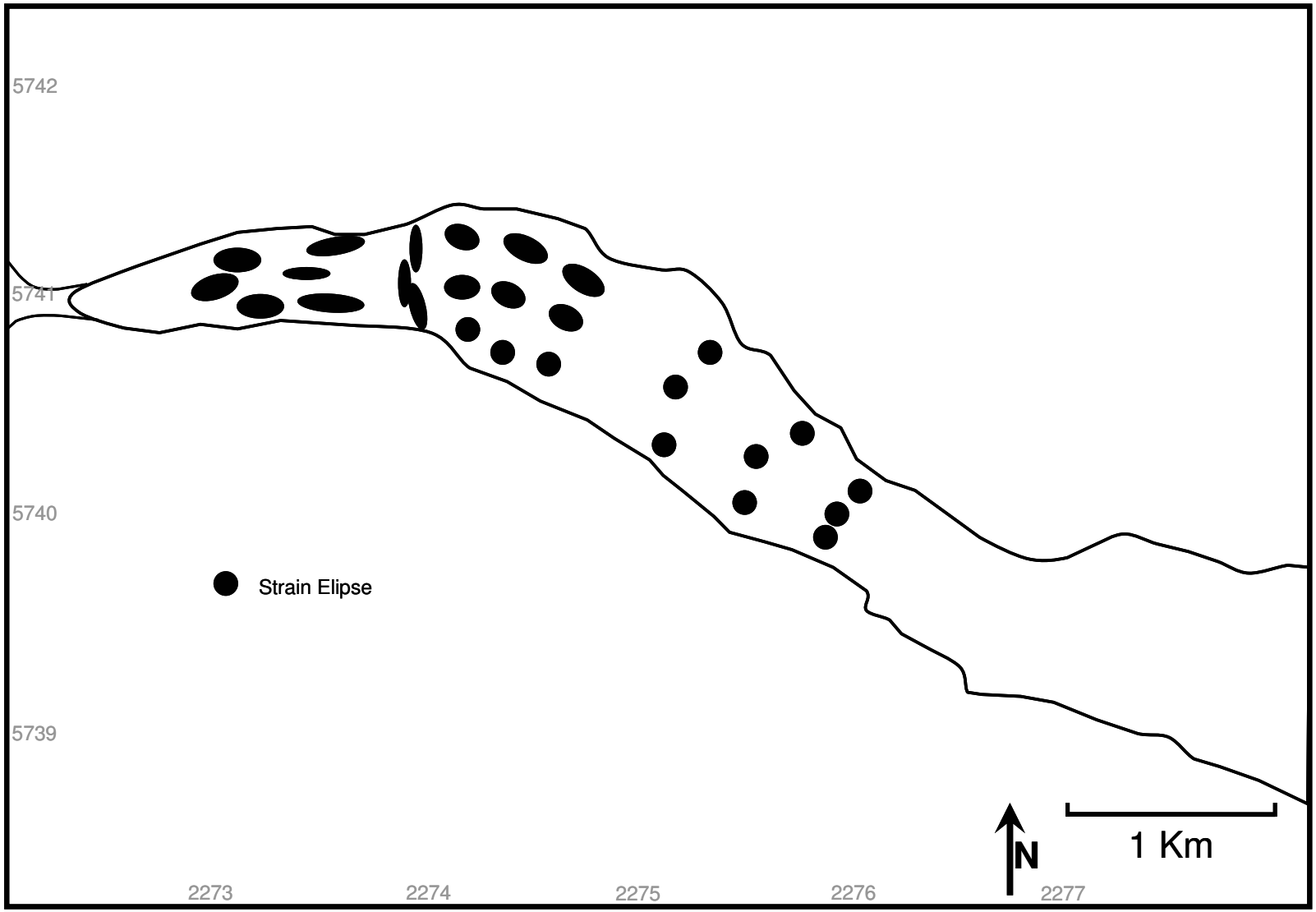

Figure 5.4: Deformation of three initially circular strain ellipses moving through the glacier system from the highest point of the study area at the top of Victoria Flat, down to the snout.

5.4.2 Microstructure of Ice

Internal processes and structures of Fox Glacier may be further investigated by studying the microstructure of ice crystals obtained by taking cores from the glacier, making use of the GNS Science New Zealand Ice Core Research Lab. Information regarding cleavage plains, crystal defects, recrystalization and crystal deformation may be gained for sample sites along the length of the glacier to determine trends in microstructure and microstructural processes. A great deal of ice core microstructure research has been undertaken on polar and high latitude ice sheets and caps (e.g. Arnaud *et al.*, 2000; Gagliardini *et al.*, 2004; Obbard and Baker, 2007), but very little published research is available on the microstructure of temperate valley glaciers such as Fox Glacier.

5.4.3 Glacier Hydrology

The amount of water in a glacier is primarily determined by the glaciers thermal regime and environmental setting and has considerable influences on the flow and behaviour of ice. Water is central to the mechanics of movement of a glacier and hence, as we have seen, the strain rate and structure of glaciers. Research (e.g. Bingham *et al*., 2006; Carlson *et al*., 2007; Mitchell and Brown, 2007) has shown how the hydrology of a glacier's drainage system can be largely influenced by the internal structure of the glacier.

A great deal of information regarding the internal structure of glaciers can be determined from dye tracing experiments. Tracer experiments have been undertaken for over a century (Hubbard and Glasser, 2005), often making use of common salt (NaCl) as a tracer in glacial melt water, which usually has very low base levels of salt. More commonly now, however, the most commonly used tracers are fluorescent dyes (Smart and Laidlaw, 1976; Smart and Karunaratne, 2002; Campbell *et al*., 2006), particularly Rhodamine and Fluorescein.

The time taken for dyes to emerge from the glacier drainage system after being injected, along with the volume of dye measured at the glacier outlet, relative to the volume injected can provide information relating to the complexity and size of englacial conduits, channels and water stores. Return curves can be considered as the key to determining the drainage system.

5.4.4 Long-Term Mass Balance Measurements

A glaciers mass balance describes its mass inputs and outputs over various temporal and spatial scales providing a quantitative expression of volumetric change and net balance through time (Hubbard and Glasser, 2005). The net balance quantifies the net difference between accumulation and ablation over the whole ice mass, and so the mass balance which has a considerable influence on ice flow velocities, strain rates and so potentially structural evolution of the glacier.

5.4.5 Origin and Significance of Debris-Charged Ridges

Debris-charged ridges, representing basal and glaciofluvial material that has emerged at the glacier surface have been noted on several glaciers globally. They generally appear in the terminal area of glaciers, and appear to originate from steeply-dipping (50-70°), fractures on the glacier surface. Whether or not the fractures are new curvilinear features formed at the glacier snout, or whether they are formed further up-glacier is open to conjecture (e.g. Glasser *et al*., 2003). It has been suggested that many fractures may permeate to the glacier bed due to compressional glaciotectonics near the snout of valley glaciers, perhaps due to thermal boundaries within the ice. This could occur where active temperate ice is being thrust over colder, stagnant ice near the snout. An alternative hypothesis would be that the fractures may relate to large-scale recumbent folding in the glacier. As highlighted by Glasser *et al*. (2003), further work is required to elucidate the exact cause (if any) of these mechanisms in elevating basal and glaciofluvial material to the ice surface in temperate glaciers. Studying the isotropic composition ($\sigma^{18}O$) of glacier ice and ice within the debris-charged ridges may help determine, via isotopic fractionation, whether ice has been re-frozen or not. This may help in determining the precise process-origins of the ridges (e.g. Glasser *et al*.)

Chapter 6: Conclusions

6.1 Objectives Revisited

This research project mapped the surface structures of Fox Glacier, using remote sensing in the form of aerial photographs and field observations, to produce a structural glaciological interpretation of the glacier surface, structural field maps of individual structures, and a schematic structural evolution of Fox Glacier. In addition, cumulative strain, and strain rates were calculated for three different areas of the lower Fox Glacier. The relationship between the observed structures and the measured strain rates has also been considered and discussed.

The research questions being addressed by this thesis were:

- What structures are present on the surface of the Fox Glacier?
- What processes are occurring to produce these structures?
- What strain rates are present on the surface of the Fox Glacier?
- How do these strain rates vary over the surface of the Fox Glacier?
- How do these strain rates relate to the observed processes and structures?

From these questions a number of objectives were developed:

1. produce a structural map of the surface of the lower part of Fox Glacier;
2. determine the spatial variation of strain rates within the measured array on the glacier surface;
3. identify spatial relationships between the structures observed on the surface of the glacier and the measured strain rates.

6.2 Structural Mapping

A high level of spatial variability in structural features has been observed on the surface of Fox Glacier. This variation can be linked to valley topography including long-profile

gradient and valley width, both of which have an influence on the rate of ice flow, and the degree of ice compression and extension.

A range of structural features have been observed from both aerial photography and field observations including primary stratification, crevasses, crevasse traces, foliation, folding, ogives, moulins, and englacial conduits. Primary stratification persists throughout the study area and becomes increasingly rotated and deformed as it moves through the study area, from almost level sedimentary levels, to near vertical banding. Crevasse traces also persist throughout the study area, suggesting a continual change in the stress state within the surface ice of Fox Glacier. High stresses, changes in temperature, and strain have rotated and deformed primary stratification in the lower part of the study area, to produce steeply-dipping foliation.

Crevasses appear to vary in type, size and orientation according to the processes that have caused them, with chevron crevasses being created by frictional resistance of the valley walls, transverse crevasses produced by longitudinal extension, and splaying crevasses produced where compression causes the glacier to expand laterally, modifying the stress pattern. Crevasse traces are interpreted to result from either crevasse closure, or represent unopened crevasses similar to tensional veins.

Aerial photographs used for structural mapping were taken more than twenty years prior to field observations and in situ strain rate measurements, potentially having implications for the accuracy of any associations made.

6.3 Strain & Deformation

A great deal of spatial variability occurs in the cumulative strain and strain rates measured on the surface of the Fox Glacier, with the variations being linked to valley topography including long-profile gradient and width.

The highest strain rates of 208.78 y^{-1} and -162.06 y^{-1} were recorded in the lower part of the study area, in the area of most ice disturbance. The lowest strain rates of 0.73 y^{-1} and -1.10 y^{-1} were recorded in the upper part of the study area, in an area of most subdued topography. Strain rates were measured over a relatively short study period during the glaciers most active season, and so extrapolation of results to the whole year should be viewed with extreme caution.

An association can be made between observed glaciological structural features and measured strain rates, suggesting strain rate has an influence on the type, magnitude, location and frequency of these structures.

6.4 Summary

This study has identified how structurally active the lower half of Fox Glacier is. A tentative relationship has been identified between the observed structures and measured surface strain rates. This study focused on the surface of the lower part of Fox Glacier. It would be interesting to study this apparent relationship in more detail in three ways. Firstly, studying how the identified relationship between strain and structure is manifest in three dimensions using ground penetrating radar (GPR) would be intriguing. Secondly, how the structure-strain relationship is manifested further up the glacier towards the névé would be another stimulating research focus. Third, how the structure and strain is apparent in other New Zealand glaciers, including debris-covered examples in Mount Cook National Park would be another intriguing avenue for future research. An important relationship has been identified between strain rates, structure, and the topography of Fox Valley. This project has discussed the current structure and strain rate situation across the surface of Fox Glacier, and how they may inter-relate. To conclude, the exact process mechanisms of ice flow and deformation are reflected in the structure of glacier ice. Developing predictive models of the structural evolution of glaciers may help further understanding of how glaciers respond to a change in climatic input, especially climatic warming. This is particularly important for larger ice sheet outlet glaciers such as Jakobshavn isbræ, Greenland, whose structure and flow appear to reflect and control dynamics of the ice sheet behind (Mayer and Herzfeld, 2000; Bamber *et al.*, 2007).

Appendices

Appendix 1: Fourier Classification of Folding

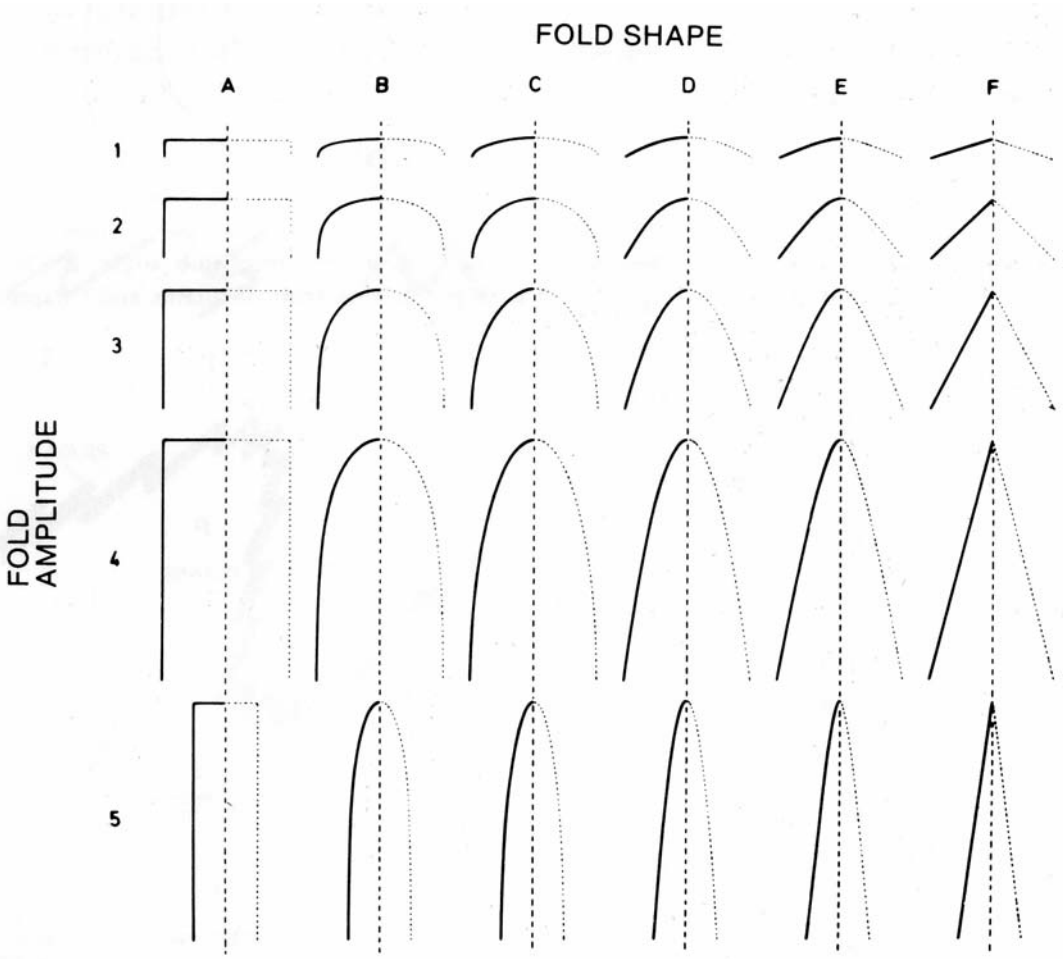

Appendix 2: Software Used During Study

Georient equal angle stereographic projection software. Available to download for free from: http://www.holcombe.net.au/software/rodh_software_georient.htm

MohrView Mohr-Coulomb failure analysis grapher. Available to download from: http://www.scientificsoftwaregroup.com/pages/product_info.php?products_id=150

Appendix 3: Structural Mapping Data

Primary Stratification	
Dip	Strike
76	24
81	24
72	60
76	60
73	14
80	242
76	330
76	178
80	138
65	184
52	180
40	176
33	218
48	180
32	179
90	208
90	210
88	210
90	244
90	246
90	208
78	217
85	220
74	188
88	152
90	136
83	156
74	132
90	146
85	144
68	142

Crevasse Traces	
Dip	Strike
45	178
50	190
50	154
48	204
52	242
50	194
48	142
68	198
68	138
65	208

70	180
70	128
68	104
66	200
90	182
90	184
90	184
80	215
90	198
90	198
86	194
86	208
88	196
90	198
90	198
90	198
88	182
84	232
88	234
88	194
88	180

Foliation	
Dip	Strike
45	188
50	172
50	144
50	128
65	152
87	120
81	120
87	126
87	95
78	84
87	90

Crevasse Orientation (degrees from North)
292
312
298
298
300
392
324

235
235
236
238
138
136
310
308
306
320
338
214
212
212
138
2
334
334
344
30
22
8
252
254
258
268
254
240

Appendix 4: Surficial Debris Data

True Left of Glacier

Length (a)	Width (b)	Depth (c)	Roundness
70	45	22	A
83	50	28	A
74	41	31	SA
104	38	34	SA
143	46	22	VA
67	32	14	SA
88	58	21	SA
97	52	25	A
60	44	32	SA
55	55	27	SA
81	30	22	A
90	50	30	A
116	75	15	VA
90	40	27	A
85	38	33	VA
123	75	36	SA
81	57	21	A
180	100	31	VA
100	69	29	A
81	53	27	SA
170	118	33	A
132	51	35	A
92	83	22	SA
85	61	31	SA
138	67	15	A
110	66	21	SA
57	50	33	A
134	34	15	A
115	42	27	A
95	57	25	SA
120	76	31	A
121	74	41	A
140	130	24	VA
119	51	30	SA
78	61	25	A
60	35	20	A
78	70	25	SA
81	67	25	SA
130	35	30	A
81	46	20	A
75	60	25	SA
100	75	35	A
115	44	27	SA

85	50	12	A
60	40	5	VA
77	41	17	A
90	54	49	SA
94	41	23	A
80	35	26	A
58	48	9	A

True Right of Glacier

Length (a)	Width (b)	Depth (c)	Roundness
90	57	22	A
150	80	26	A
120	57	44	VA
118	95	41	VA
150	66	32	A
120	61	54	VA
150	52	25	A
100	61	57	VA
106	71	40	A
126	72	53	A
118	80	44	A
190	78	31	VA
190	60	40	A
113	59	21	A
118	61	25	A
79	49	19	A
52	28	12	SA
100	78	24	A
130	38	35	A
93	66	42	A
98	75	45	VA
177	55	37	A
115	78	44	SA
100	54	54	A
77	55	29	A
90	67	36	A
100	82	47	SA
192	73	58	SA
116	68	14	A
153	82	32	VA
80	62	32	A
92	55	21	A
125	56	26	A
196	97	80	A
95	50	25	A
180	24	12	VA
76	46	18	VA
125	77	18	A

75	54	30	VA
192	73	58	SA
130	72	40	SA
95	50	29	VA
105	69	46	A
77	70	19	A
160	90	32	VA
77	55	35	SA
89	60	20	VA
115	84	50	A
113	100	76	VA
89	60	64	VA

Centre of Glacier

Length (a)	Width (b)	Depth (c)	Roundness
84	47	41	A
41	30	20	A
85	47	31	SR
41	40	23	A
89	78	67	SR
61	45	33	A
45	39	22	SA
51	32	13	SR
49	34	13	A
57	49	37	A
38	26	15	SA
73	57	30	VA
84	66	48	SR
120	44	44	SA
33	19	16	A
50	50	34	SR
98	75	52	A
108	54	27	A
104	73	65	A
70	60	36	SR
125	73	67	VA
87	77	46	SA
110	94	49	A
66	55	33	VA
50	40	26	SA
99	63	30	SA
79	57	27	A
95	82	38	SA
28	27	18	SR
50	43	14	SR
30	24	13	VA
55	28	12	A
75	38	38	VA

44	38	25	SR
63	60	442	VA
41	20	15	SR
65	40	19	A
58	33	32	A
54	29	16	A
52	48	22	A
57	44	30	A
34	17	15	SA
47	14	14	SA
63	48	27	SR
33	22	13	A
110	103	58	SR
80	69	48	A
56	37	26	SR
35	35	16	A
63	42	27	A

Appendix 5: Strain Data

1000	2270973	5741412	248.339	GPS Base Station 1
1001	2270840	5741495	239.457	GPS Base Station 2
	Long x	Lat y		
Transect A #1				
6006	2274475	5740941	767.077	a1
6007	2274478	5740867	770.545	a6
6008	2274407	5740920	762.897	a10
6009	2274408	5740840	764.898	a2
6010	2274442	5740807	768.683	a7
6011	2274348	5740829	762.331	a11
6012	2274389	5740789	764.518	a3
6013	2274434	5740745	767.3	a8
6014	2274337	5740766	763.705	a12
6015	2274381	5740736	763.979	a4
6016	2274424	5740694	764.954	a9
6017	2274372	5740681	764.421	a5
6018	2274332	5740708	763.608	a13
Transect A #2				
7000	2274466	5740873	769.764	a6
7001	2274463	5740947	764.878	a1
7002	2274395	5740926	760.756	a10
7003	2274396	5740846	762.917	a2
7004	2274430	5740813	766.898	a7
7005	2274377	5740795	762.776	a3
7006	2274336	5740835	760.539	a11
7007	2274325	5740772	763.165	a12
7008	2274370	5740742	762.617	a4
7009	2274423	5740751	766.025	a8
7010	2274413	5740700	763.833	a9
7011	2274361	5740686	764.092	a5
7012	2274321	5740714	763.368	a13
Transect B #1				
3001	2272577	5740899	458.567	b4
3003	2272533	5740873	449.513	b13
3005	2272529	5740917	454.179	b12
3006	2272561	5740952	462.406	b3
3008	2272616	5740928	468.75	b8
5008	2272570	5740826	466.133	b5
5009	2272614	5740878	468.205	b9
3012	2272523	5740999	454.799	b11
3013	2272586	5740984	471.609	b7

5014	2272514	5741042	457.582	b10
5015	2272528	5741015	451.046	b2
5016	2272554	5741041	463.079	b6
5017	2272524	5741069	450.772	b1

Transect B #2

7013	2272496	5741067	444.114	b1
7015	2272488	5741038	451.687	b10
7016	2272521	5741036	455.617	b6
7017	2272502	5741010	445.73	b2
7018	2272495	5740994	449.486	b11
7019	2272557	5740976	465.82	b7
7020	2272532	5740945	455.693	b3
7021	2272500	5740911	447.144	b12
7022	2272582	5740923	459.996	b8
7023	2272548	5740891	450.693	b4
7024	2272585	5740871	458.731	b9
7025	2272545	5740821	460.574	b5
7026	2272504	5740867	443.14	b13

Transect C #1

4009	2272346	5741062	418.114	c1
4010	2272385	5741018	435.464	c6
4011	2272349	5741005	428.616	c10
4012	2272361	5740973	432.779	c2
4013	2272392	5740937	439.065	c7
4014	2272419	5740817	436.917	c5
4015	2272386	5740828	425.598	c13
4016	2272435	5740851	434.152	c9
4017	2272392	5740865	428.111	c4
4018	2272439	5740897	434.747	c8
4020	2272356	5740867	424.197	c12
4021	2272364	5740915	429.701	c3
4023	2272335	5740931	428.249	c11

Transect C #2

7027	2272405	5740852	427.941	c9
7028	2272412	5740893	430.617	c8
7029	2272358	5740826	420.08	c13
7030	2272365	5740863	422.275	c4
7031	2272340	5740874	423.132	c12
7032	2272364	5740935	433.281	c7
7033	2272336	5740912	423.979	c3
7034	2272307	5740958	424.445	c11
7035	2272323	5741063	412.813	c1
7036	2272359	5741019	426.742	c6
7037	2272298	5741025	414.201	c10
7038	2272359	5740995	428.928	c2

Terminal Face

8000	2271947	5740759	299.285	t1	True Left
8001	2271899	5740808	291.796	t2	
8002	2271851	5740890	275.501	t3	
8003	2271840	5740928	267.965	t4	
8004	2271881	5740987	268.039	t5	
8005	2271890	5741011	267.238	t6	
8006	2271952	5741106	269.139	t7	True Right

References

Allen, C. Kamb, W. Meier, M. and Sharp, R. 1960. Structure of the Lower Blue Glacier, Washington. *Journal of Geology*, **68** (6): 601-625.

Alley, R.1992. Flow-law hypotheses for ice-sheet modelling. *Journal of Glaciology*, **38**: 245-256.

Alpine Guides Westland. 2007. Available at http://www.foxguides.co.nz. Accessed on Monday 12th March, 2007.

Ambach, W. 1968. The formation of crevasses in relation to the measured distribution of strain-rates and stresses. *Archives for Meteorology, Geophysics, and Bioclimatology. Serial A*, **17**: 78-87.

Amir, A. 2005. Theoretical issues of searching aerial photographs: a bird's eye view. *International Journal of Foundations of Computer Science*, **16** (6): 1075-1097.

Ancey, C. 2007. Plasticity and geophysical flows: A review. *Journal of Non-Newtonian Fluid Mechanics*, **142** (1-3): 4-35.

Anderson, B. and Mackintosh, A. 2006. Temperature change is the major driver of late-glacial and Holocene glacier fluctuations in New Zealand. *Geology*, **34** (2): 121-124.

Arnaud, L. Weiss, J. Gay, M. and Duval, P. 2000. Shallow-ice microstructure at Dome Concordia, Antarctica. *Annals of Glaciology*, **30**: 8-12.

Bamber, J. Alley, R. and Joughin, I. 2007. Rapid response of modern day ice sheets to external forcing. *Earth and Planetary Science Letters*, **257** (1-2): 1-13.

Barnes, J. 1997. *Basic Geological Mapping, 3rd Edition. The Geological Field Guide Series*. John Wiley & Sons Ltd, Chichester.

Bell, J. 1910. *A geographical report on the Franz Josef Glacier, with topographical maps and data by R.P. Grenville and botanical notes by Leonard Cockayne*. New Zealand Geological Survey. Wellington, New Zealand.

Benn, D. and Ballantyne, C. 1994. Reconstructing the transport history of glacigenic sediments: a new approach based on the co-variance of clast form indices. *Sedimentary Geology*, **91**: 215-227.

Benn, D. and Evans, D. 1998. *Glaciers & Glaciation*. Hodder Arnold, London.

Benn, D. Wiseman, S. and Hands, K. 2001. Growth and drainage of supraglacial lakes on debris-mantled Ngozumpa Glacier, Khumbu Himal, Nepal. *Journal of Glaciology*, **47** (159): 626-238.

Bingham, R. Nienow, P. Sharp, M. and Copland, L. 2006. Hydrology and dynamics of a polythermal (mostly cold) high arctic glacier. *Earth Surface Processes and Landforms*, **31**: 1463-1479.

Blachut, T, and Müller, F. 1966. Some fundamental considerations on glacier mapping. *Canadian Journal of Earth Sciences*, **6**: 747-759.

Boulton, G. 1996. Theory of glacial erosion, transport and deposition as a consequence of subglacial sediment deformation. *Journal of Glaciology*, **42** (140): 43-62.

Boulton, G. 1978. Boulder shapes and grain-size distributions of debris as indicators of transport paths through a glacier and till genesis. *Sedimentology*, **25**:773-799.

Boulton, G. and Jones, A. 1979. Stability of temperate ice caps and ice sheets resting on beds of deformable sediment. *Journal of Glaciology*, **24**: 29-43.

Bugmann, H. Gurung, A. Ewert, F. Heberli, W. Guisan, A. Fagre, D. and Kaab, A. 2007. Modelling the biophysical impacts of global change in mountain biosphere reserves. *Mountain Research and Development*. **27** (1) 66-77.

Campbell, F. Nienow, P. and Purves, R. 2006. Role of the supraglacial snowpack in mediating meltwater delivery to the glacier system as inferred from dye tracer investigations. *Hydrological Processes*, **20** (4): 969-985.

Carassa, G. 1992. Foliation on Tyndall Glacier, Southern Patagonia. *Bulletin of Glacial Research*, **10**: 75-77.

Carlson, A. Jenson, J. and Clark, P. 2007. Modelling the subglacial hydrology of the James Lobe of the Laurentide Ice Sheet. *Quaternary Science Reviews*, **26** (9-10): 1384-1397.

Case, J. Chilver, A. and Ross, C. 1999. *Strength of Materials and Structures, 4th Edition*. Arnold-Hodder Headline group, London..

Chinn, T. 2000. Satellite Image Atlas of Glaciers of the World: Irian Jaya, Indonesia, and New Zealand (H-2 Glaciers of New Zealand). United States Geological Survey Professional Paper 1386-H. Available at: http://pubs.usgs.gov/prof/p1386h/contents.html. Accessed on Tuesday 6th March 2007.

Clark, C. 1997. Reconstructing the evolutionary dynamics of palaeo-ice sheets using multi-temporal evidence, remote sensing and GIS. *Quaternary Science Reviews*, **16** (9): 1067–1092.

Coates, G. and Chinn, T. 1992. *The Franz Josef and Fox Glaciers*. DSIR Geology and Geophysics, New Zealand.

Cutnell, J. and Johnson, K. 2004. *Physics, 6th Edition*. John Wiley & Sons, Inc, United States.

Davies, T. Smart, C. and Turnbull, J. 2003. Water and sediment outbursts from advanced Franz Josef Glacier, New Zealand. *Earth Surface Processes and Landforms*, **28** (10): 1081-1096.

Dickinson, G. 1969. *Maps and Air Photographs*. Edward Arnold, London.

Douglas, C. 1896. *Report on Cooks River District: Appendix to the Journal of the House of Representatives of New Zealand*, **1** (C1): 110-112, Wellington.

Dowdeswell, J. and Williams, M. 1997. Surge-type glaciers in the Russian High Arctic identified from digital satellite imagery. *Journal of Glaciology*, **43**: 489-494.

Echelmeyer, K. and Kamb, B. 1986. Stress-gradient coupling in glacier flow, 2. Longitudinal averaging in the flow response to small perturbations in ice thickness and surface slope. *Journal of Glaciology*, **32** (111): 285-298.

Echelmeyer, K. and Wang, Z. 1987. Direct observation of basal sliding and deformation of basal drift at sub-freezing temperatures. *Journal of Glaciology*, **33**: 83-98.

Engelder, T. and Marshak, S. 1998. *Analysis of data from rock-deformation experiments*. *In* Marshak, S. and Mitra, G. (*eds.*). Basic Methods of Structural Geology. Prentice Hall. New Jersey.

Ewing, K. and Marcus, M. (1966). Cartographic representation and symbolization in glacier mapping. *Canadian Journal of Earth Sciences*, **6**: 761-769.

Farbrot, H. Isaksen, K. Eiken, T. Kääb, T. and Sollid, J. 2005. Composition and internal structures of a rock glacier on the strandflat of western Spitzbergen, Svalbard. *Norwegian Journal of Geography*, **59** (2): 139-148.

Fischer, U. Iverson, N. Hooyer, T. Cohen, D. Jackson, M. Moore, P. Lappegard, G. and Kohler, J. 2003. Motion of a temperate glacier over a soft bed: subglacial experiments at Engabreen, Norway. *Geophysical Research Abstracts*, **5**: 10565.

Fisher, J. 1962. Ogives of the Forbes type on Alpine glaciers and a study of their origins. *Journal of Glaciology*, **4** (31): 53-61.

Fitzharris, B. Lawson, W. and Owens, I. 1999. Research on glaciers and snow in New Zealand. *Progress in Physical Geography*, **23** (4): 469–500.

Forbes, J. 1845. Illustrations of the viscous theory of glacier motion. *Philosophical Transactions of the Royal Society of London,* **136**: 143-155.

Forbes, J. 1859. *Occasional papers on the theory of glaciers*. Adam and Charles Black. Edinburgh.

Fountain, A. 1993. Geometry and flow conditions of subglacial water at South Cascade Glacier, Washington State, USA: an analysis of tracer injections. *Journal of Glaciology*, **39**: 143-156.

Gagliardini, O. Durand, G. and Wang, Y. 2004. Grain area as a statistical weight for polycrystal constituents. *Journal of Glaciology*, **50** (168): 87-95.

Gao, J. and Liu, Y. 2001. Applications of remote sensing, GIS and GPS in glaciology: A review. *Progress in Physical Geography*, **25**: 520-540.

Gardner, A. and Sharp, M. 2007. Influence of the arctic circumpolar vortex on the mass balance of Canadian High Arctic glaciers. *Journal of Climate*, **20** (18): 4586-4598.

Gellatly, A. 1985. Glacier fluctuations in the central Southern Alps, New Zealand: documentation and implications for environmental change during the last 1000 years. *Zeitschrift für Gletscherkunde und Glazialgeologie*, **21**: 259-264.

Glasser, N. Hambrey, M. Bennett, M. and Huddart, D. 2003. Comment: Formation and reorientation of structure in the surge-type glacier Kongsvegen, Svalbard. *Journal of Quaternary Science*, **18** (1): 95-97.

Glasser, N. Hambrey, M. Crawford, K. Bennett, M. and Huddart, D. 1998. The structural glaciology of Kongsvegen, Svalbard, and its role In landform genesis. *Journal of glaciology*, **44** (146): 136-148.

Glasser, N. Hambrey, M. Crawford, K. Bennett, M. and Huddart, D. 2000 (Correction). The structural glaciology of Kongsvegen, Svalbard, and its role In landform genesis. *Journal of glaciology*, **44** (146): 136-148.

Glasser, N. Hambrey, M. Etienne, J. Jansson, P. and Pettersson, P. 2003. The origin and significance of debris-charged ridges at the surface of Storglaciaren, northern Sweden. *Geografiska Annaler Series A-Physical Geography*, **85A** (2): 127-147.

Glasser, N. Jansson, K. Mitchell, W. and Harrison, S. 2006. The geomorphology and sedimentology of the 'Témpanos' moraine at Laguna San Rafael, Chile. *Journal of Quaternary Science*, **21** (6): 629-643.

Glen, J. 1955. The creep of polycrystalline ice. *Proceedings of the Royal Society, Series A*, **228** (1175): 519-538.

Goodsell, B. Anderson, B. and Lawson, W. 2003. Supraglacial routing of subglacial water at Franz Josef Glacier, South Westland, New Zealand. *Journal of Glaciology*, **49** (166): 469-470.

Goodsell, B. Hambrey, M. and Glasser, N. 2002. Formation of band ogives and associated structures at Bas Glacier d'Arolla, Valais, Switzerland. *Journal of Glaciology*, **48** (161): 287-300.

Goodsell, B. Hambrey, M. Glasser, N. Nienow, P. and Mair, D. 2005[a]. The Structural Glaciology of a Temperate Valley Glacier: Haut Glacier d'Arolla, Valais, Switzerland. *Arctic, Antarctic, and Alpine Research*, **37** (2): 218-232.

Goodsell, B. Anderson, B. Lawson, W. and Owens, I. 2005[b]. Outburst flooding at Franz Josef Glacier, South Westland, New Zealand. *New Zealand Journal of Geology and Geophysics*, **48**: 95-104.

Gudmundsson, G. Iken, A. and Funk, M. 1997. Measurements of ice deformation at the confluence area of Unteraagletscher, Bernese Alps, Switzerland. *Journal of Glaciology*, **43** (145): 548-556.

Gunn, B. 1964. Flow rates and secondary structures of Fox and Franz Josef Glaciers, New Zealand. *Journal of Glaciology*, **5** (38): 173-190.

Hambrey, M. 1976. Structure of the glacier Charles Rabots Bre, Norway. *Geological Society of America Bulletin*, **87** (11): 1629-1637.

Hambrey, M. 1994. *Glacial Environments*. UCL Press. London.

Hambrey, M. and Alean, J. 2004. *Glaciers 2nd Edition*. Cambridge University Press, Cambridge.

Hambrey, M and Dowdeswell, J. 1994. Flow regime of the Lambert Glacier-Emery Ice Shelf system, Antarctica: Structural evidence from Landsat imagery. *Annals of Glaciology,* **20**: 401-406.

Hambrey, M. Dowdeswell, J. Murray, T. and Porter, P. 1996. Thrusting and debris entrainment in a surging glacier: Bakaninbreen, Svalbard. *Annals of Glaciology*, **22**.

Hambrey, M. and Ehrmann, W. 2004. Modification of sediment characteristics during glacial transport in high-alpine catchments: Mount Cook area, New Zealand. *Boreas*, **33** (4): 300-318.

Hambrey, M. and Milnes, A. 1977. Structural Geology of an Alpine Valley Glacier (Griesgletscher, Valais, Switzerland). *Eclogae Geologicae Helvetiae*, **77**: 667-684.

Hambrey, M. and Lawson, W. 2000. *Structural styles and deformation fields in glaciers: a review*. *In* Maltman, A. Hubbard, B. and Hambrey, M. (*eds*). Deformation of glacial materials. Geological Society, London, Special Publications, **176**: 59-83.

Hambrey, M. and Müller, F. 1978. Structures and Ice Deformation in the White Glacier, Axel Heiberg Island, Northwest Territories, Canada. *Journal of Glaciology*, **20** (82): 41-66.

Hambrey, M. Murray, T. Glasser, N. Hubbard, A. Hubbard, B. Stuart, G. Hansen, S. and Kohler, J. 2005. Structure and changing dynamics of a polythermal valley glacier on a centennial timescale: Midre Lovénbreen, Svalbard. *Journal of Geophysical Research*, **110**: F01006.

Hamelin, B. Bastie, P. Duval, P. Chevy, J. Montagnat, M. 2004. Lattice distortion and basal slip bands in deformed ice crystals revealed by hard x-ray diffraction. *Journal de Physique IV*, **118**: 27-33.

Harper, J. Humphrey, N. and Pfeffer, W. 1998. Three-dimensional deformation measured in an Alaskan Glacier. *Science*, **281** (5381): 1340-1342.

Harper, J. Humphrey, N. Pfeffer, W. Huzurbazar, S. Bahr, D. and Welch, B. 2001. Spatial variability in the flow of a valley glacier: Deformation of a large array of boreholes. *Journal of Geophysical Research*, **106** (B5): 8547-8562.

Harvey, A. 2001. Coupling between hillslopes and channels in upland fluvial systems: implications for landscape sensitivity, illustrated from the Howgill Fells, northwest England. *Catena*, **42** (2-4): 225-250.

Herbst, P. Neubauer, F. and Schöpfer, M. 2006. The development of brittle structures in an alpine valley glacier: Pasterzenkees, Austria, 1887-1997. *Journal of Glaciology*, **52** (176): 128-136.

Hibbeler, R. 1997. *Mechanics of Materials, 3rd Edition*. Prentice Hall. New Jersey.

Higuchi, K. and Tanaka, Y. 1982. Flow pattern of meltwater in mountain snow cover. *Hydrological Sciences Journal*, **27** (2): 256.

Hochstein, M. Watson, M, Malengreau, B. Nobes, D. and Owens, I. 1998. Rapid melting of the terminal section of the Hooker Glacier (Mt Cook National Park, New Zealand). *New Zealand Journal of Geology and Geophysics*, **41** (3): 203-218.

Holdsworth, G. 1969. Primary transverse crevasses. *Journal of Glaciology*, 8 (52): 107-129.

Holmlund, P. 1988. Internal geometry and evolution of moulins, Storglaciaren, Sweden. *Journal of Glaciology*, **34** (117): 242-248.

Holz, R. 1973. *The surveillant science. Remote sensing in the environment*. Houghton Mifflin Company, Boston.

Hooke, R. 2005. *Principles of Glacier Mechanics, 2nd Edition.* Cambridge University Press, Cambridge..

Hooke, R. Calle, P. Holmlund, P. Nilsson, M. and Stroeven, A. 1989. A 3 year record of seasonal variations in surface velocity, Storglaciären, Sweden. *Journal of Glaciology*, **35** (120): 235-247.

Hooke, R. and Hudleston, P. 1978. Origin of foliation in glaciers. *Journal of Glaciology*, **20**: 285-299.

Hooker, B. and Fitzharris, B. 1999. The correlation between climatic parametres and the retreat and advance of Franz Josef Glacier, New Zealand. *Global and Planetary Change*, **22** (1-4): 39-48.

Hoydal, O. 1996. A force-balance study of ice flow and basal conditions of Jutulstraumen, Antarctica. *Journal of Glaciology*, **42** (142): 413-425.

Hubbard, A. Blatter, H. Nienow, P. Mair, D. and Hubbard, B. 1998. Comparison of a three-dimensional model for glacier flow with field data at Haut Glacier d'Arolla, Switzerland. *Journal of Glaciology*, **44**: 368-378.

Hubbard, A. and Hubbard, B. 2000. The potential contribution of high-resolution glacier flow modelling to structural glaciology. *In* Maltman, A. Hubbard, B. and Hambrey, M (*eds*). Deformation of Glacial Materials. *Special Publication of the Geological Society*, **176**: 135-146.

Hubbard, B. and Glasser, N. 2005. *Field Techniques in Glaciology and Glacial Geomorphology*. John Wiley & Sons, Ltd. Chichester.

Hudleston, P. 1976. Recumbent folding in the base of the Barnes Ice Cap, Baffin Island, Northwest Territories, Canada. *Geological Society of America Bulletin*, **87** (12): 1678-1683.

Humphrey, N. Kamb, B. Fahnestock, M. and Engelhardt, H. 1993. Characteristics of the bed of the lower Columbia Glacier, Alaska. *Journal of Geophysical Research*, **98**: 837-846.

Irvine-Flynn, T. Moorman, B. Williams, J. and Walter, F. 2006. Seasonal changes in ground-penetrating radar signature observed at a polythermal glacier, Bylot Island, Canada. Earth Surface Processes and Landforms, **31** (7): 892-909.

Jaeger, J. and Cook, N. 1979. *Fundamentals of Rock Mechanics, 3rd Ed*. Chapman & Hall. London.

Jansson, K. 2005. Map of the glacial geomorphology of north-central Quebec, Labrador, Canada. *Journal of Maps*. 46– 56.

Johnson-laird, P. 1999. Deductive reasoning. *Annual Review of Psychology*, **50**: 109-135.

Karato, S. Zang, S. Zimmerman, M. Daines, M. Kohlstedt, D. 1998. Experimental Studies of Shear Deformation of Mantle Materials: Towards Structural Geology of the Mantle. *Pure and Applied Geophysics*, **151** (2-4): 589-603.

Kaser, G. Mountain Glaciers. In, Knight, P. 2006. *Glacier and Environmental Change*. Blackwell, Oxford. 268-271.

Kehle, R. 1964. Deformation of the Ross Ice Shelf, Antarctica. *Geological Society of America Bulletin*, **75**: 259-286.

King, C. and Lewis, W. 1961. A tentative theory of ogive formation. *Journal of Glaciology*, **3** (29): 913-939.

Kirkbride, M. and Spedding, N. 1996. The influence on englacial drainage on sediment-transport pathways and till texture of temperate valley glaciers. *Annals of Glaciology,* **22**: 160-166.

Knight, P. 2006. (*ed.*) *Glacier Science and Environmental Change*. Blackwell Science Ltd, Oxford.

Kuhn, M. 1984. Mass budget imbalances as criterion for a climatic classification of glacier. *Gegrafiska Annnaler*, **66A**: 229-238.

Langley, K. Hamran, S. Hogda, K. Storvold, R. Brandt, O. Hagen, J. and Kohler, J. Use of C-Band ground penetrating radar to determine backscatter sources within glaciers. *IEEE Transactions on Geosciences and Remote Sensing*, **45** (5): 1236-1246.

Larsen, N. Piotrowski, J. and Menzies, J. 2007. Microstructural evidence of low-strain, time-transgressive subglacial deformation. *Journal of Quaternary Science*, **22** (6): 593-608.

Läufer, A. and Phillips, G. 2005. Brittle structural architecture of the Lambert Glacier Region (E Antarctica) and its relation to Gondwana break-up. *Geophysical Research Abstracts*, **7**: 06814.

Lawson, W. Sharp, M. and Hambrey, M. 1994. The structural geology of a surge-type glacier. *Journal of Structural Geology,* **16** (10): 1447-1462.

Mager, S. and Fitzsimons, S. 2007. Formation of glaciolacustrine Late Pleistocene end moraines in the Tasman Valley, New Zealand. *Quaternary Science Reviews*, **26** (5-6): 243-258.

Mair, D. Sharp, M. and Willis, I. 2002. Evidence for basal cavity opening from analysis of surface uplift during and early melt-season high velocity event: Haut Glacier d'Arolla, Switzerland. *Journal of Glaciology*, **48** (161): 208-216.

Mair, D. Willis, I. Hubbard, B. Fischer, H. Nienow, P. and Hubbard, A. 2003. Hdrological controls on patterns of surface, internal and basal motion during three "spring events": Haut Glacier D'Arolla, Switzerland. *Geographical Research Abstracts*, **5**: 09821.

Mair, R. and Kuhn, M. 1994. Temperature and movement measurements at a bergschrund. *Journal of Glaciology*, **40** (136): 561-565.

Mayer, H. and Herzfeld, U. 2000. Structural glaciology of the fast-moving Jakobshavn Isbræ, Greenland, compared to the surging Bering Glacier, Alaska, USA. *Annals of Glaciology*, **30**: 243-249.

McClay, K. 1997. *The Mapping of Geological Structure. The Geological Field Guide Series*. John Wiley & Sons Ltd. Chichester.

McKinzey, K. Lawson, W. Kelly, D. and Hubbard, A. 2004. A revised little ice age chronology of the Franz Josef Glacier, Westland, New Zealand. *Journal of the Royal Society of New Zealand*, **34** (4): 381-394.

Meier, M. Kamb, W. Allen, C. and Sharp, R. 1974. Flow of Blue Glacier, Olympic Mountains, Washington, USA. *Journal of Glaciology,* **13** (68): 187-212.

Milnes, A. Hambrey, M. 1976. A method of estimating approximate cumulative strains in glacier ice. *Tectonophysics*, **34**: T23-T27.

Mitchell, A. and Brown, G. 2007. Diurnal hydrological-physiochemical controls and sampling methods for minor and trace elements in an alpine glacial hydrological system. *Journal of Hydrology*, **332** (1-2): 123-143.

Moeller, C. Mickelson, D. Anderson, M. and Winguth, C. 2007. Groundwater flow beneath Late Weichselian Glacier ice in Nordfjord, Norway. *Journal of Glaciology*, **53** (180): 84-90.

Naruse, R. and Skvarca, P. 2000. Dynamic features of thinning and retreating Glaciar Upsala, a Lacustrine calving glacier in Southern Patagonia. *Arctic, Antarctic and Alpine Research*, **32** (4): 485-491.

NASA, 2001. Landsat 7 Enhanced Thematic Mapper (ETM) plus image of Mount Cook region, New Zealand (produced 31 March 2001). Available at: http://www.earthobservatory.nasa.gov/Newsroom/NewImages/images.php3?img_id=15331. Accessed on Thursday 29th March 2007.

Nesje, A. and Dahl, S. 2000. *Glaciers and Environmental Change: Key Issues in Environmental Change*. Hodder Arnold, London..

New Zealand Aerial Mapping. 2007. Available at http://www.nzam.com. Accessed on Friday 30th March 2007.

Nicholson, L. & Benn, D. 2006. Calculating ice melt beneath a debris layer using meteorological data. *Journal of Glaciology*, **52** (278): 463-470.

Nienow, P. Hubbard, A. Hubbard, B. Chandler, D. Mair, D. Sharp, M. and Willis, I. 2005. Hydrological controls on diurnal ice flow variability in valley glaciers. *Journal of Geophysical Research- Earth Surface,* **110**: F04002.

Nye, J. 1957. *Physical Properties of Crystals*. Clarendon Press, Oxford..

Nye, J. 1958. Surges in glaciers. *Nature*, **181**: 1450-1451.

Nye, J. 1959. A method of determining the strain-rate tensor at the surface of a glacier. *Journal of Glaciology*, **3** (25): 409-419.

Obbard, R. and Baker, I. 2007. The microstructure of meteoric ice from Vostok, Antarctica. *Journal of Glaciology*, **53** (180): 41-62.

Ødegård, R. Isaksen, K. Eiken, T. and Sollid, J. 2003. Terrain Analyses and Surface Velocity Measurements of the Hiorthfjellet Rock Glacier, Svalbard. *Permafrost and Periglacial Processes*, **14**: 359-365.

Oerlemans, J. Anderson, B. Hubbard, A. Huybrechts, P. Jóhannesson, T. Knap, W. Schmeits, M. Stroeven, A. Van de Wal, R. Wallinga, J. and Zuo, Z. 1998. Modelling the response of glaciers to climate warming. *Climate Dynamics*, 14 (4): 267-274.

Paterson, W. 1994. *The Physics of Glaciers 3rd Edition*. Elsevier Science, Amsterdam.

Pattyn, F. and Naruse, R. 2003. The nature of complex ice flow in Shirase Glacier catchment, East Antarctica. *Journal of Glaciology*, **49** (166): 429-436.

Petrenko, V. and Whitworth, R. 1999. *Physics of Ice*. Oxford University Press, Oxford.

Posamentier, H. 1978. Thoughts on ogive formation. *Journal of Glaciology*, **20** (82): 218-220.

Punkari, M. 1982. Glacial geomorphology and dynamics in the eastern parts of the Shield interpreted using Landsat imagery. *Photogrammetric Journal Finland*, **9**: 77– 93.

Purdie, H. 2005. *Intra-annual variations in ablation and surface velocity on the lower Fox Glacier, South Westland, New Zealand.* MSc thesis, Massey University, Palmerston North, New Zealand.

Purdie, H. Brook, M. and Fuller, I. 2007 (in press). Seasonal variation in ablation and surface velocity on a temperate maritime glacier: Fox Glacier , New Zealand . *Arctic, Antarctic and Alpine Research*.

Purdie, H. Brook, M. Fuller, I. and Appleby, J. 2008 (in press). Recent changes and dynamics of 'Te Moeka o Tuawe' Fox Glacier, South Westland , New Zealand . *New Zealand Geographer*.

Ragan, D. 1969. Structures at the base of an icefall. *Journal of Geology*, **77**: 647-667.

Raymond, C. 1969. Flow *in a transverse section of Athabasca Glacier, Alberta, Canada*. PhD thesis, California Institute of Technology, Pasadena, California.

Rohl, K. and Roehl, K. 2006. Thermo-erosional notch development at fresh-water-calving Tasman Glacier, New Zealand. *Journal of Glaciology*, **52** (177): 203-213.

Samyn, D. Fitzsimons, S. and Lorrain, R. 2005. Strain-induced phase changes within cold basal ice from Taylor Glacier, Antarctica, indicated by textural and gas analyses. *Journal of Glaciology*, **51** (175): 611-619.

Sara, W. 1974. *Glaciers of Westland National Park: A New Zealand Geological Survey Handbook*. New Zealand Geological Survey, DSIR. Greymouth, New Zealand.

Scofield, J. Lindstrom, D. and Hughes, T. 1988. Surface strain rates, Byrd Glacier, Antarctica. *Annals of Glaciology*, **12**: 207.

Sinnott, R. 1984. Virtues of the Haversine. *Sky and Telescope*, **68** (2): 159-159.

Smart, C. and Karunaratne, K. 2002. Characterisation of fluorescence background in dye tracing. *Environmental Geology*, **42** (5): 492-498.

Smart, P. and Laidlaw, I. 1976. An evaluation of some fluorescent dyes for water tracing. *Water Resource Research*, **13** (1): 15-33.

Smith, M. Rose, J. and Booth, S. 2006. Geomorphological mapping of glacial landforms from remotely sensed data: An evaluation of the principal data sources and an assessment of their quality. *Geomorphology*, **76**: 148– 165.

Soons, J. 1992. The West Coast of the South Island. *In* Soons, J. and Selby, M. (*eds*). *Landforms of New Zealand 2nd Edition*. Longman Paul Ltd. Auckland..

Speight, R. 1935. Notes on the Franz Josef Glacier. *Transactions of the New Zealand Institute*, **64**: 315-322.

Stenborg, T. 1973. Studies of the internal drainage of glaciers. *Geografiska Annaler*, **51A** : 13-41.

Sugden, D. and John, B. 1976. *Glaciers and Landscapes*. Arnold. London.

Sugiyama, S. Naruse, R. and Murav'yev, Y. 2005. Surface strain anomaly induced by the storage and drainage of englacial water in Koryto glacier, Kamchatka, Russia. *Annals of Glaciology*, **40**: 232-236.

Swift, D. Nienow, P. Hoey, T. and Mair, W. 2005. Seasonal evolution of runoff from Haut Glacier d'Arolla, Switzerland and implications for glacial geomorphic processes. *Journal of Hydrology*, **309** (1-4): 133-148.

Thomas, I. Lewis, A. and Ching, N. 1978. Snowfield assessment from Landsat. *In* Ellis, P. Thomas, I. and McDonnell, M (*eds*). *LANDSAT over New Zealand: monitoring our resources from space. The final report of the New Zealand LANDSAT II investigation. DSIR Bulletin 221*. New Zealand Department of Scientific and Industrial Research, Wellington.

Thorsteinsson, T. 2001. An analytical approach to deformation of anisotropic ice-crystal aggregates. *Journal of Glaciology*, **47** (148): 507-516.

Tyndall, J. 1859. On the veined structure of glaciers, with observations on white seams, air bubbles and dirt bands. *Philosophical Transactions of the Royal Society of London*, **149**: 279-307.

Vaughan, D, 1993. Relating the Occurrence of Crevasses to Surface Strain Rates. *Journal of Glaciology*, **39** (142): 255-265.

Vere, D. and Benn, D. 1989. Structure and debris characteristics of medial moraines in Jotunheimen, Norway: implications for moraine classification. *Journal of Glaciology*, **35**: 276-280.

Waddington, E. 1986. Wave ogives. *Journal of Glaciology*, **32** (112): 325-334.

Warren, C. and Kirkbride, M. 2003. Calving speed and climatic sensitivity of New Zealand lake-calving glaciers. *Annals of Glaciology*, **36**: 173-178.

Washburn, B. 1935. Morainic bandings of Malaspina and other Alaskan glaciers. *Geological Society of America Bulletin*, **46** (12): 1879-1890.

Weertman, J. 1964. The theory of glacier sliding. *Journal of Glaciology*, **5**: 287-303.

Weertman, J. 1983. Creep deformation of ice. *Annual Reviews of Earth and Planetary Sciences*, **11**: 215-240.

Williams, R. and Hall, D. 1998. Use of remote-sensing techniques. *In* Haeberli, W. Hoelzle, M. and Suter, S (*eds*). *Into the second century of worldwide glacier monitoring: prospects and strategies*. United Nations Educational, Scientific, and Cultural Organisation (UNESCO), Paris.

Wilson, W. 1896. The Fox Glacier*, Appendix to the Journal of the House of Representatives of New Zealand*, **1** (C1): 108-109.

Woodward, J. and Burke, M. 2007. Applications of ground-penetrating radar to glacial and frozen materials. *Journal of Environmental and Engineering Geophysics*, **12** (1): 69-85.

Woodward, W. Murray, T. Clark, R. and Stuart, G. 2003. Glacier surge mechanics inferred from ground-penetrating radar: Kongsvegen, Svalbard. *Journal of Glaciology*, **49** (167): 473-480.

Woodward, J. Murray, T. and McCaig, A. 2002. Formation and reorientation of structure in the surge-type glacier Kongsvergen, Svalbard. *Journal of Quaternary Science*, **17** (3): 201-209.

Woodward, J. Murray, T, and McCaig, A. 2003. Reply: Formation and reorientation of structures in the surge-type glacier Kongsvegen, Svalbard. *Journal of Quaternary Science*, **18** (1): 99-100.

Wu, T. and Christensen, R. 1964. Measurement of surface strain-rate on Taku Glacier, Alaska. *Journal of Glaciology*, **5** (39): 305-313.

Yamaguchi, S. Sawagaki, T. Matsumoto, T. Muravyev, Y. and Naruse, R. 2007. Influence of debris cover on ogive-like surface morphology of Bilchenok Glacier in Kamchatka. *Arctic, Antarctic, and Alpine Research*, **39** (2): 332-339.

Yamamoto, T. Matsuoka, K, and Naruse, R. 2004. Observation of internal structures of snow covers with a ground penetrating radar. *Annals of Glaciology*, **34** (1): 228-234.

Young, N. and Hyland, G. 2002. Velocity and strain rates derived from InSAR analysis over the Amery Ice Shelf, East Antarctica. *Annals of Glaciology*, **34** (1): 228-234.